

**CHARACTERIZATION OF ASYMMETRIC ANNULAR-SLOT
ANTENNAS AND DESIGN OF A TUNABLE ASYMMETRIC
ANNULAR-SLOT ANTENNA WITH FERROELECTRIC
MATERIAL**

by

Antonio Amador-Pérez

A thesis submitted in partial fulfillment of the requirements for the degree of

MASTER of SCIENCE
in
ELECTRICAL ENGINEERING

UNIVERSITY OF PUERTO RICO
MAYAGÜEZ CAMPUS
2006

Approved by:

Jose Colom Ustariz, PhD
Member, Graduate Committee

Date

Félix Fernández, PhD.
Member, Graduate Committee

Date

Rafael Rodriguez Solis, PhD
President, Graduate Committee

Date

David González-Barreto, Ph.D.
Representative of Graduate Studies

Date

Isidoro Couvertier, PhD
Chairperson of the Department

Date

ABSTRACT

A statistical characterization of an annular slot ring antenna using DOE is presented. The models give an understanding on the effects of the antenna design parameters on the responses of the antenna. These models are validated by comparing the values from simulated antennas with the values predicted by the models. Also, antennas were fabricated and measured to further validate the results and optimum designs were obtained for maximum bandwidth and for perfect match using the models.

A tunable antenna using ferroelectric material operating at around 30 GHz is presented. One design with a magnesium oxide substrate of thickness equal to 0.302 mm presents a tunability of 14.78% when the dielectric permittivity of BSTO_3 is varied from 600 to 1200. A directivity of only -8.8 dB was achieved for this antenna. A second design is presented with a substrate of thickness equal to 0.800 mm; this antenna has two resonant frequencies around 30 GHz, one with a tunability of 1.27%, the second with a tunability of 3.31%. The directivity of this antenna was between 0.567 dB and 1.313 dB.

RESUMEN

Una caracterización estadística de una antena de ranura anular utilizando diseño de experimentos es presentada. Los modelos obtenidos proveen un entendimiento acerca del efecto de los parámetros de diseño sobre las respuestas de la antena. Estos modelos son validados comparando los valores de antenas simulados con los valores predichos por los modelos. Además, se fabricaron y midieron antenas para la validación de los modelos y se obtuvieron diseños óptimos de ganancia máxima y de pareo exacto de impedancia utilizando los modelos.

Una antena sintonizable utilizando material ferroeléctrico operando a 30 GHz es presentada. Un diseño con un sustrato de óxido de magnesio con grosor igual a 0.302 mm y una sintonización de 14.78% cuando la permisividad eléctrica de BSTO_3 es variada de 600 a 1200. Esta antena alcanzó una directividad de solo -8.8 dB. Un segundo diseño es presentado con un sustrato de grosor igual a 0.800 mm; esta antena presentó dos frecuencias de resonancia cerca de 30 GHz; una con sintonización de 1.27%, y la segunda con sintonisibilidad 3.31%. La directividad de esta antena fue de 0.567 dB y 1.313 dB.

To my wife, for her encouragement, help and support and for being there with me every step of the way. I love you

ACKNOWLEDGEMENTS

I want to recognize several persons who collaborated directly and indirectly with my research at the University of Puerto Rico at Mayagüez. Their guidance and support made this work possible.

First of all I would like to thank my advisor, Dr. Rafael A. Rodríguez Solís, for giving me the opportunity to be a part of his research group and to be there to answer my questions time and time again. I would also like to thank the rest of my graduate committee: Dr. José Colom Ustáriz and Dr. Félix Fernández and a special thanks to Dr. David González-Barreto from the Industrial Engineering Department for always making time to answer my questions.

My thanks to the members of the Radiation Laboratory group, David del Río, Juan Torres, Silvia Herrera, Víctor Marrero and Pablo Lozada, each one helped me in many aspects and made my time at UPRM enjoyable.

Very special thanks to my parents Sony and Giggie, they loved me and supported me in every decision in my life and without them I would not be where I am right now. I also would like to thank my brother who was a safe heaven every time I wanted to forget about

responsibilities for a while and my grandparents Jameson and Nicha for always making sure that I had everything I needed.

Finally, I would like to thank my wife Silvia Sofia Herrera for her patience and understanding and for helping me focus on the task at hand.

TABLE OF CONTENTS

ABSTRACT.....	II
RESUMEN	III
ACKNOWLEDGEMENTS.....	V
TABLE LIST.....	ERROR! BOOKMARK NOT DEFINED.
FIGURE LIST	IX
1 INTRODUCTION.....	1
1.1 JUSTIFICATION	1
1.2 OBJECTIVES	2
1.3 PROJECT DESCRIPTION.....	3
1.4 WORK ORGANIZATION.....	4
2 LITERATURE REVIEW	5
2.1 SLOTLINES	5
2.2 COPLANAR WAVEGUIDE TRANSMISSION LINES	6
2.3 ANNULAR SLOT ANTENNAS	7
2.3.1 <i>CPW fed Slot Ring Antenna</i>	8
2.4 DESIGN OF EXPERIMENTS.....	9
2.4.1 <i>Characterization of Antennas Using DOE</i>	10
2.5 FERROELECTRIC MATERIALS	11
2.5.1 <i>Tunable Components Using Ferroelectric Material</i>	13
2.6 CHAPTER CONCLUSIONS	15
3 METHODOLOGY	17
3.1 PURPOSE	17
3.2 PROCEDURE	17
3.3 CHAPTER CONCLUSIONS	25
4 RESULTS AND DISCUSSION	26
4.1 STATISTICAL CHARACTERIZATION RESULTS.....	26
4.2 TUNABLE ANTENNA DESIGN RESULTS	70
5 CONCLUSIONS AND FUTURE WORK.....	82
5.1 CONCLUSIONS.....	82
5.2 FUTURE WORK.....	83

List of Tables

Tables	Page
Table 3.2.1 Levels of the 2 ⁴ factorial design.....	19
Table 3.2.2 Antenna Dimensions.....	22
Table 4.1.1 Results of the simulations.....	27
Table 4.1.2 Calculated effects using Designer and HFSS.....	28
Table 4.1.3 Validation of Resonant Frequency Models.....	47
Table 4.1.4 Validation of Resistance Models.....	47
Table 4.1.5 Validation of Bandwidth Models.....	47
Table 4.1.6 Validation of Gain Model.....	48
Table 4.1.7 Optimum Designs.....	48
Table 4.1.8 Result data from fabricated antennas.....	66
Table 4.1.9 Comparison between the fabricated antenna model and the simulated antenna models.....	67
Table 4.1.10 Validation of Fabricated Antenna Resonant Frequency Model.....	69
Table 4.1.11 Validation of Fabricated Antenna Resistance at Resonance Model.....	69
Table 4.1.12 Validation of Fabricated Antenna Bandwidth Model.....	69
Table 4.1.13 Validation of Fabricated Antenna Directivity Model.....	70
Table 5.2.1 Levels of the proposed DOE for the tunable antenna.....	84

List of Figures

Figures	Page
Figure 2.1.1. Electrical field distribution in a slotline.	5
Figure 2.2.1 Coplanar Waveguide Geometry	6
Figure 2.2.2. Excitation modes in a coplanar waveguide: (a) even or coplanar mode and (b) odd or slot-line mode	7
Figure 2.3.1 Electric Field of a CPW fed annular slot antenna taken from [7]	8
Figure 2.5.1. The ABO_3 perovskite structure.	12
Figure 3.2.1. Schematic of an Annular Slot Ring Antenna with its design parameters.....	18
Figure 3.2.2 Electric Field of the CPW fed annular slot antenna central design.....	20
Figure 3.2.3 Graphical representation of all 25 designs.	21
Figure 3.2.4. Typical response of an annular slot ring antenna: a) radiation pattern in the E-plane (-o-) and H-plane (-x-), and b) input impedance.....	23
Figure 3.2.5. Material characteristics of the CPW fed annular slot ring antenna with thin film ferroelectric material.....	24
Figure 4.1.1 Input impedance from 8 to 12 GHz for Central design using Designer (--) and HFSS (--).....	29
Figure 4.1.2 Input impedance from 8 to 12 GHz for abcd design using Designer (--) and HFSS (--).....	30
Figure 4.1.3 Input impedance from 8 to 12 GHz for Abcd design using Designer (--) and HFSS (--).....	30
Figure 4.1.4 Input impedance from 8 to 12 GHz for aBcd design using Designer (--) and HFSS (--).....	31
Figure 4.1.5 Input impedance from 8 to 12 GHz for ABcd design using Designer (--) and HFSS (--).....	31
Figure 4.1.6 Input impedance from 8 to 12 GHz for abCd design using Designer (--) and HFSS (--).....	32
Figure 4.1.7 Input impedance from 8 to 12 GHz for AbCd design using Designer (--) and HFSS (--).....	32
Figure 4.1.8 Input impedance from 8 to 12 GHz for aBCd design using Designer (--) and HFSS (--).....	33
Figure 4.1.9 Input impedance from 8 to 12 GHz for ABCd design using Designer (--) and HFSS (--).....	33
Figure 4.1.10 Input impedance from 8 to 12 GHz for abcD design using Designer (--) and HFSS (--).....	34

Figure 4.1.11 Input impedance from 8 to 12 GHz for AbcD design using Designer (--) and HFSS (--).....	34
Figure 4.1.12 Input impedance from 8 to 12 GHz for aBcD design using Designer (--) and HFSS (--).....	35
Figure 4.1.13 Input impedance from 8 to 12 GHz for ABcD design using Designer (--) and HFSS (--).....	35
Figure 4.1.14 Input impedance from 8 to 12 GHz for abCD design using Designer (--) and HFSS (--).....	36
Figure 4.1.15 Input impedance from 8 to 12 GHz for AbCD design using Designer (--) and HFSS (--).....	36
Figure 4.1.16 Input impedance from 8 to 12 GHz for aBCD design using Designer (--) and HFSS (--).....	37
Figure 4.1.17 Input impedance from 8 to 12 GHz for ABCD design using Designer (--) and HFSS (--).....	37
Figure 4.1.18 Input impedance from 8 to 12 GHz for a design using Designer (--) and HFSS (--).....	38
Figure 4.1.19 Input impedance from 8 to 12 GHz for A design using Designer (--) and HFSS (--).....	38
Figure 4.1.20 Input impedance from 8 to 12 GHz for b design using Designer (--) and HFSS (--).....	39
Figure 4.1.21 Input impedance from 8 to 12 GHz for B design using Designer (--) and HFSS (--).....	39
Figure 4.1.22 Input impedance from 8 to 12 GHz for c design using Designer (--) and HFSS (--).....	40
Figure 4.1.23 Input impedance from 8 to 12 GHz for C design using Designer (--) and HFSS (--).....	40
Figure 4.1.24 Input impedance from 8 to 12 GHz for d design using Designer (--) and HFSS (--).....	41
Figure 4.1.25 Input impedance from 8 to 12 GHz for D design using Designer (--) and HFSS (--).....	41
Figure 4.1.26 Effect of the outer radius in the resonant frequency and the resistance at resonance of the antenna.....	43
Figure 4.1.27 Effect of the inner radius in the resonant frequency and the resistance at resonance of the antenna.....	43
Figure 4.1.28 Effect of the offset between the centers of the circles in the resistance at resonance of the antenna.....	44
Figure 4.1.29 Effect of the inset in the resistance at resonance of the antenna.....	45
Figure 4.1.30 Closest Match in Designer.....	49
Figure 4.1.31 Closest Match in HFSS.....	49
Figure 4.1.32 Optimum Bandwidth in Designer.....	50
Figure 4.1.33 Optimum Bandwidth in HFSS.....	50
Figure 4.1.34 Fabricated Antennas.....	51

Figure 4.1.35 CPW fed asymmetric annular slot ring antenna.....	52
Figure 4.1.36 Log magnitude of the reflection coefficient of the fabricated central design antenna measured (--) and simulated in Designer (--) and HFSS (--).....	52
Figure 4.1.37 Log magnitude of the reflection coefficient of the fabricated abcd design antenna measured (--) and simulated in Designer (--) and HFSS (--).....	53
Figure 4.1.38 Log magnitude of the reflection coefficient of the fabricated Abcd design antenna measured (--) and simulated in Designer (--) and HFSS (--).....	53
Figure 4.1.39 Log magnitude of the reflection coefficient of the fabricated aBcd design antenna measured (--) and simulated in Designer (--) and HFSS (--).....	54
Figure 4.1.40 Log magnitude of the reflection coefficient of the fabricated ABcd design antenna measured (--) and simulated in Designer (--) and HFSS (--).....	54
Figure 4.1.41 Log magnitude of the reflection coefficient of the fabricated abCd design antenna measured (--) and simulated in Designer (--) and HFSS (--).....	55
Figure 4.1.42 Log magnitude of the reflection coefficient of the fabricated AbCd design antenna measured (--) and simulated in Designer (--) and HFSS (--).....	55
Figure 4.1.43 Log magnitude of the reflection coefficient of the fabricated aBCd design antenna measured (--) and simulated in Designer (--) and HFSS (--).....	56
Figure 4.1.44 Log magnitude of the reflection coefficient of the fabricated ABCd design antenna measured (--) and simulated in Designer (--) and HFSS (--).....	56
Figure 4.1.45 Log magnitude of the reflection coefficient of the fabricated abcD design antenna measured (--) and simulated in Designer (--) and HFSS (--).....	57
Figure 4.1.46 Log magnitude of the reflection coefficient of the fabricated AbcD design antenna measured (--) and simulated in Designer (--) and HFSS (--).....	57
Figure 4.1.47 Log magnitude of the reflection coefficient of the fabricated aBcD design antenna measured (--) and simulated in Designer (--) and HFSS (--).....	58
Figure 4.1.48 Log magnitude of the reflection coefficient of the fabricated ABcD design antenna measured (--) and simulated in Designer (--) and HFSS (--).....	58
Figure 4.1.49 Log magnitude of the reflection coefficient of the fabricated abCD design antenna measured (--) and simulated in Designer (--) and HFSS (--).....	59
Figure 4.1.50 Log magnitude of the reflection coefficient of the fabricated AbCD design antenna measured (--) and simulated in Designer (--) and HFSS (--).....	59
Figure 4.1.51 Log magnitude of the reflection coefficient of the fabricated aBCD design antenna measured (--) and simulated in Designer (--) and HFSS (--).....	60
Figure 4.1.52 Log magnitude of the reflection coefficient of the fabricated ABCD design antenna measured (--) and simulated in Designer (--) and HFSS (--).....	60
Figure 4.1.53 Log magnitude of the reflection coefficient of the fabricated a design antenna measured (--) and simulated in Designer (--) and HFSS (--).....	61
Figure 4.1.54 Log magnitude of the reflection coefficient of the fabricated A design antenna measured (--) and simulated in Designer (--) and HFSS (--).....	61
Figure 4.1.55 Log magnitude of the reflection coefficient of the fabricated b design antenna measured (--) and simulated in Designer (--) and HFSS (--).....	62

Figure 4.1.56 Log magnitude of the reflection coefficient of the fabricated B design antenna measured (--) and simulated in Designer (--) and HFSS (--).....	62
Figure 4.1.57 Log magnitude of the reflection coefficient of the fabricated c design antenna measured (--) and simulated in Designer (--) and HFSS (--).....	63
Figure 4.1.58 Log magnitude of the reflection coefficient of the fabricated C design antenna measured (--) and simulated in Designer (--) and HFSS (--).....	63
Figure 4.1.59 Log magnitude of the reflection coefficient of the fabricated d design antenna measured (--) and simulated in Designer (--) and HFSS (--).....	64
Figure 4.1.60 Log magnitude of the reflection coefficient of the fabricated D design antenna measured (--) and simulated in Designer (--) and HFSS (--).....	64
Figure 4.2.1 Tunable antenna with substrate thickness equal to 0.302 mm	71
Figure 4.2.2 Resonance frequency and resistance at frequency of the 0.305mm substrate antenna with a ferroelectric material with relative permittivity equal to 600.....	72
Figure 4.2.3 Resonance frequency and resistance at frequency of the 0.305mm substrate antenna with a ferroelectric material with relative permittivity equal to 1200.....	72
Figure 4.2.4 Log magnitude of the reflection coefficient of the 0.305mm substrate antenna with a ferroelectric material with relative permittivity equal to 600	73
Figure 4.2.5 Log magnitude of the reflection coefficient of the 0.305mm substrate antenna with a ferroelectric material with relative permittivity equal to 1200	73
Figure 4.2.6 VSWR of the 0.305mm substrate antenna with a ferroelectric material with relative permittivity equal to 600.....	74
Figure 4.2.7 VSWR of the 0.305mm substrate antenna with a ferroelectric material with relative permittivity equal to 1200.....	74
Figure 4.2.8 Directivity of the 0.305mm substrate antenna with a ferroelectric material with relative permittivity equal to 600.....	75
Figure 4.2.9 Directivity of the 0.305mm substrate antenna with a ferroelectric material with relative permittivity equal to 1200.....	75
Figure 4.2.10. Tunable antenna with substrate thickness equal to 0.800 mm	76
Figure 4.2.11 Resonance frequency and resistance at frequency of the 0.800mm substrate antenna with a ferroelectric material with relative permittivity equal to 600.....	77
Figure 4.2.12 Resonance frequency and resistance at frequency of the 0.800mm substrate antenna with a ferroelectric material with relative permittivity equal to 1200.....	77
Figure 4.2.13 Log magnitude of the reflection coefficient of the 0.800mm substrate antenna with a ferroelectric material with relative permittivity equal to 600	78
Figure 4.2.14 Log magnitude of the reflection coefficient of the 0.800mm substrate antenna with a ferroelectric material with relative permittivity equal to 1200	78
Figure 4.2.15 VSWR of the 0.800mm substrate antenna with a ferroelectric material with relative permittivity equal to 600.....	79
Figure 4.2.16 VSWR of the 0.800mm substrate antenna with a ferroelectric material with relative permittivity equal to 1200.....	79
Figure 4.2.17 Directivity of the 0.800mm substrate antenna with a ferroelectric material with relative permittivity equal to 600.....	80

Figure 4.2.18 Directivity of the 0.800mm substrate antenna with a ferroelectric material with relative permittivity equal to 1200..... 80

1 INTRODUCTION

1.1 Justification

Annular slot ring antennas are attractive for wireless applications because they are planar, compact in size, simple to fabricate, have low cost and light weight, and can be easily integrated to microwave circuits. Recently, there have been publications where the inner circular conductor of an coplanar waveguide fed annular slot ring antenna is moved making the slot wider in the side opposite to the feed of the antenna. Using this design the bandwidth of the antenna is increased considerable and also, there is no need to use any type of matching line between the transmission line and the antenna. Even though there has been some publications using this configuration, no formal characterization has been reported for this particular design.

Recent publications have used a technique called Design of Experiments to make statistical characterizations of antennas. Design of Experiments (DOE) is a statistical analysis that allows experiments that not only let us know which variables are having an effect in our responses but also which interactions of variables are affecting our response. This research uses DOE to characterize an annular slot ring antenna.

Once the antenna has been properly characterized the configuration will be used to design a tunable antenna. Tunable antennas are becoming increasingly popular due to the continuous developments in wireless communication technologies. Thin film ferroelectric materials such as Barium Strontium Titanate Oxide, $\text{Ba}_x\text{Sr}_{1-x}\text{TiO}_3$, (BSTO) have been used to produce tunable components. Application of a DC biasing voltage varies the thin film dielectric constant, causing a resonant frequency shift.

This research is important because it will provide a statistical characterization of annular slot ring antenna using DOE. This kind of characterization has not been done for this type of antenna. Also, this research will explore the effects of changing the permittivity of a ferroelectric material in the resonant frequency of the annular asymmetric slot ring antenna.

1.2 Objectives

The first objective of this research work is to characterize an asymmetric annular slot ring antenna. Design of experiments (DOE) will be used to analyze the effects of the antenna design parameters and their interactions on the resonant frequency, the input impedance, the bandwidth and the broadside gain.

Another objective is the use of a thin ferroelectric material to make an asymmetric annular slot ring antenna tunable. The antennas must satisfy the following characteristics:

1. A voltage standing wave ratio less than 2.
2. A directivity of at least 2 decibels.
3. An input impedance of 50 Ohms.

1.3 Project Description

The Asymmetric Annular Slot Ring Antenna (AASRA) is simple to fabricate, has low cost, light weight, is compact in size, can radiate at low elevation angles and can be easily integrated to microwave circuits. In this project, two types of AASRA were designed, one for the statistical characterization and the other for the tunable antenna design.

Design of Experiments (DOE) techniques were used to make the statistical characterization of the AASRA. For the DOE design, a substrate of relative permittivity (ϵ_r) equal to 6.15 and a thickness of 1.28 mm were chosen. A full 2^4 factorial design with one central point was used. Initially, an antenna was designed for a resonant frequency around 10 GHz. The antenna parameters were adjusted to achieve input impedance with a value close to 50 ohms. The input parameters of the antenna, which are dimensions of the antenna, are varied in order to find the effects of these parameters in the output characteristics of the AASRA. Also, the effects of the interactions of the input parameters are evaluated. The output characteristics of the AASRA are the resonance frequency, the resistance at resonance, the VSWR and peak gain. This analysis will present solutions to optimize the antenna performance.

For the second type of AASRA a substrate of Magnesium Oxide (MgO) was used with a $\epsilon_r = 9.8$. A layer of $\text{Ba}_x \text{Sr}_{1-x} \text{TiO}_3$ (BSTO) is deposited on top of the MgO crystal with a thickness of 400 nm. BSTO can have a ϵ_r between 400 and 1200 depending on the bias voltage that is applied to it. The resulting shift in resonant frequency which occurs when the BSTO changes its dielectric permittivity due to an applied bias voltage is studied.

1.4 Work Organization

Chapter 2 present the theory and background publications of annular slot antennas, coplanar waveguides, Design of Experiments and how it has been used to characterized antennas and finally, tunable components using BSTO including antennas. Chapter 3 presents the methodology used while characterized he Asymmetric Annular Slot Ring Antenna (AASRA) and the design of the tunable antenna. In Chapter 4 the results are presented and explained. Finally, Chapter 5 presents the conclusion, as well as the recommendations for future work.

2 Literature Review

2.1 Slotlines

The planar transmission structure known as a slotline consists of a narrow slot etched in the metallization on one side of a dielectric substrate. They are suitable for microwave integrated circuits because they have a planar geometry. They can be used as high impedance lines, series stubs, short circuits and baluns. Slotlines can also be used as resonant or nonresonant antennas [1].

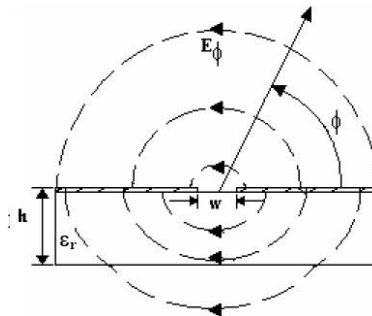


Figure 2.1.1. Electrical field distribution in a slotline.

The electric field of a slotline is oriented across the slot in the metallized side of the substrate. In far field, the slotline electric field has only one component in the phi (Φ) direction. The field distributes the energy between the substrate and air region as seen in Figure 2.1.1. That is the reason why the effective dielectric constant of the slotline (ϵ_{re}) is

smaller than the substrate permittivity (ϵ_r). In an infinitely thick substrate, the effective substrate permittivity ϵ_{re} is given by equation 2.1.1

$$\epsilon_{re} = \frac{\epsilon_r + 1}{2} \quad 2.1.1$$

2.2 Coplanar Waveguide Transmission Lines

Coplanar waveguides consist of two slot lines of width w and a central conductor of width s on top of a substrate of thickness h as shown in Figure 2.1.1. It is possible to connect circuit components in shunt easily because all conductors are on the same plane so there is no need for via holes. They have less radiation at discontinuities than microstrip patches, low conductor losses and good grounding. They are light in weight, conformal and can be easily integrated to microwave active devices as seen in [2] and [3].

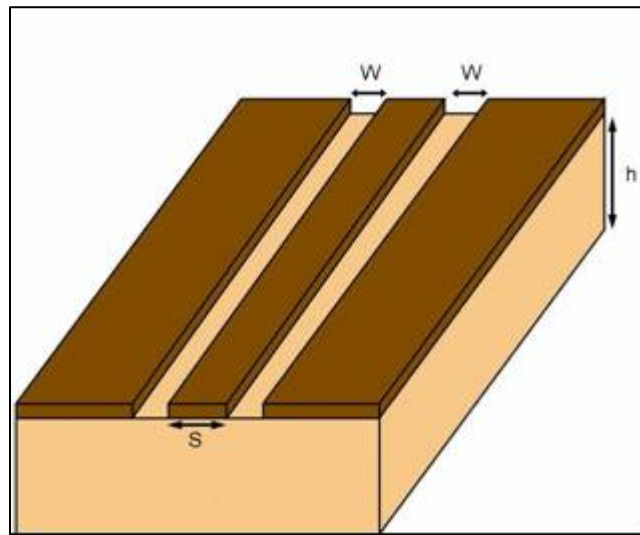


Figure 2.2.1 Coplanar Waveguide Geometry

A disadvantage of CPW is that in addition to the coplanar waveguide mode (also called even mode) of excitation, there can be the unintentional excitation of the parasitic slot-line mode (also called odd mode) [4], both are shown on Figure 2.1.2. To suppress excitation of the slot-line mode, airbridges are used to equalize the ground planes along the feedline.

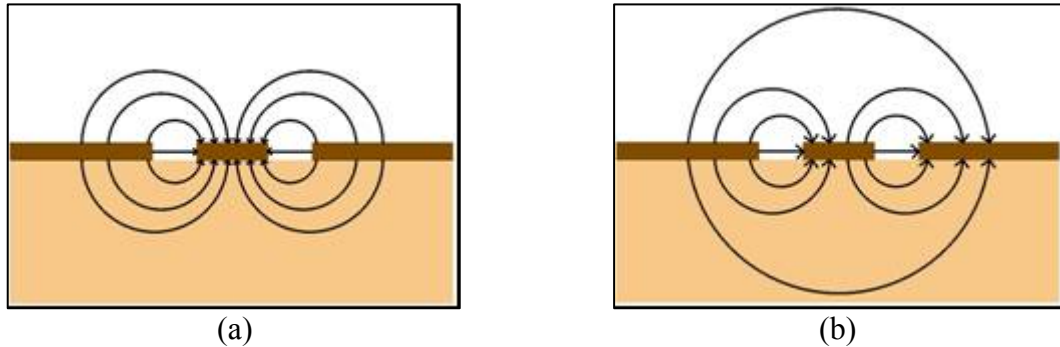


Figure 2.2.2. Excitation modes in a coplanar waveguide: (a) even or coplanar mode and (b) odd or slot-line mode

2.3 Annular Slot Antennas

Slot antennas are attractive because they are easy to analyze, design and fabricate. Their radiation pattern can be bidirectional or unidirectional and is possible to have radiation at low elevation angles. They can have linear or circular polarization and their cross-polarization level is very low, they have wider bandwidth than patch antennas, low spurious radiation and good isolation between radiating elements [5].

Due to the annular geometry of this antenna, the circumference length necessary for the phase of the currents to be of equal is determined by Bessel functions [6]. Figure 2.3.1,

taken from [7], shows the electrical field distribution of an annular slot ring antenna.. It can be seen from this figure that the horizontal components of the electric field is cancelled while the vertical components are aligned, consequently this antenna exhibits vertical polarization.

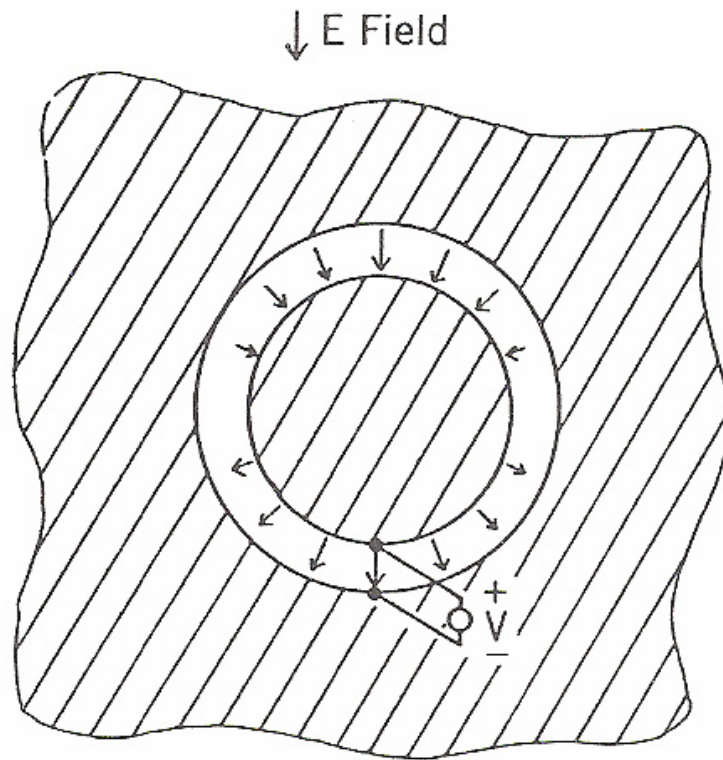


Figure 2.3.1 Electric Field of a CPW fed annular slot antenna taken from [7]

2.3.1 CPW fed Slot Ring Antenna

CPW fed slot ring antennas (SRA) have been studied recently because they are simple to fabricate, have low cost, light weight, are compact in size, can radiate at low elevation angles and can be easily integrated to microwave circuits. These characteristics make them attractive for mobile communications.

In [8], a SRA was analyzed using a spectral domain moment method to examine different feeding methods. It was concluded that CPW fed slot ring antennas performed better because they have a wider bandwidth than stripline fed slot ring antennas and a more symmetric radiation pattern than microstrip fed slot ring antennas because of the strong field exited near the microstrip.

An eccentric microstrip fed annular SRA was presented in [8]. It was shown that moving the inner circular conductor improved the bandwidth of the antenna. Using this technique it is possible to design a wide-band CPW fed circular antenna as shown in [9], where a bandwidth of 143.2% was achieved.

2.4 Design of Experiments

Design of Experiments (DOE) is a statistical analysis that allows determining the variables and interactions of variables that have an effect in the responses. In a 2^k factorial design the variables in an experiment are set with two levels: low or high. An experiment for every possible combination of variable levels is performed for a total of 2^k experiments where k is the number of variables. Using a DOE model with center points determine the linearity of the model. If the model is not linear, axial points are added in order to construct a second order model [10].

2.4.1 Characterization of Antennas Using DOE

DOE has been used in the analysis and characterization of folded slot antennas in [11]. It was shown that the input impedance of the resonance frequency at λ_g can be decreased by increasing the width of the slot opposite to the feedline. Also, when the width of the slot at the side of the feedline is increased, the usually low input impedance of the resonance frequency at $3\lambda_g/2$ is increased making it a useful parameter

A concentric Rectangular Slot Ring Antenna (RSRA) was analyzed in [12]. The author used Functional Data Analysis (FDA) in combination with DOE. This technique showed that the model presented in the publication was valid only at certain frequency intervals. The factors which had a bigger effect on the responses were identified and whether the factors should be increased or decreased in order to optimized the desired responses.

In [13] DOE was used to improve the radiation pattern of a Log Periodic Folded Slot Antenna (LPFSA). The width of the phasing slot inside each folded slot was determined to be between 20% and 33% of the space inside the folded slot to improve the far field performance of the antenna.

2.5 Ferroelectric Materials

Ferroelectric materials have usually high dielectric constants that can be varied when an electric field is applied to them. Ferroelectric materials are a subclassification of pyroelectric materials that show a spontaneous polarization that is temperature-dependant. The orientation of said polarization can be changed by applying an external dc electric field. Therefore, the dielectric constant of ferroelectric materials also presents a dependency on temperature [14].

Most ferroelectric materials present a Perovskite structure, a cube containing three ions, which is shown in Figure 2.4.1. It is a face-centered cubic (FCC) ABO_3 structure with A atoms in the corner, O atoms on the faces and a B center atom. There are minimum-energy off-centered positions that can be occupied by the B atom. Dipoles are created when the B atom is shifted by an applied electric field [14].

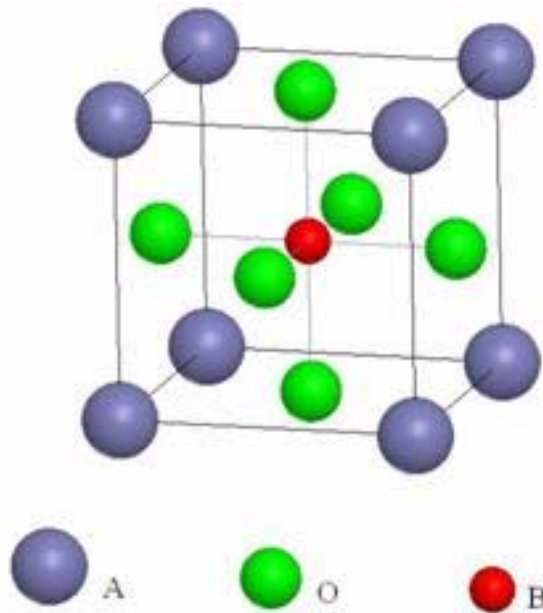


Figure 2.5.1. The ABO_3 perovskite structure.

As said before, the dielectric constant of ferroelectric materials is also dependent on temperature. They possess a Curie temperature (T_c), above which ferroelectric materials become paraelectric. As temperature increases, the thermal motion energy also increases and the electric field necessary to orientate the domains for zero polarization decreases. As temperature decreases, the material undergoes a phase transformation which alters the crystal structure from tetragonal to rhombohedral [14].

$BaTiO_3$ (BTO) and $SrTiO_3$ (STO) are types of materials with an ABO_3 structure. STO does not have a Curie temperature (T_c) above 0 K and BTO has a T_c temperature of about 400K. The most studied material for microwave applications is $Ba_xSr_{1-x}TiO_3$, (BSTO), where x goes from 0 to 1. Varying the value of x changes the value of T_c , the higher the value of x

the lower the Curie temperature. For applications at room temperature a value of $x=0.5$ is usually selected [15].

The change in dielectric constant ϵ_r caused by an external electric field is described by tunability and is defined as:

$$\xi = \frac{\epsilon_{r0} - \epsilon_{re}}{\epsilon_{r0}} \times 100\% \quad \mathbf{2.5.1}$$

In equation 2.1, ϵ_{r0} is the dielectric constant of the ferroelectric material without external dc electric field and ϵ_{re} is the dielectric constant when the material is biased by an external dc electric field [14].

Usually, materials with large tunability have higher loss tangent [14]. A figure of merit K defined in Equation 2.5.2.

$$K = \frac{\xi}{\tan \delta} \quad \mathbf{2.5.2}$$

In equation 2.2, ξ and $\tan \delta$ are the tunability and the loss tangent of the material respectively.

2.5.1 Tunable Components Using Ferroelectric Material

Ferroelectric materials have been used in the development of tunable components. This, in spite the difficulties presented in this technology [16]. The difficulties are:

- (a) Large loss tangent: This result in low Q resonators and lossy delay lines.
- (b) Large dielectric constant: This result in low-impedance transmission lines and problems with surface wave modes.
- (c) Requires large bias voltages and the design of complex bias networks.

Phase shifters for three different frequencies are presented in [17]. They provided 460 degrees of phase shift with an insertion loss of 8.8dB at 8GHz, 265 degrees of phase shift with an insertion loss of 5.8dB at 20GHz and 180 degrees of face shift with an insertion loss 4dB at 30GHz. In [16] a tunable ring resonator with a frequency tunability factor of over 12%, a bandpass filter with tunability factor greater than 9% and a tunable local oscillator are also presented.

2.5.1.1 Tunable antennas using ferroelectric material

Ferroelectric materials exhibit high dielectric permittivity. Microstrip antennas in substrates with high permittivity exhibit poor efficiency and narrow bandwidth. These are consequences of the energy loss caused by the excitation of surface modes. A microstrip patch printed on a BSTO substrate was shown in [18]. This antenna showed a negative gain when measured with respect to a standard gain log periodic dipole.

A way to solve this problem is with the use of a multi-layer patch antenna. Multi-layer patch antennas have better bandwidth and can have dual band performance. In [18], a

superstrate layer was added over the previous structure separated by an air gap. The air gap spacing was varied to optimize the structure and an improvement of 5dBi over the single layer structure was achieved. Also, [19] presents a second structure where a conductive layer with a parasitic patch is added on top of the superstrate. An improvement of 6dBi over the single layer structure was shown.

In order to reduce the height of the structure, [20] propose the elimination of the air gap from the previous structures. The feeder patch on the bottom also serves as a ground plane on top of which is the substrate, then the BSTO and finally the parasitic patch on the top. A gain improvement of at least 7dBi compared to the single layered structure is achieved.

A tunable folded-slot antenna with thin film ferroelectric material was presented in [21]. The antenna was modeled using the finite difference time domain (FDTD) technique. The antenna had a bandwidth of 10.73% and a resonant tunable frequency of 6.29% was obtained. The resonant frequency decreased as the dielectric constant of the ferroelectric thin film was increased.

2.6 Chapter Conclusions

In this chapter, a literature review of slotlines, coplanar waveguides, annular slot antennas and tunable antennas using ferroelectric material were presented. Also, the results of publications involving the use of design of experiments for antenna characterization were

introduced. In the next chapter, the methodology used to accomplish this thesis research will be described.

3 METHODOLOGY

3.1 Purpose

This research is focused on the design and characterization of an asymmetric annular slot ring antenna using Design of Experiments. The effects of the dimensions of the antenna on the response of the antenna will be determined. The desired responses are the frequency of operation, the input impedance at resonance, the voltage standing wave ratio (VSWR) bandwidth, and the gain of the antenna.

3.2 Procedure

The annular slot ring antenna that will be used for this research has six design parameters, as shown in Figure 1. The outer radius of the slot (R_o), the inner radius (R_i), the offset distance between the inner and outer circles (d), the length of the CPW insert (s), the CPW slots width (s) and the width of the CPW central conductor (g). Also, the height of the substrate (h) and the relative permittivity (ϵ_r) are needed for the proper characterization of the antenna.

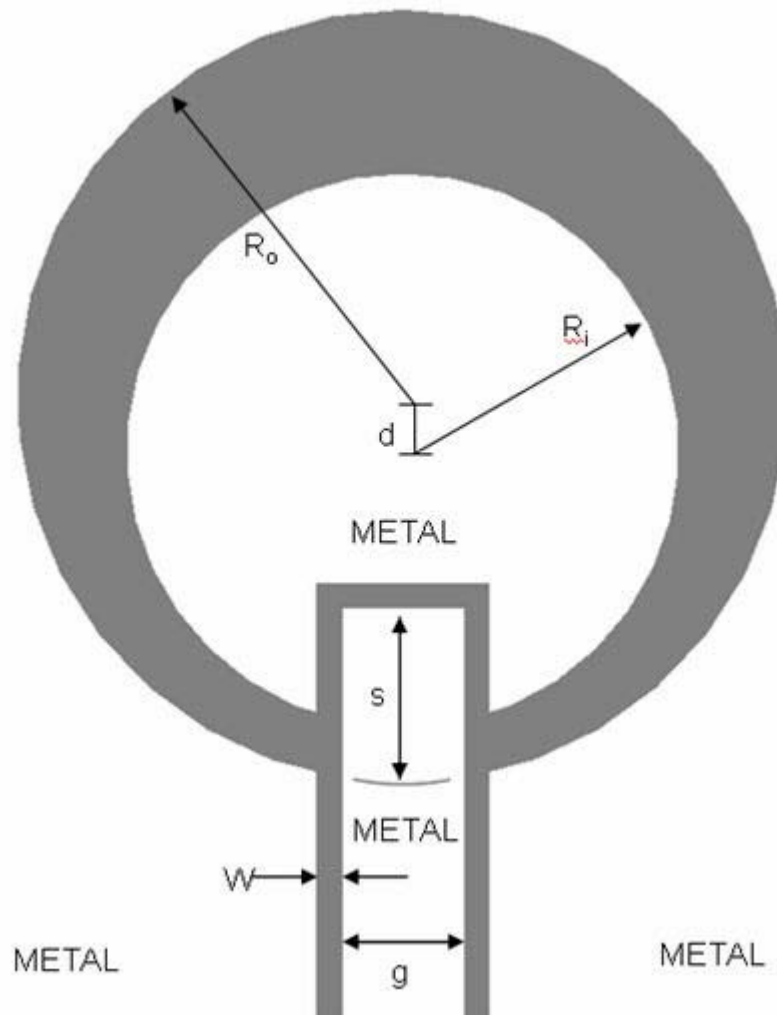


Figure 3.2.1. Schematic of an Annular Slot Ring Antenna with its design parameters

To make the statistical characterization simpler, some parameters were maintained constant. The relative permittivity of the substrate was 6.15 and its width was 1.28 mm. The CPW fed line had a center conductor of 1.02 mm and a slot width of 0.2 mm. A full 24 factorial design with one central point and 8 axial points was used for the DOE design. The axial points in these experiments have one factor in either low or high value while all the

other factors are set to its central value. It would be preferable to have the axial points at values higher and lower than the rest of the factorial design but it was not possible due to the physical dimensions of the antenna. Initially, an antenna was designed for a resonance frequency around 10 GHz. The antennas for the characterization will be in the X band in order to be able to fabricate and measure them with the equipment available in the Radiation Laboratory of the University of Puerto Rico at Mayagüez (UPRM).

The antenna parameters were adjusted to achieve input impedance with a value close to 50 ohms. The parameter values of this initial design are used as the central point values. Central points and axial points are used to determine the linearity of the statistical model. The factors in the design were R_o , R_i , d and s and their values can be seen in table 3.2.1. Figure 3.2.2 shows the electric field of the central design.

Table 3.2.1 Levels of the 2^4 factorial design.

	Low level	High level
Factor	In millimeters	In millimeters
R_o	3.05mm	3.35mm
R_i	2.15mm	2.45mm
d	0.35mm	0.55mm
s	0.95mm	1.05mm

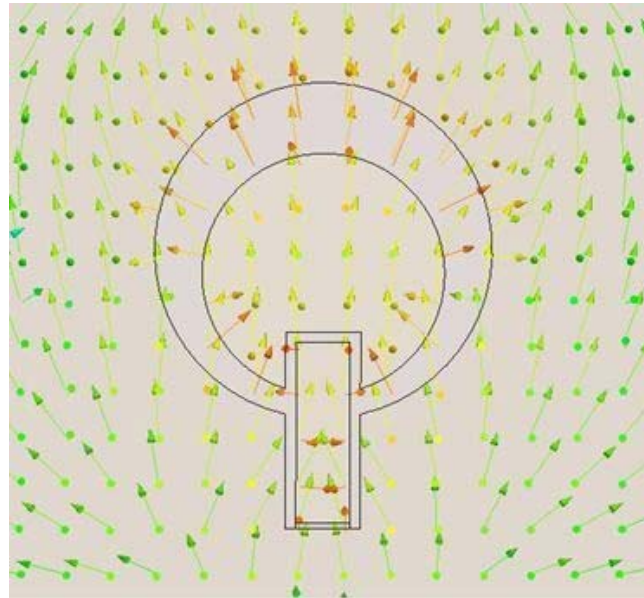


Figure 3.2.2 Electric Field of the CPW fed annular slot antenna central design

Figure 3.2.3 shows a diagram of all 25 designs for the DOE analysis represented by points. The outer axis represents factors A and B and inner axis represents factors C and D. The point in the middle of the diagram corresponds to the center value. The outer horizontal axial points represent the A factor axial values and the inner horizontal axial points represent the C factor axial values. Finally, the outer vertical axial points represent the B factor axial values and the inner vertical axial points represent the D factor axial values.

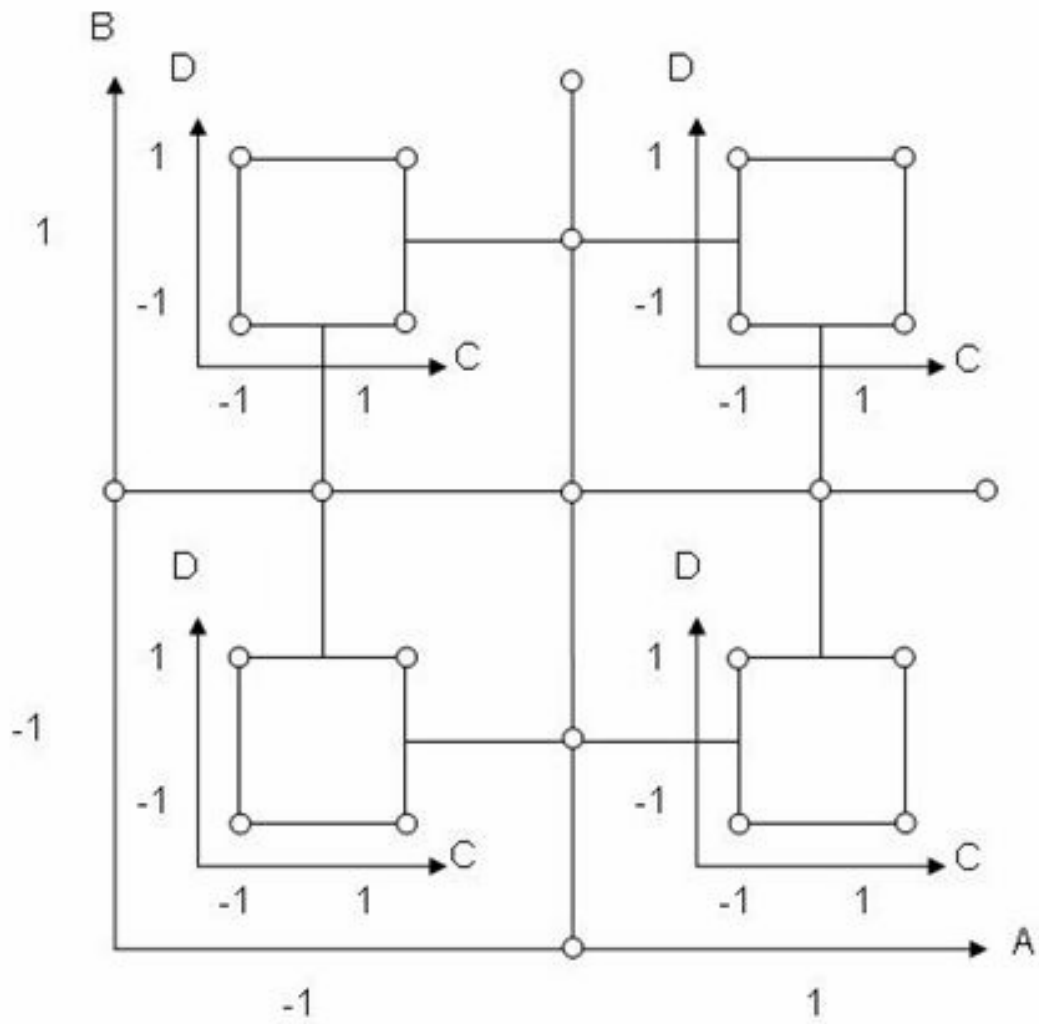


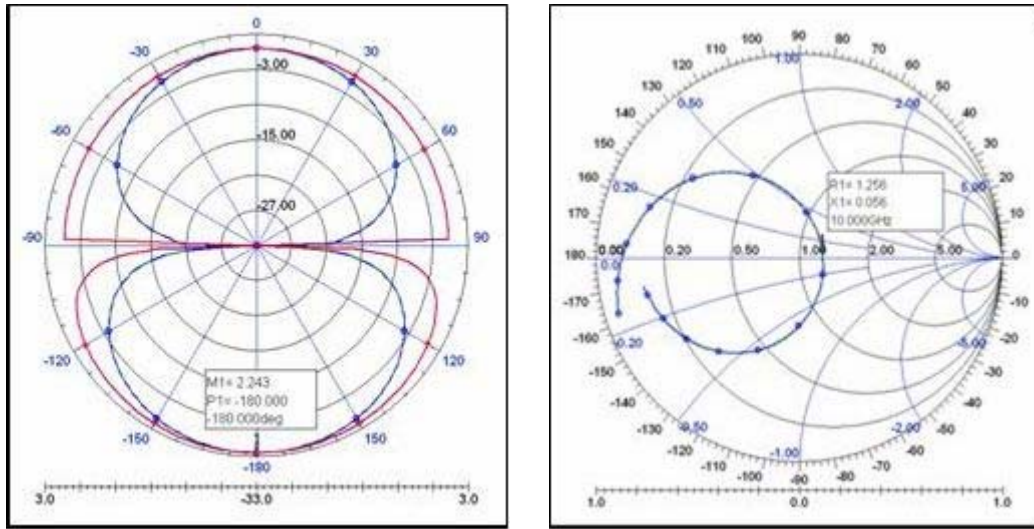
Figure 3.2.3 Graphical representation of all 25 designs.

Table 3.2.2 shows the dimensions in millimeters of the four factors in each of the 25 designs.

Table 3.2.2 Antenna Dimensions

	R _o (mm)	R _i (mm)	d (mm)	s (mm)
central	3.20	2.30	0.45	1.00
abcd	3.05	2.15	0.35	0.95
Abcd	3.35	2.15	0.35	0.95
aBcd	3.05	2.45	0.35	0.95
ABcd	3.35	2.45	0.35	0.95
abCd	3.05	2.15	0.55	0.95
AbCd	3.35	2.15	0.55	0.95
aBCd	3.05	2.45	0.55	0.95
ABCd	3.35	2.45	0.55	0.95
abcD	3.05	2.15	0.35	1.05
AbcD	3.35	2.15	0.35	1.05
aBcD	3.05	2.45	0.35	1.05
ABcD	3.35	2.45	0.35	1.05
abCD	3.05	2.15	0.55	1.05
AbCD	3.35	2.15	0.55	1.05
aBCD	3.05	2.45	0.55	1.05
ABCD	3.35	2.45	0.55	1.05
a	3.05	2.30	0.45	1.00
A	3.35	2.30	0.45	1.00
b	3.20	2.15	0.45	1.00
B	3.20	2.45	0.45	1.00
c	3.20	2.30	0.35	1.00
C	3.20	2.30	0.55	1.00
d	3.20	2.30	0.45	0.95
D	3.20	2.30	0.45	1.05

The experiment was performed twice, each time using a different electromagnetic simulator: Designer, which uses the method of moments and HFSS (High Frequency Structure Simulator) which uses the finite element method. The factorial design was analyzed for the effects in each response: resonant frequency, input impedance at frequency, bandwidth and gain.



a)

b)

Figure 3.2.4. Typical response of an annular slot ring antenna: a) radiation pattern in the E-plane (-o-) and H-plane (-x-), and b) input impedance.

In the second part of this research work the Finite Element Method (FEM) is used to analyze an annular slot antenna with a thin film ferroelectric operating in the Ka Band. The resonant frequency, input impedance, bandwidth (VSWR<2), radiation pattern and gain of the antenna will be presented.

Figure 3.2.3 shows the layers and material characteristics of the proposed tunable annular slot ring antenna. A thin film ferroelectric material, BSTO, with relative permittivity of 400 and a thickness of 0.4 μm is deposited on a Magnesium Oxide (MgO) crystal with relative permittivity of 9.8 and a thickness of 0.305 mm. The metallization layer is a 2 μm layer of gold.

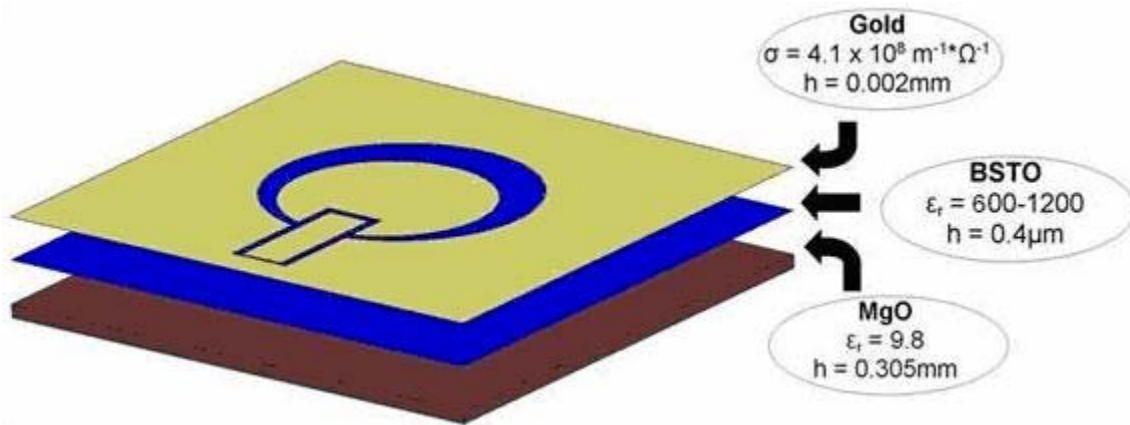


Figure 3.2.5. Material characteristics of the CPW fed annular slot ring antenna with thin film ferroelectric material.

HFSS will be used to simulate the antenna structure. A relative permittivity (ϵ_r) of 600 for BSTO will be used in the design of the antenna because it is the center value that the material can achieved not clear. The input impedance will be adjusted to 50 Ohms by using the stub and widening the slot opposite to the CPW line. When this design is optimized ϵ_r will be changed to the maximum value of 1200.

Equation 3.2.1 will be used as a starting point to calculate the slot length corresponding to one guided wavelength. This equation is valid for $0.0015 \leq w/\lambda_0 \leq 0.075$ and $3.8 \leq \epsilon_r \leq 9.8$. However, it is only valid for a slotline of constant width. The antenna design under study does not have a constant width because the center of the inner conductor has an offset in relation to the center of the circle that forms the outer edge of the slot. For this reason a value of w equal to the width of the slots in the coplanar waveguide that provide 50 Ohms for a selected inner conductor width in our particular substrate will be used to

calculate our approximate wavelength. Using Bessel equations and the wavelength of the slot it is possible to calculate the circumference necessary for the antenna to resonate.

$$\frac{\lambda_g}{\lambda_0} = 0.9217 - 0.277 \ln(\epsilon_r) + 0.0322 \left(\frac{W}{h} \right) \left[\frac{\epsilon_r}{\frac{W}{h} + 0.453} \right]^{\frac{1}{2}} - 0.01 \ln \left(\frac{h}{\lambda_0} \right) \left[4.6 - \frac{3.65}{\epsilon_r^2 \sqrt{\frac{W}{\lambda_0} \left(9.06 - 100 \frac{W}{\lambda_0} \right)}} \right]$$

Equation 3.2.1

3.3 Chapter Conclusions

In this chapter the methodology used to complete this research was described. The antenna structures, design process, simulation software and characterization method were presented. In the next chapter we will present the results, analyze and explain them.

4 RESULTS AND DISCUSSION

This chapter discusses the results from the simulations for the DOE and the antennas fabricated to validate the results. Result for the simulations of the tunable antenna using thin film ferroelectric materials are also shown.

4.1 Statistical Characterization Results

Table 4.1.1 shows the results of the simulations using Designer and HFSS. A capital letter means that the factor is at the high level, and a, b, c and d correspond to R_o , R_i , d and s respectively. These results are analyzed using Design-Expert to find the effects of the variables in each response. Table 4.1.2 shows the calculated effects for the simulations using Designer and HFSS; only the significant effects are shown in the table.

Table 4.1.1 Results of the simulations.

	f_0 (GHz)		R at f_0 (Ohm)		Max. gain at f_0 (dB)		Bandwidth (MHz)	
	Designer	HFSS	Designer	HFSS	Designer	HFSS	Designer	HFSS
central	10.02	10.02	68.34	63.14	2.24	3.72	740	730
abcd	10.48	10.49	75.34	69.50	2.24	3.89	760	790
Abcd	9.89	9.90	82.67	75.49	2.21	3.63	700	770
aBcd	10.00	9.94	61.38	57.05	2.24	3.70	620	580
ABcd	9.52	9.64	72.77	64.01	2.24	3.55	650	700
abCd	10.57	10.64	57.18	56.59	2.24	3.94	850	810
AbCd	10.00	10.11	65.66	60.52	2.24	3.78	870	870
aBCd	9.89	9.95	37.55	37.77	2.16	3.56	490	450
ABCd	9.57	9.65	54.77	48.85	2.21	3.54	670	640
abcD	10.44	10.47	82.93	78.90	2.24	3.84	660	720
AbcD	9.85	9.82	90.78	85.04	2.21	3.70	540	620
aBcD	10.00	10.01	68.87	62.64	2.21	3.68	610	620
ABcD	9.50	9.58	80.08	69.46	2.21	3.46	600	680
abCD	10.56	10.62	63.58	61.89	2.24	3.91	840	840
AbCD	9.98	10.07	72.59	67.92	2.24	3.74	830	860
aBCD	9.92	9.97	44.71	41.89	2.16	3.56	520	490
ABCD	9.57	9.67	61.36	53.44	2.21	3.57	680	690
a	10.29	10.40	62.82	58.99	2.22	3.79	720	730
A	9.76	9.82	73.38	65.40	2.22	3.57	740	760
b	10.23	10.26	74.15	69.65	2.25	3.79	800	810
B	9.78	9.86	61.33	56.85	2.22	3.56	650	650
c	9.96	9.92	77.46	70.63	2.22	3.65	670	690
C	10.05	10.13	59.32	55.42	2.22	3.76	750	750
d	10.02	10.07	64.66	61.09	2.25	3.74	740	720
D	10.00	10.07	71.41	66.61	2.22	3.71	720	750

Table 4.1.2 Calculated effects using Designer and HFSS

	f_{res}		R at f_{res}		Bandwidth		Gain	
	D	H	D	H	D	H	D	H
constant	10.00	10.04	67.56	62.48	734.17	733.33	2.19	3.70
A(R_o)	-0.25	-0.24	5.54	3.61		31.11	0.003	-0.072
B(R_i)	-0.24	-0.23	-6.78	-7.42	-75.56	-88.33		-0.110
C(d)			-9.75	-8.25	38.33	12.78		
D(s)			3.57	3.16				
A ² (R_o^2)							0.044	
C ² (d^2)					50.28	-35.00		
AB(R_oR_i)			1.49	0.90		38.12		0.021
AC($R_o d$)						25.62		
BC($R_i d$)					-53.12	-49.38		

The first two columns of Table 4.1.2 show that both Designer and HFSS agree that decreasing the R_o or R_i will increase the f_{res} as expected. Also the interactions R_oR_i , and R_iD have a smaller effect of increasing the f_{res} as they are increase. HFSS shows that d has a small positive effect (increases the response as it increases) in f_{res} but Designer does not show that effect. The next two columns show that both simulators agree that as R_o and s increase, the resistance at f_{res} increases, and as R_i and d increase the resistance at f_{res} decreases. Both simulators agree that the interaction R_oR_i has a smaller effect of increasing the impedance as they are increased.

Table 3 also shows that Designer and HFSS agree that decreasing R_i or increasing d will increase the bandwidth of the antenna. Also, both agree that as the interaction $R_i d$ decreases the bandwidth increases. Only HFSS shows that the bandwidth of the antenna increases as R_o and the interactions R_oR_i and $R_o d$ are increased.

Finally, both simulators agree that R_i has a negative effect in the antenna gain. Only Designer shows that the interaction $R_i d$ has a negative effect and only HFSS show that R_o also has a negative effect on the gain. The difference in the gain responses is mainly due to the difference in ground size in HFSS and Designer. Designer assumes an infinite ground plane while HFSS uses the actual size of the ground

Figures 4.1.2 to 4.1.27 show the smith charts of all 25 designs. The figures include both Designer and HFSS data. The resonant frequency is indicated

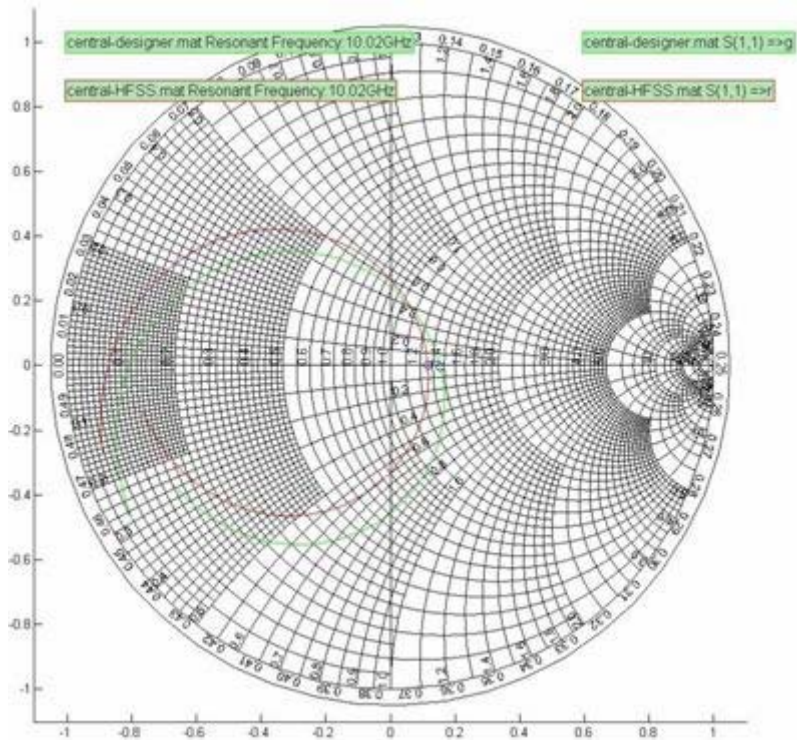


Figure 4.1.1 Input impedance from 8 to 12 GHz for Central design using Designer (--) and HFSS (--)

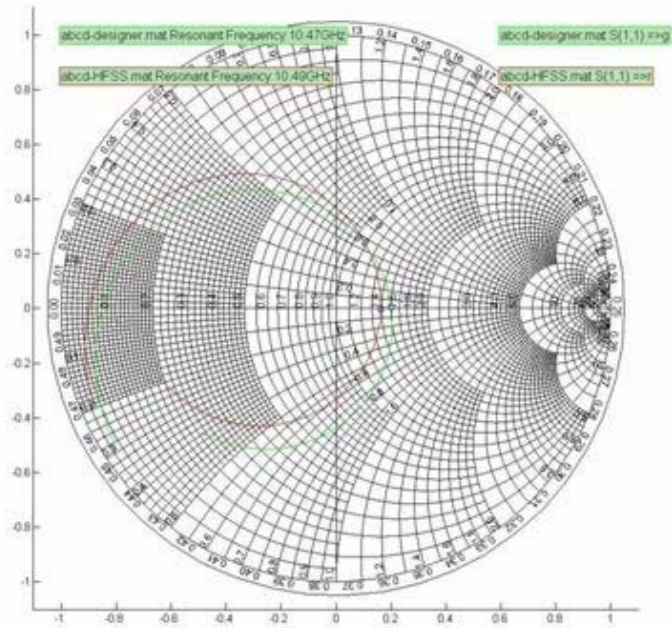


Figure 4.1.2 Input impedance from 8 to 12 GHz for abcd design using Designer (--) and HFSS (--)

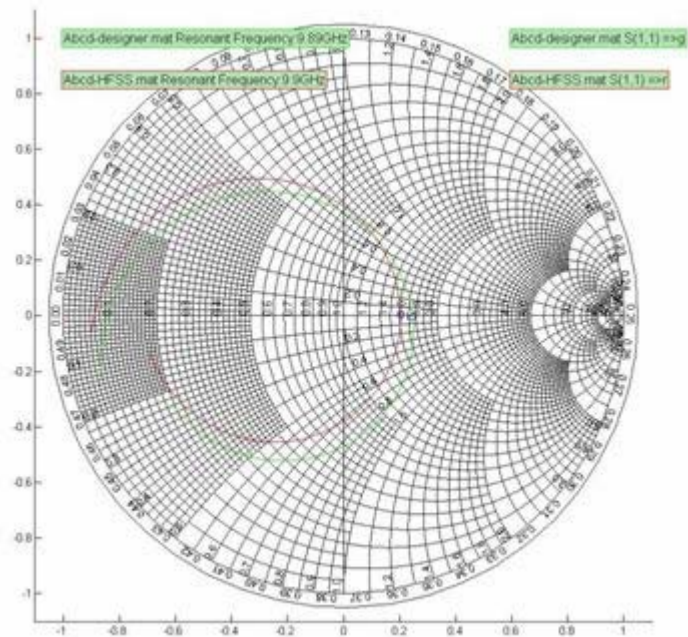


Figure 4.1.3 Input impedance from 8 to 12 GHz for Abcd design using Designer (--) and HFSS (--)

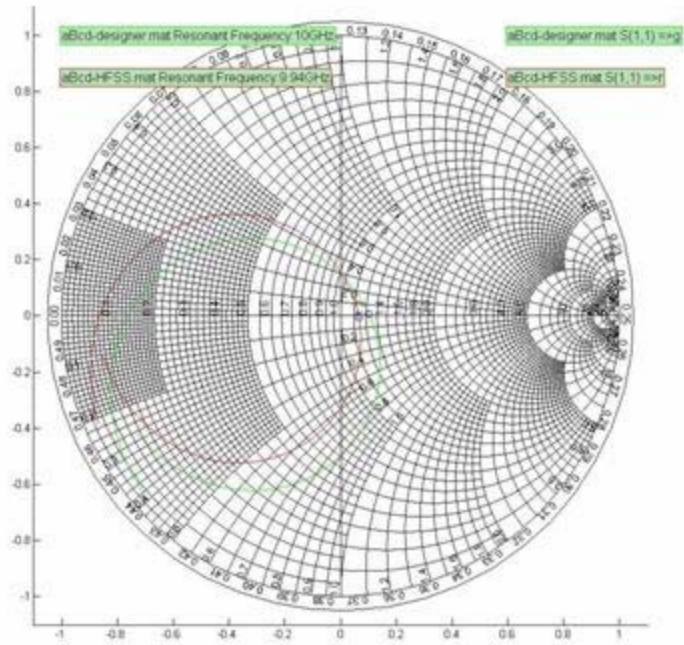


Figure 4.1.4 Input impedance from 8 to 12 GHz for aBcd design using Designer (--) and HFSS (--)

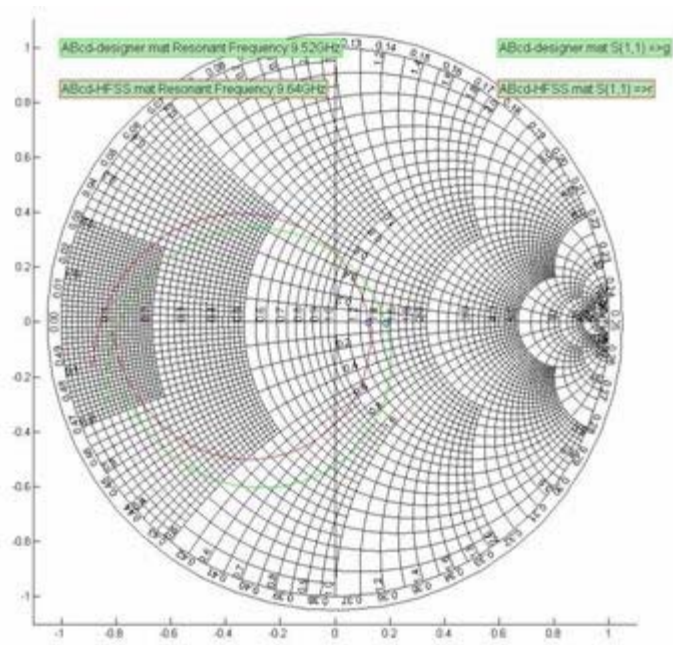


Figure 4.1.5 Input impedance from 8 to 12 GHz for ABcd design using Designer (--) and HFSS (--)

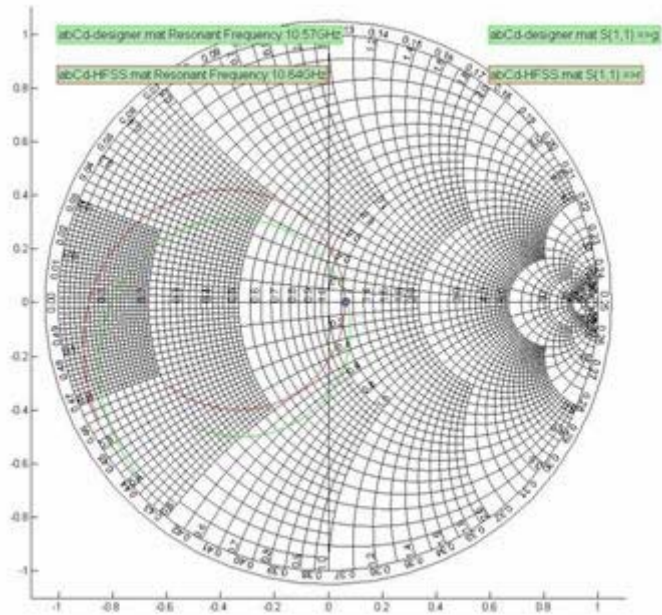


Figure 4.1.6 Input impedance from 8 to 12 GHz for abCd design using Designer (--) and HFSS (--)

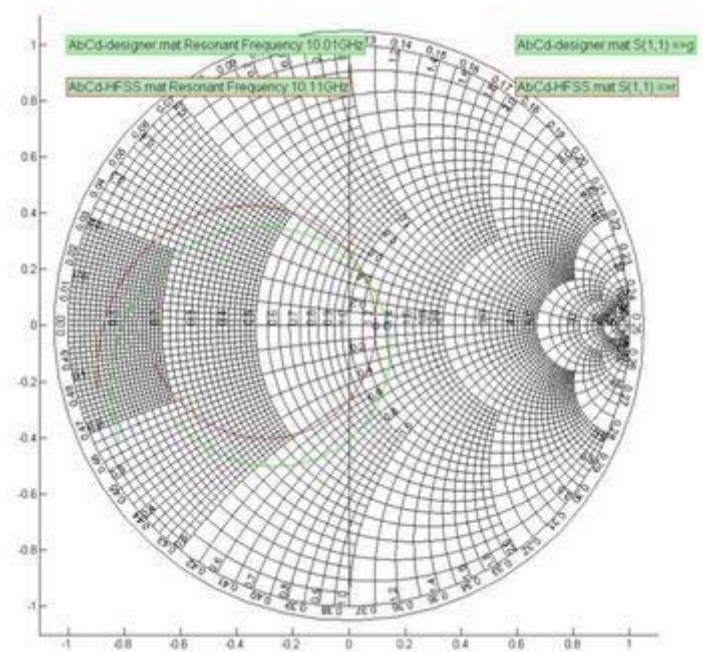


Figure 4.1.7 Input impedance from 8 to 12 GHz for AbCd design using Designer (--) and HFSS (--)

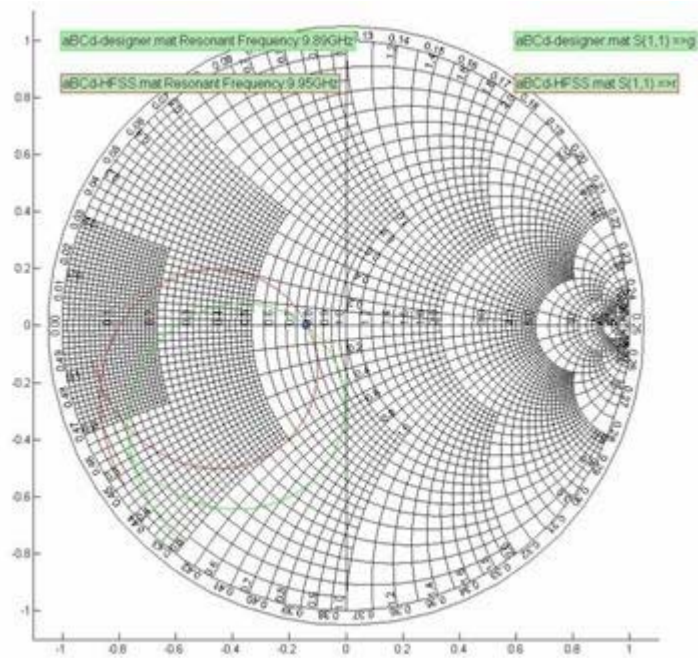


Figure 4.1.8 Input impedance from 8 to 12 GHz for aBCd design using Designer (--) and HFSS (--)

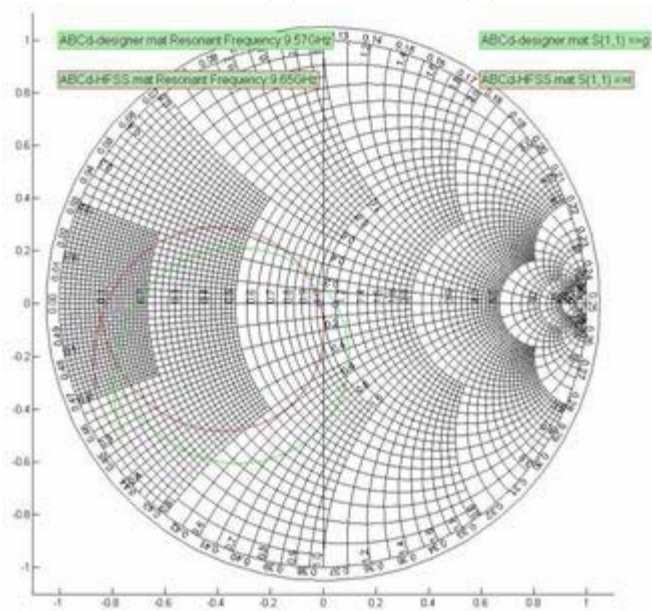


Figure 4.1.9 Input impedance from 8 to 12 GHz for ABCd design using Designer (--) and HFSS (--)

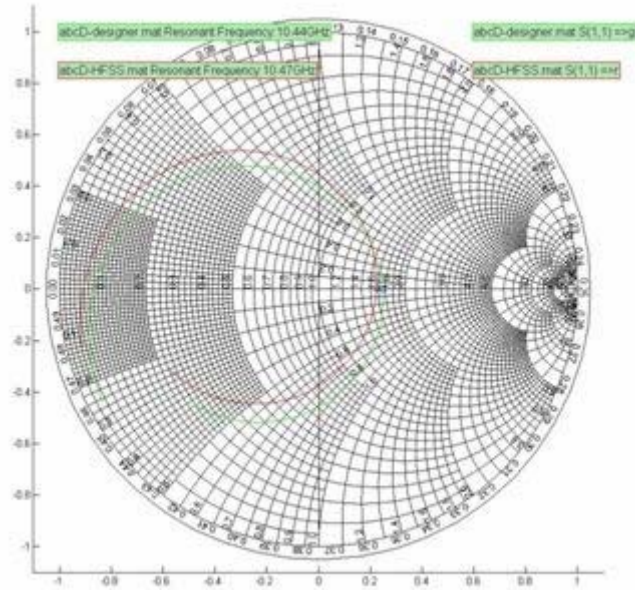


Figure 4.1.10 Input impedance from 8 to 12 GHz for abcD design using Designer (--) and HFSS (--)

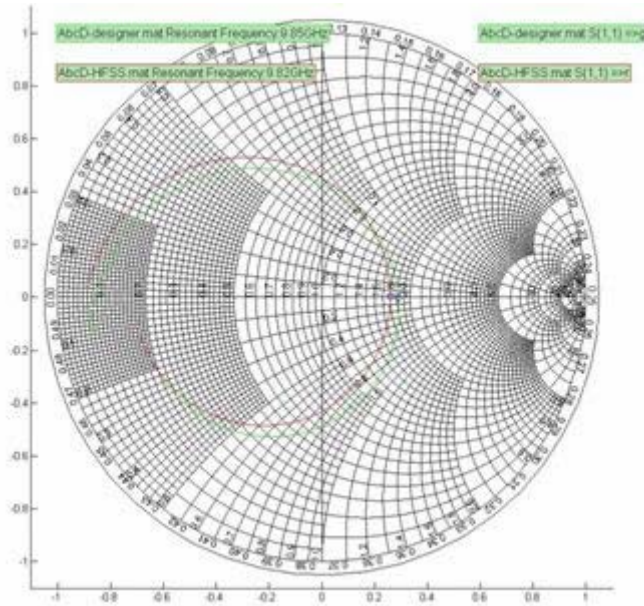


Figure 4.1.11 Input impedance from 8 to 12 GHz for AbcD design using Designer (--) and HFSS (--)

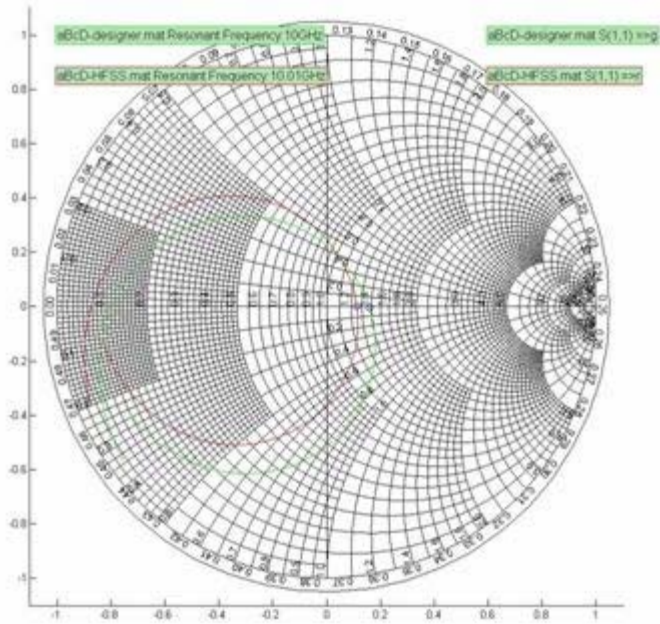


Figure 4.1.12 Input impedance from 8 to 12 GHz for aBcD design using Designer (--) and HFSS (—)

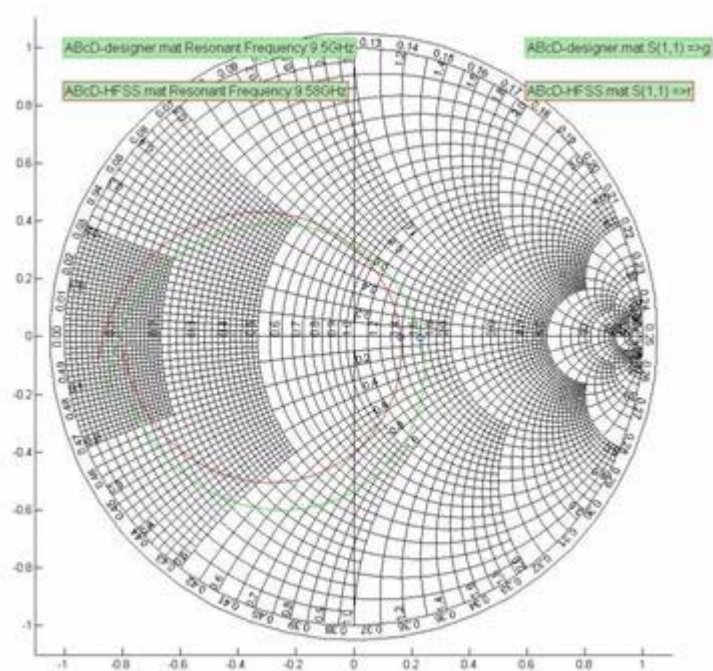


Figure 4.1.13 Input impedance from 8 to 12 GHz for ABcD design using Designer (--) and HFSS (—)

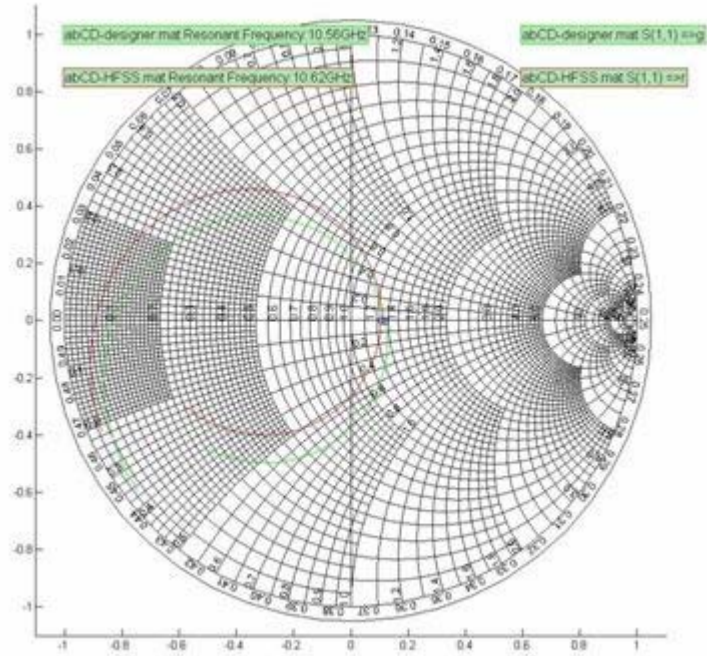


Figure 4.1.14 Input impedance from 8 to 12 GHz for abCD design using Designer (--) and HFSS (--)

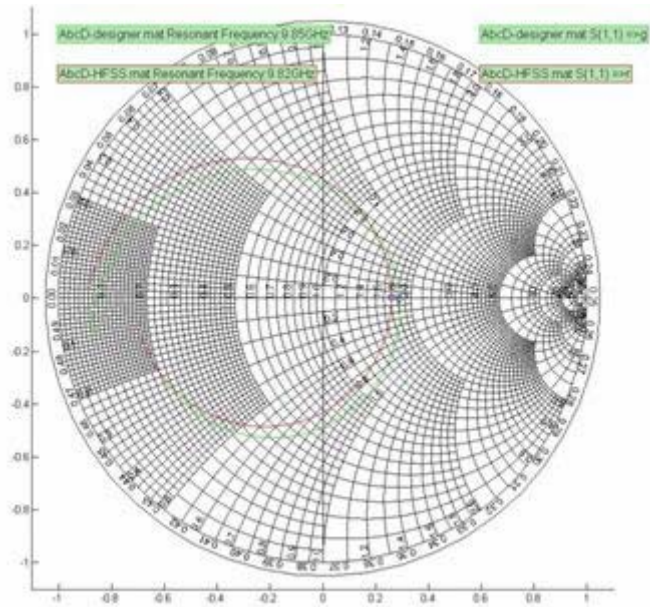


Figure 4.1.15 Input impedance from 8 to 12 GHz for AbCD design using Designer (--) and HFSS (--)

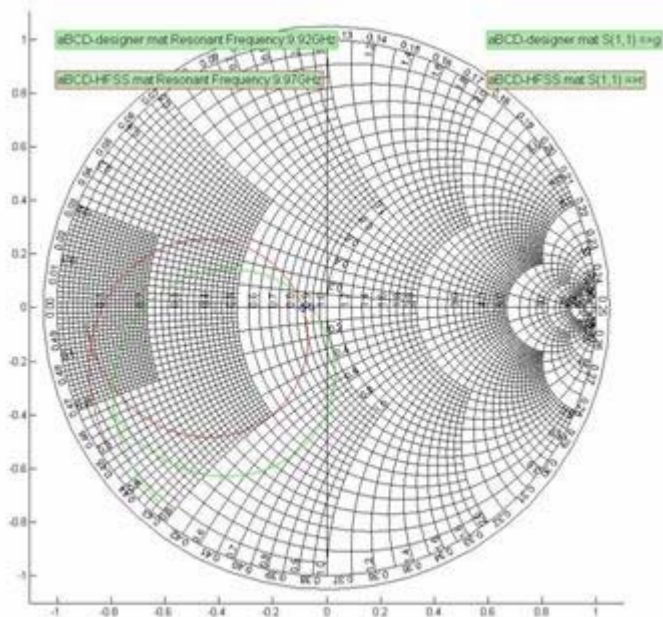


Figure 4.1.16 Input impedance from 8 to 12 GHz for aBCD design using Designer (--) and HFSS (--)

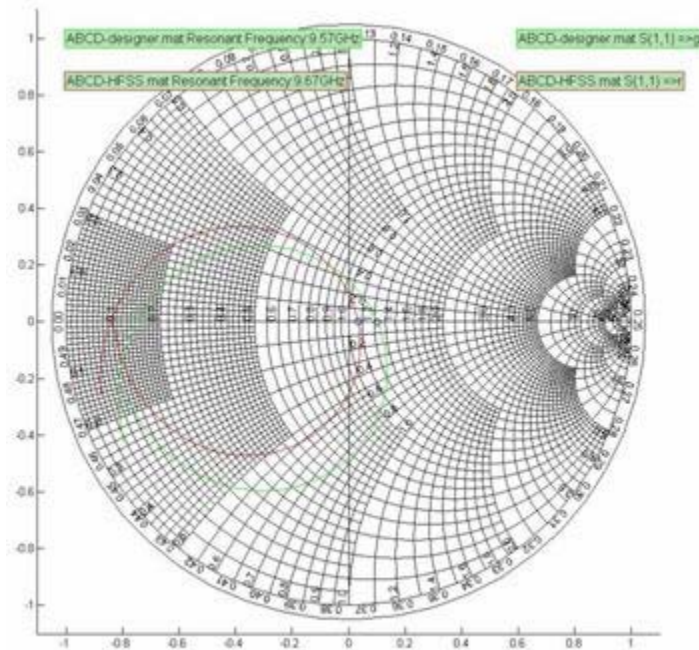


Figure 4.1.17 Input impedance from 8 to 12 GHz for ABCD design using Designer (--) and HFSS (--)

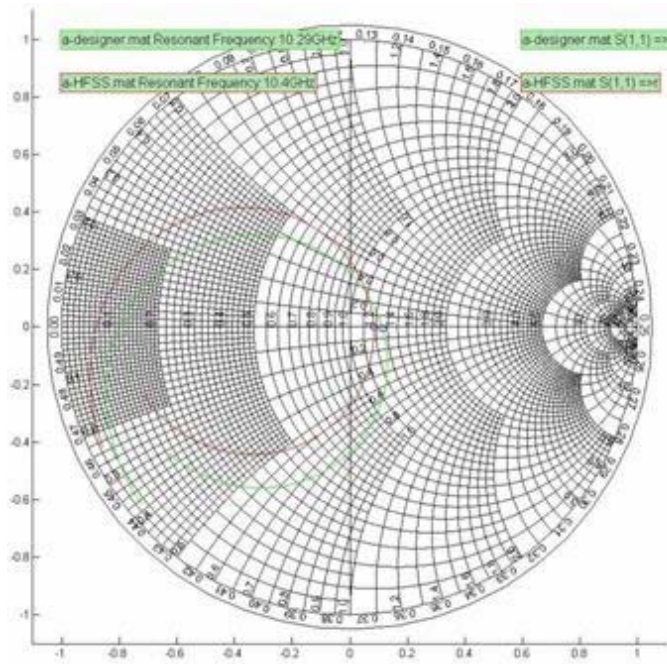


Figure 4.1.18 Input impedance from 8 to 12 GHz for a design using Designer (--) and HFSS (--)

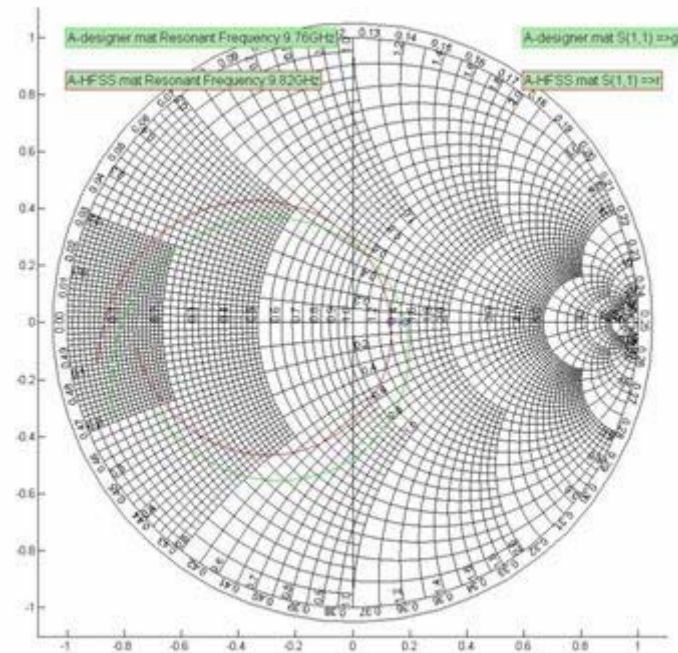


Figure 4.1.19 Input impedance from 8 to 12 GHz for A design using Designer (--) and HFSS (--)

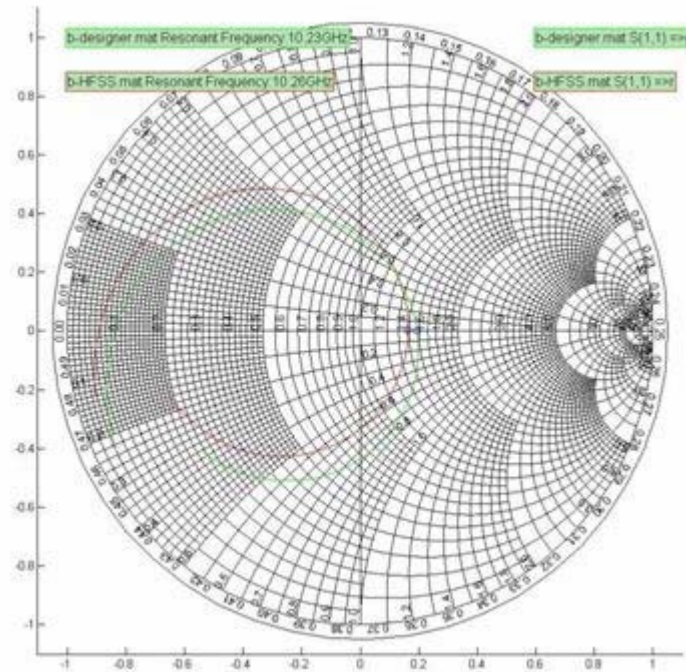


Figure 4.1.20 Input impedance from 8 to 12 GHz for b design using Designer (--) and HFSS (--)

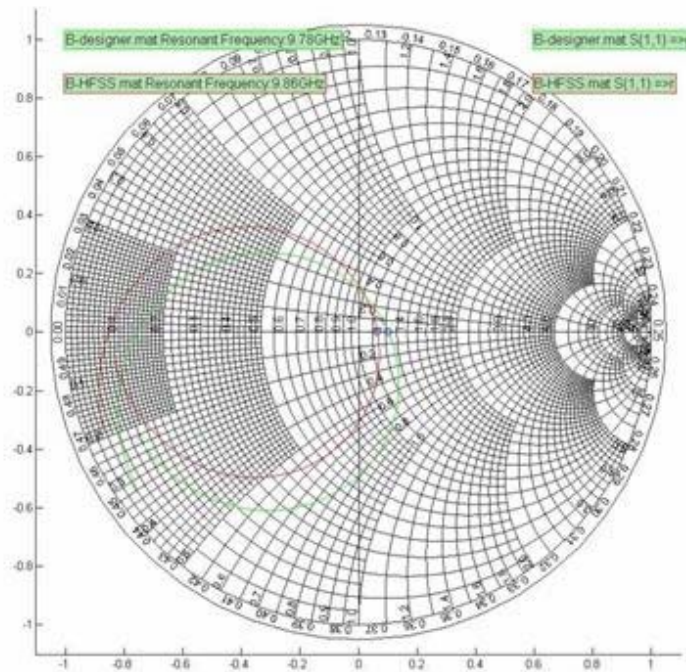


Figure 4.1.21 Input impedance from 8 to 12 GHz for B design using Designer (--) and HFSS (--)

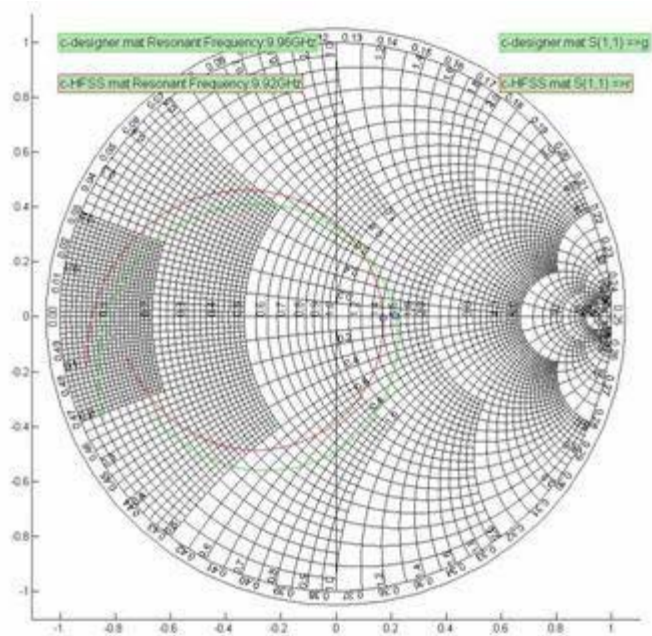


Figure 4.1.22 Input impedance from 8 to 12 GHz for c design using Designer (--) and HFSS (--)

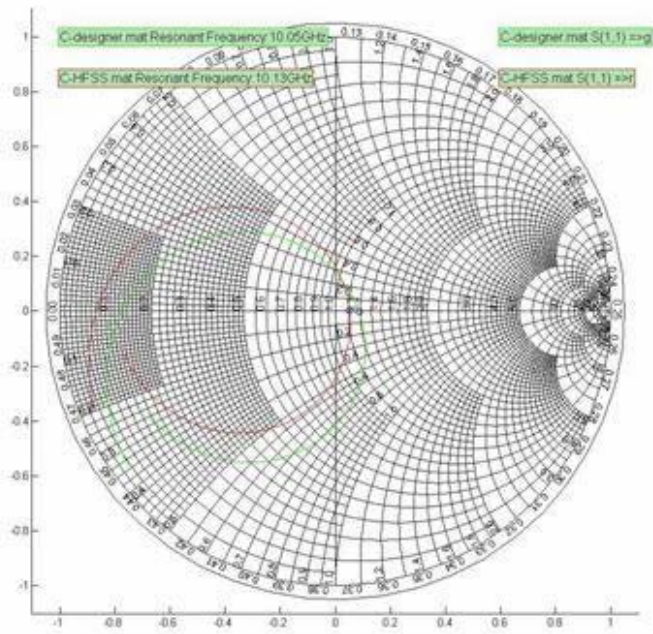


Figure 4.1.23 Input impedance from 8 to 12 GHz for C design using Designer (--) and HFSS (--)

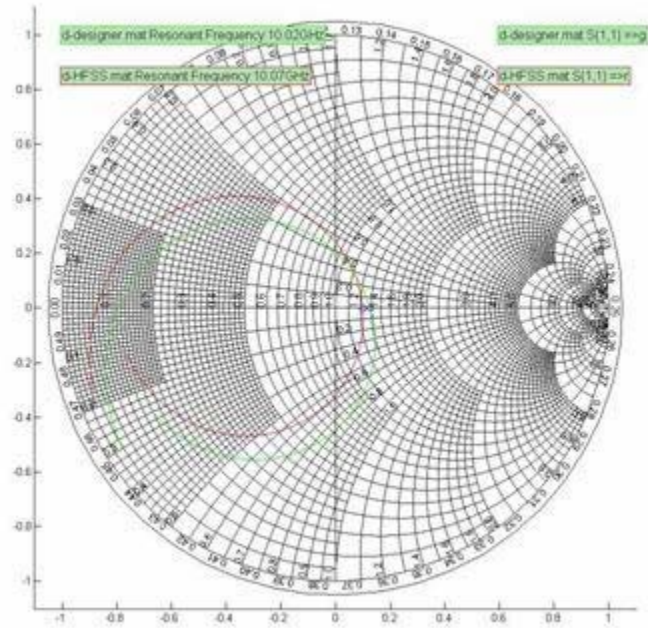


Figure 4.1.24 Input impedance from 8 to 12 GHz for d design using Designer (--) and HFSS (--)

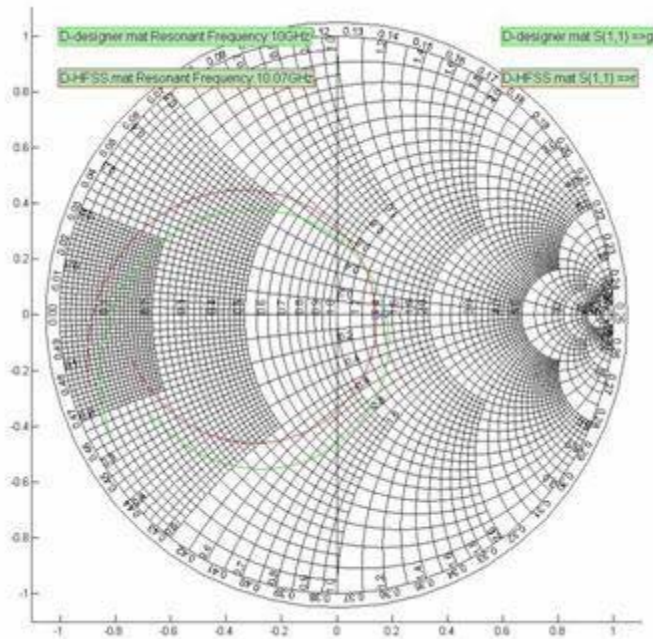


Figure 4.1.25 Input impedance from 8 to 12 GHz for D design using Designer (--) and HFSS (--)

The result of the model using Designer is presented in equations 4.1.1 to 4.1.4 and the results of the model using HFSS is shown in equations 4.1.5 to 4.1.8

Designer:

$$\mathbf{F} = 10.00 - 0.25\mathbf{A} - 0.24\mathbf{B} \quad \mathbf{4.1.1}$$

$$\mathbf{R} = 67.56 + 5.54\mathbf{A} - 6.78\mathbf{B} - 9.75\mathbf{C} + 3.57\mathbf{D} + 1.49\mathbf{AB} \quad \mathbf{4.1.2}$$

$$\mathbf{BW} = 734.17 - 75.56\mathbf{B} + 38.33\mathbf{C} - 50.28\mathbf{C}^2 - 53.12\mathbf{BC} \quad \mathbf{4.1.3}$$

$$\mathbf{G} = 2.19 + 0.003\mathbf{A} + 0.044\mathbf{A}^2 \quad \mathbf{4.1.4}$$

HFSS:

$$\mathbf{F} = 10.04 - 0.24\mathbf{A} - 0.23\mathbf{B} \quad \mathbf{4.1.5}$$

$$\mathbf{R} = 62.48 + 3.61\mathbf{A} - 7.42\mathbf{B} - 8.25\mathbf{C} + 3.16\mathbf{D} + 0.90\mathbf{AB} \quad \mathbf{4.1.6}$$

$$\mathbf{BW} = 733.33 + 31.11\mathbf{A} - 88.33\mathbf{B} + 12.78\mathbf{C} - 35.00\mathbf{C}^2 + 38.12\mathbf{AB} + 25.62\mathbf{AC} - 49.38\mathbf{BC} \quad \mathbf{4.1.7}$$

$$\mathbf{G} = 3.70 - 0.072\mathbf{A} - 0.11\mathbf{B} + 0.021\mathbf{AB} \quad \mathbf{4.1.8}$$

In Figure 4.1.26 we show again the input impedance of the aBcD and ABcD designs. It can be seen that increasing the outer radius decreases the resonance frequency and increases the resistance at resonance. This agrees with equations 4.1.1 and 4.1.5 where the coefficient of the A factor is negative meaning a decrease in resonance frequency when the factor is increased, and with equations 4.1.2 and 4.1.6 where the coefficient of the A factor is positive meaning an increase in the resistance at resonance when the factor is increased

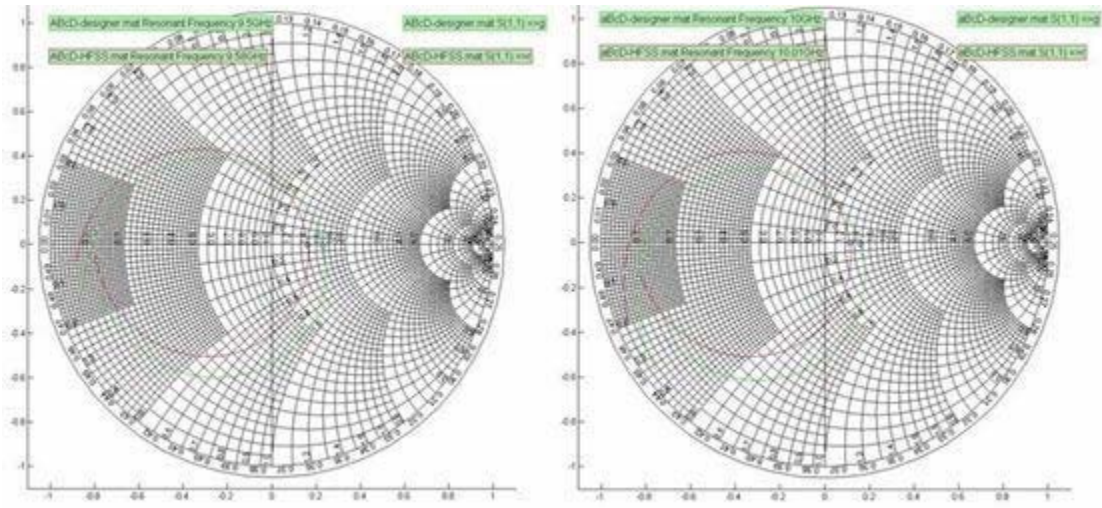


Figure 4.1.26 Effect of the outer radius in the resonant frequency and the resistance at resonance of the antenna.

Figure 4.1.27 show the input impedance of the ABcD and AbcD designs. It can be seen that increasing the inner radius decreases the resonance frequency and decreases the resistance at resonance. This agrees with equations 4.1.1 and 4.1.5 where the coefficient of the B factor is negative and equations 4.1.2 and 4.1.6 where the coefficient of the B factor is also negative.

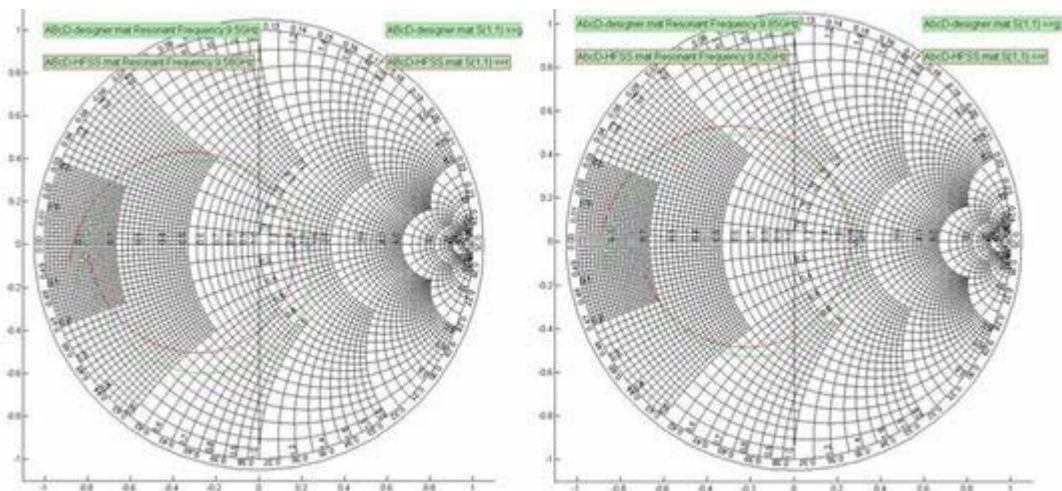


Figure 4.1.27 Effect of the inner radius in the resonant frequency and the resistance at resonance of the antenna

Equations 4.1.2 and 4.1.6 show that the C factor (offset between the circles) has a negative coefficient. This agrees with the results in figure 4.1.28 where the input impedance of designs aBCd and aBcd are shown. Increasing the offset decreases the resistance at resonance

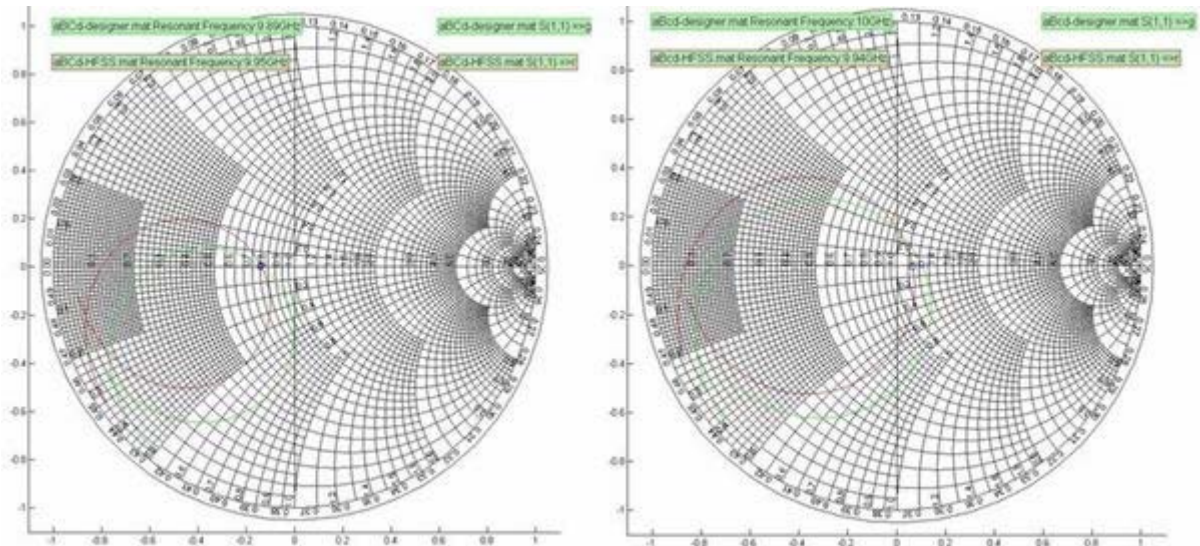


Figure 4.1.28 Effect of the offset between the centers of the circles in the resistance at resonance of the antenna.

Equations 4.1.2 and 4.1.6 show that the D factor (inset of the CPW line in the inner conductor) has a positive coefficient. This agrees with the results in figure 4.1.29 where the input impedance of designs ABCD and ABCd are shown. Increasing the inset increases the resistance at resonance

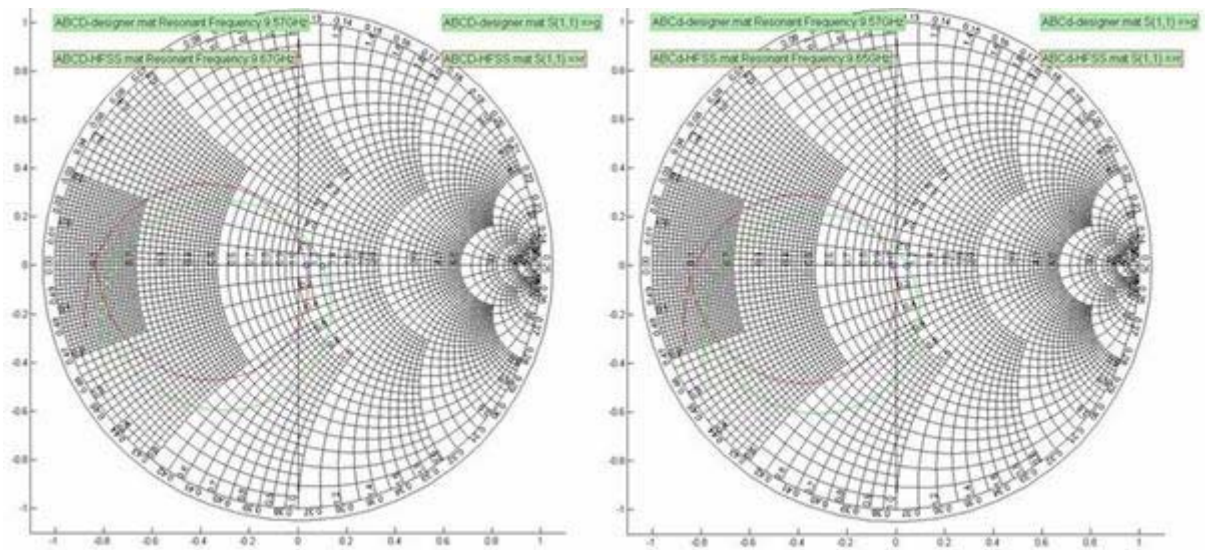


Figure 4.1.29 Effect of the inset in the resistance at resonance of the antenna.

A third model was made with the same data were the electromagnetic simulator was added as a 5th factor. Designer is the low level and HFSS the high level. It is 2⁵ factorial designs with two central points and 16 axial points. The result of that model is presented in equations 4.1.9 to 4.1.12 and compared with the equations of the previous models.

Combined Model:

$$\mathbf{F} = 10.02 - 0.24\mathbf{A} - 0.23\mathbf{B} \quad \mathbf{4.1.9}$$

$$\mathbf{R} = 65.02 + 4.57\mathbf{A} - 7.10\mathbf{B} - 9.00\mathbf{C} + 3.37\mathbf{D} - 2.54\mathbf{E} + 1.19\mathbf{AB} \quad \mathbf{4.1.10}$$

$$\mathbf{BW} = 733.75 + 21.39\mathbf{A} - 81.94\mathbf{B} + 25.56\mathbf{C} - 42.64\mathbf{C}^2 + 35.63\mathbf{AB} - 51.25\mathbf{BC} \quad \mathbf{4.1.11}$$

$$\mathbf{G} = 2.96 - 0.061\mathbf{B} + 0.74\mathbf{E} \quad \mathbf{4.1.12}$$

The model showed that the electromagnetic simulator does not affect the value of the resonant frequency and the model is almost identical to the individual ones from Designer

and HFSS. The model for the resistance at resonance shows that HFSS increases the resistance by about 2.5 Ohms and the coefficient of the rest of the factors is about an average of the coefficient of the individual models. This agrees with what is seen in the impedance plots. For example, in figures 4.1.1 where we see the impedance plot of the central design, the resonance frequency of both Designer and HFSS is 10.02 GHz and the impedance at resonance is about 0.05 units higher which is equivalent to 2.5 Ohms when the reference impedance is 50 Ohms

The bandwidth model does not present a significant change by the electromagnetic simulator but it eliminates the AC ($R_{o,d}$) interaction which previously appeared only in the HFSS model. Finally, for the gain the simulator is the most significant factor followed way behind by the inner radius which previously only appeared in the HFSS model.

To validate the models, designs were tested inside the experiment area. To generate the DOE we used low (-1) and high (1) values and generate our models from that data. Now, we set the variables at intermediate levels. Tables 4.1.3 to 4.1.6 compare what our models predict with the simulation of that design in both electromagnetic simulators for each of our four responses. The Joint Model produces two values, one for each simulator. The results show that the models agree very well with the simulated results.

Table 4.1.3 Validation of Resonant Frequency Models

				Resonant Frequency (GHz)					
				Designer			HFSS		
R_o	R_i	d	s	Sim	Pred.	J.Pred.	Sim	Pred.	J.Pred.
-0.5	-0.5	-0.5	-0.5	10.24	10.24	10.25	10.28	10.27	10.26
-0.5	-0.5	-0.7	0.7	10.22	10.24	10.26	10.22	10.27	10.26
0.5	0.7	-0.5	-0.7	9.72	9.71	9.73	9.73	9.76	9.73
0.7	0.5	0.7	-0.5	9.76	9.70	9.73	9.86	9.76	9.73
0.7	-0.7	-0.7	-0.7	9.93	9.99	10.01	10.00	10.03	10.01
0.7	-0.7	-0.7	0.7	9.92	9.99	10.01	9.94	10.03	10.01

Table 4.1.4 Validation of Resistance Models

				Resistance at f_r (Ohms)					
				Designer			HFSS		
R_o	R_i	d	s	Sim	Pred.	J.Pred.	Sim	Pred.	J.Pred.
-0.5	-0.5	-0.5	-0.5	71.45	71.64	71.94	66.73	67.15	66.86
-0.5	-0.5	-0.7	0.7	77.94	77.88	77.78	71.48	72.60	72.70
0.5	0.7	-0.5	-0.7	68.51	68.48	67.44	60.83	61.31	62.36
0.7	0.5	0.7	-0.5	61.17	59.95	59.64	55.38	54.26	54.57
0.7	-0.7	-0.7	-0.7	77.72	79.78	79.09	70.23	73.32	74.01
0.7	-0.7	-0.7	0.7	83.22	84.78	83.80	78.27	77.75	78.73

Table 4.1.5 Validation of Bandwidth Models

				Bandwidth (MHz)					
				Designer			HFSS		
R_o	R_i	d	s	Sim	Pred.	J.Pred.	Sim	Pred.	J.Pred.
-0.5	-0.5	-0.5	-0.5	760	730	740	760	750	740
-0.5	-0.5	-0.7	0.7	700	700	720	740	740	720
0.5	0.7	-0.5	-0.7	680	670	690	680	700	690
0.7	0.5	0.7	-0.5	720	680	700	740	710	700
0.7	-0.7	-0.7	-0.7	720	710	720	800	740	720
0.7	-0.7	-0.7	0.7	680	710	720	720	740	720

Table 4.1.6 Validation of Gain Model

				Gain at broadside (dB)					
				Designer			HFSS		
R _o	R _i	d	s	Sim	Pred.	J.Pred.	Sim	Pred.	J.Pred.
-0.5	-0.5	-0.5	-0.5	2.28	2.20	2.25	3.94	3.79	3.72
-0.5	-0.5	-0.7	0.7	2.22	2.20	2.25	3.40	3.79	3.73
0.5	0.7	-0.5	-0.7	2.22	2.20	2.18	3.54	3.59	3.65
0.7	0.5	0.7	-0.5	2.23	2.22	2.19	3.61	3.60	3.67
0.7	-0.7	-0.7	-0.7	2.23	2.22	2.26	3.53	3.71	3.74
0.7	-0.7	-0.7	0.7	2.23	2.22	2.26	3.55	3.71	3.74

The combined model was used to find a few optimum designs. Table 4.1.7 show the predicted values of the designs with the biggest bandwidth and the design with a perfect match (resistance of 50 Ohms) at 10 GHz for HFSS and for Designer. It also gives the dimensions of the antennas.

Table 4.1.7 Optimum Designs

	A (R _o)	B(R _i)	C(d)	D(s)	F		R		BW		G	
					Pred	Sim	pred	sim	pred	sim	pred	sim
Closest Match Designer	-0.36 (3.146mm)	0.46 (2.369mm)	1.00 (0.55mm)	-1.00 (0.95mm)	10.00	10.00	50.00	50.38	640	690	2.23	2.23
Closest Match HFSS	-0.40 (3.14mm)	0.40 (2.36mm)	1.00 (0.55mm)	-1.00 (0.95mm)	10.00	10.10	50.00	47.97	710	640	3.72	3.74
Maximum Bandwidth Designer	-1.00 (3.05mm)	-1.00 (2.15mm)	0.90 (0.540mm)	-0.97 (0.9505mm)	10.49	10.57	59.92	58.05	860	820	2.22	2.25
Maximum Bandwidth HFSS	-1.00 (3.05mm)	-1.00 (2.15mm)	0.91 (0.541m)	-0.99 (0.540mm)	10.49	10.60	54.69	56.24	860	800	3.93	3.93

Figure 4.1.30 shows a design with a closest match in Designer The design with a closest match is the design which will provide a resistance at resonance closest to 50 Ohms and therefore provide the smallest VSWR value. The model predicted a resonance frequency at 10 GHz and a resistance of 50 Ohms. A resonance frequency of 10 GHz and a resistance of 50.38 Ohms were achieved. Figure 4.1.31 shows a design with a closest match in HFSS.

The model also predicted a resonance frequency at 10 GHz and a resistance of 50 Ohms. A resonance frequency of 10.1 GHz and a resistance of 47.97 Ohms were achieved.

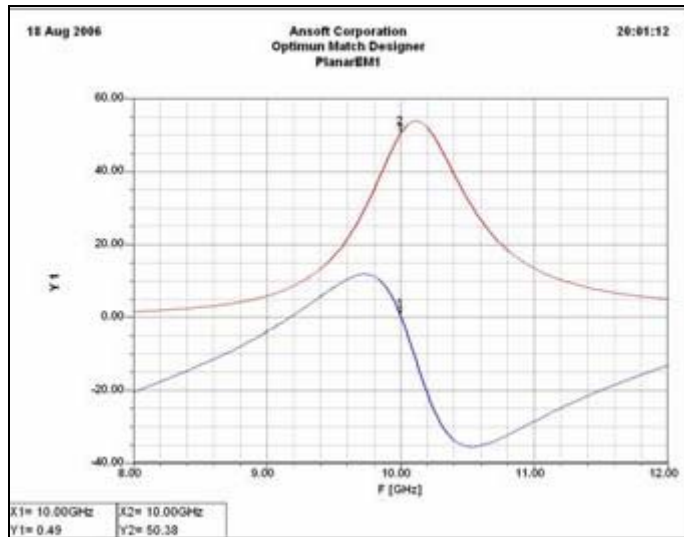


Figure 4.1.30 Closest Match in Designer

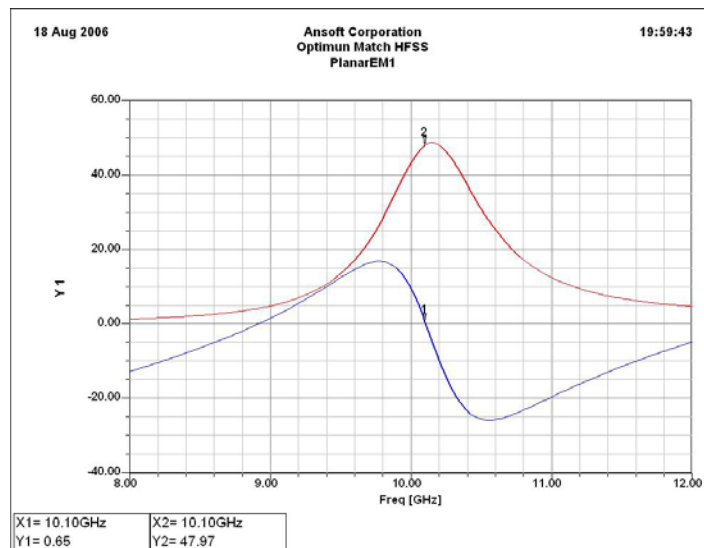


Figure 4.1.31 Closest Match in HFSS

Figure 4.1.32 shows a design with an optimum bandwidth in Designer. The model predicted a bandwidth of 860 MHz. A bandwidth of 820MHz was achieved. Figure 4.1.33 shows a design with a perfect match in HFSS. The model predicted a bandwidth of 860 MHz. A Bandwidth of 800 MHz was achieved. This results show that the models are adequate to find optimum responses.

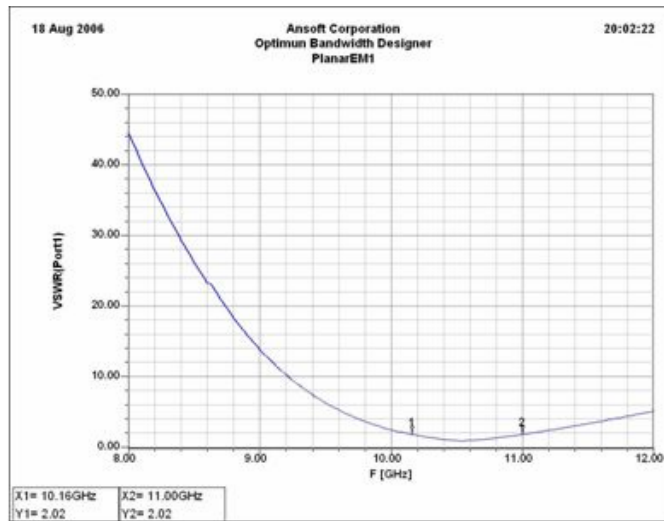


Figure 4.1.32 Optimum Bandwidth in Designer

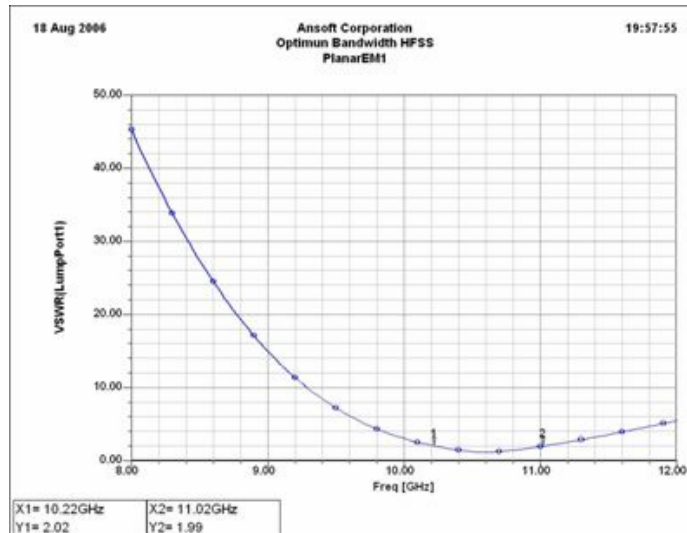


Figure 4.1.33 Optimum Bandwidth in HFSS

All 25 designs were fabricated, measured in the network analyzer and tested in the anechoic chamber twice. Figure 4.1.34 shows all the antennas and Figure 4.1.35 gives a perspective of the size of the antennas.

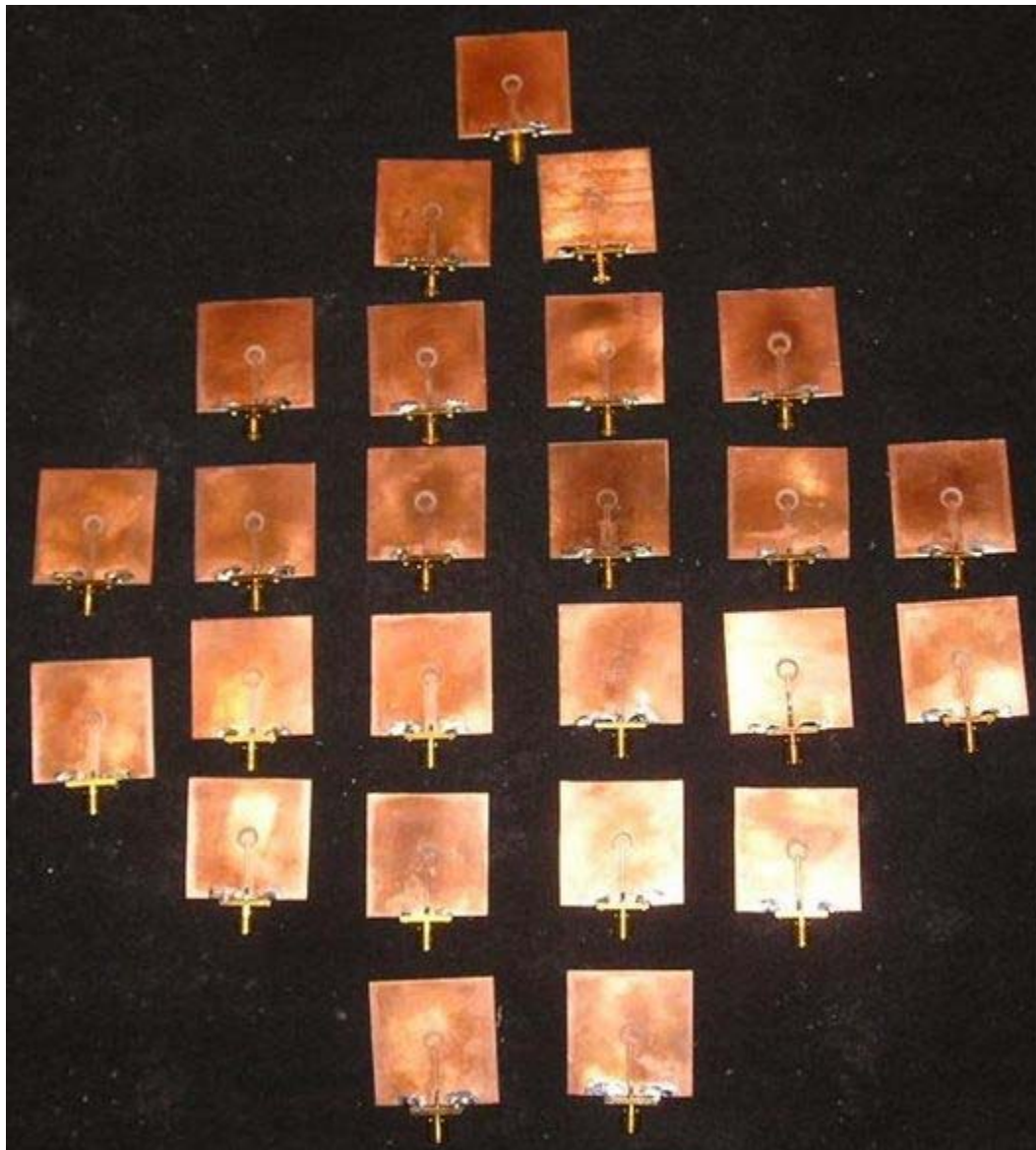


Figure 4.1.34 Fabricated Antennas

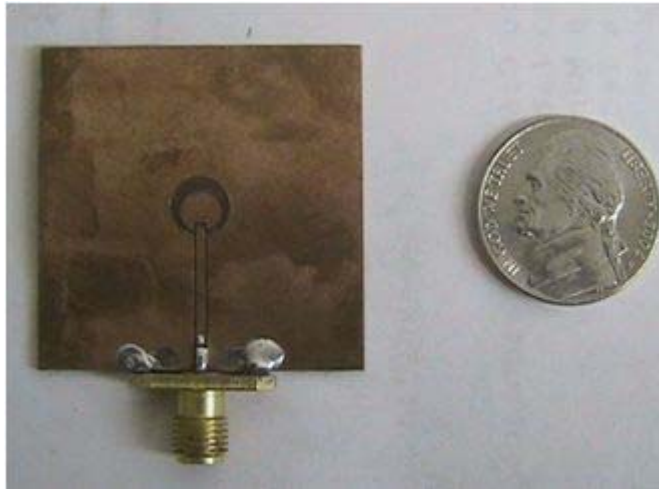


Figure 4.1.35 CPW fed asymmetric annular slot ring antenna

The fabricated antennas show very similar responses to the ones simulated. There is a difference due to the effect of the connector that is adding another resonance at around 11 GHz. Figures 4.1.36 to 4.1.560 show the log magnitude of the reflection coefficient of the antennas for the measured and both simulated antennas.

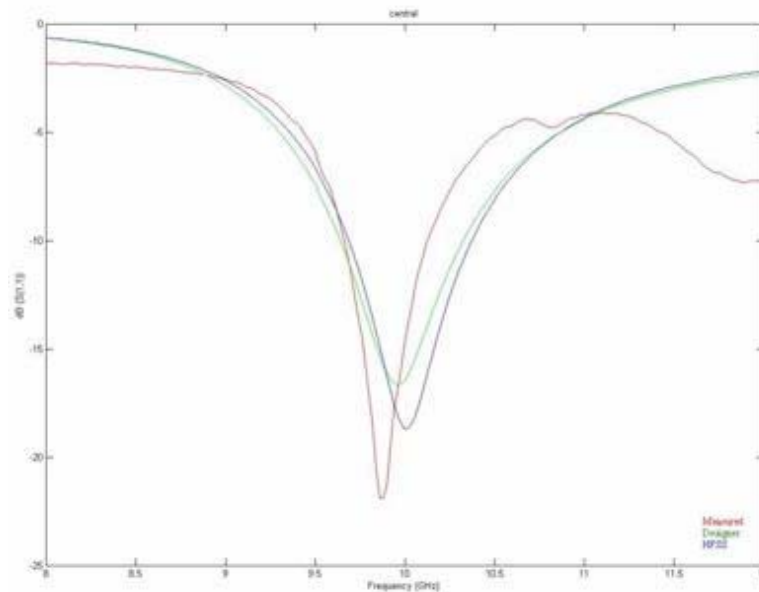


Figure 4.1.36 Log magnitude of the reflection coefficient of the fabricated central design antenna measured (--) and simulated in Designer (--) and HFSS (--)

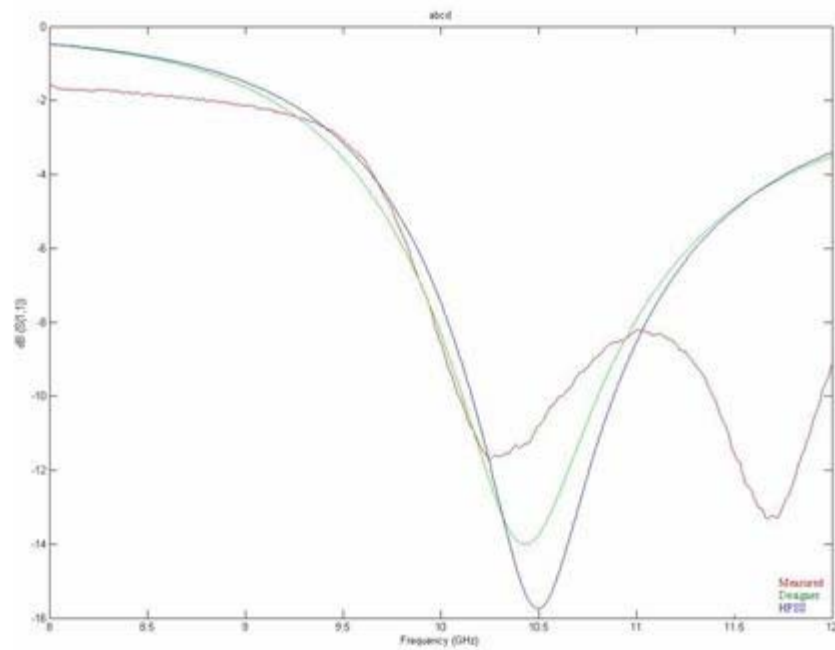


Figure 4.1.37 Log magnitude of the reflection coefficient of the fabricated abcd design antenna measured (--) and simulated in Designer (--) and HFSS (--)

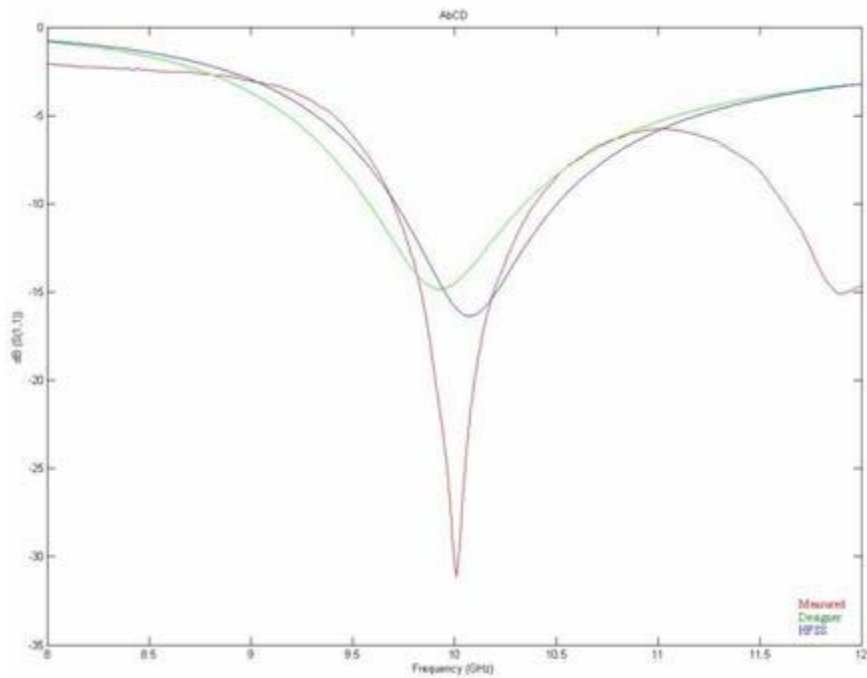


Figure 4.1.38 Log magnitude of the reflection coefficient of the fabricated Abcd design antenna measured (--) and simulated in Designer (--) and HFSS (--)

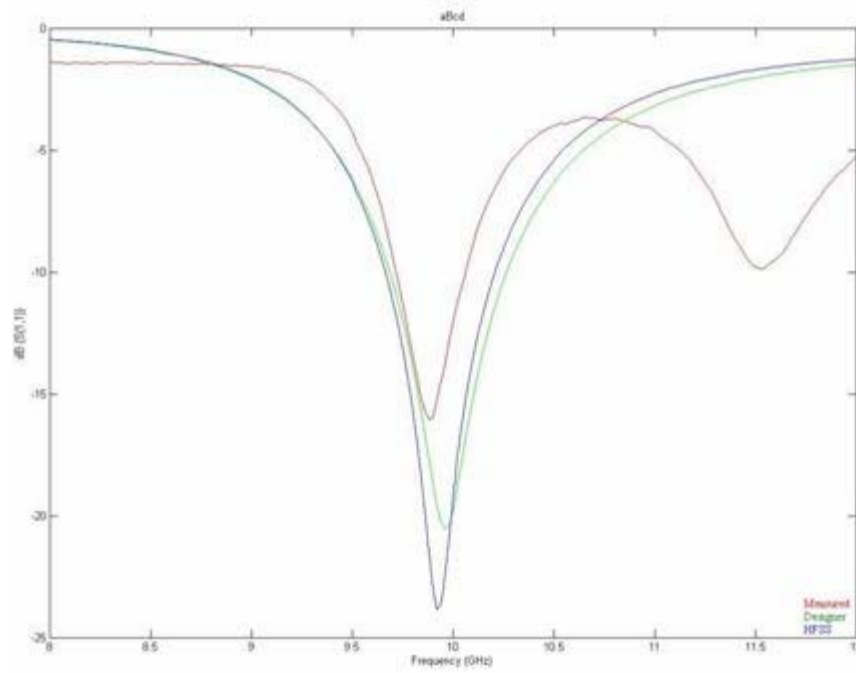


Figure 4.1.39 Log magnitude of the reflection coefficient of the fabricated aBcd design antenna measured (--) and simulated in Designer (--) and HFSS (--)

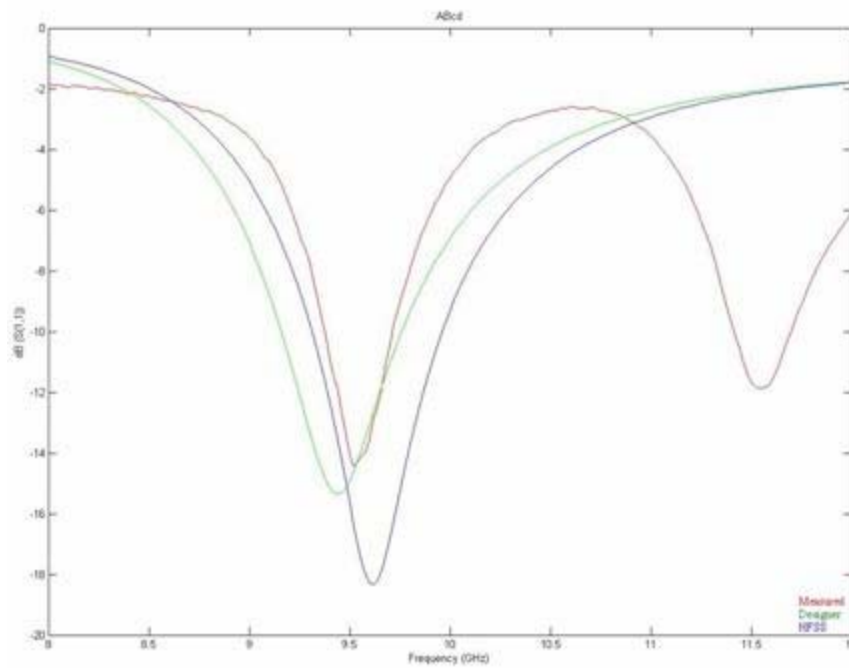


Figure 4.1.40 Log magnitude of the reflection coefficient of the fabricated ABcd design antenna measured (--) and simulated in Designer (--) and HFSS (--)

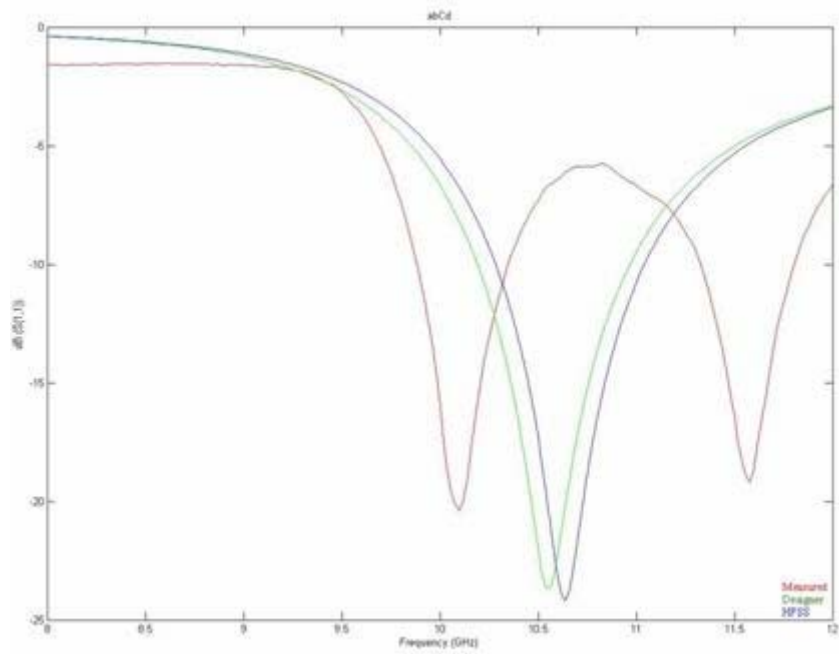


Figure 4.1.41 Log magnitude of the reflection coefficient of the fabricated abCd design antenna measured (--) and simulated in Designer (--) and HFSS (--)

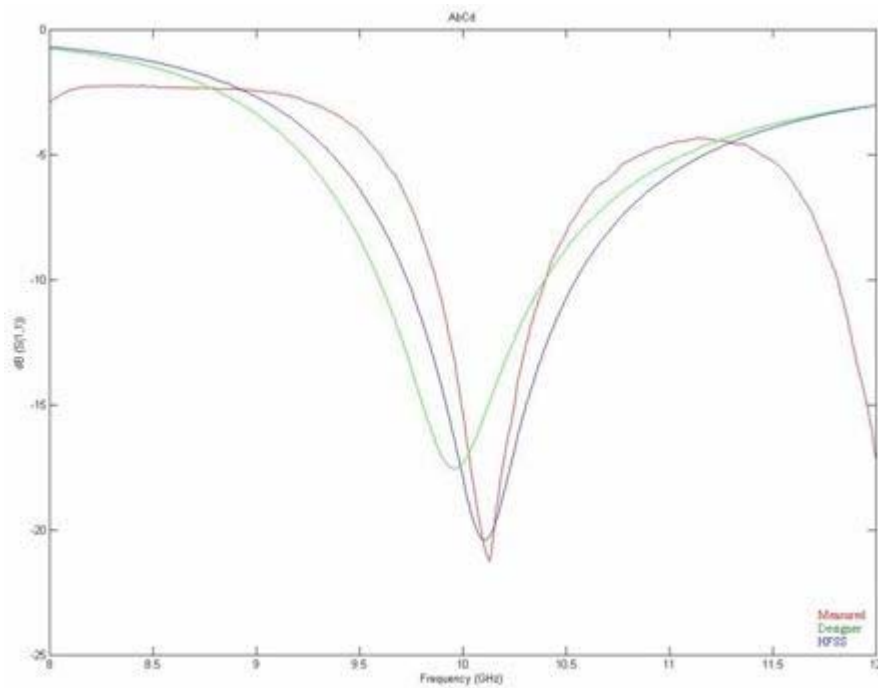


Figure 4.1.42 Log magnitude of the reflection coefficient of the fabricated AbCd design antenna measured (--) and simulated in Designer (--) and HFSS (--)

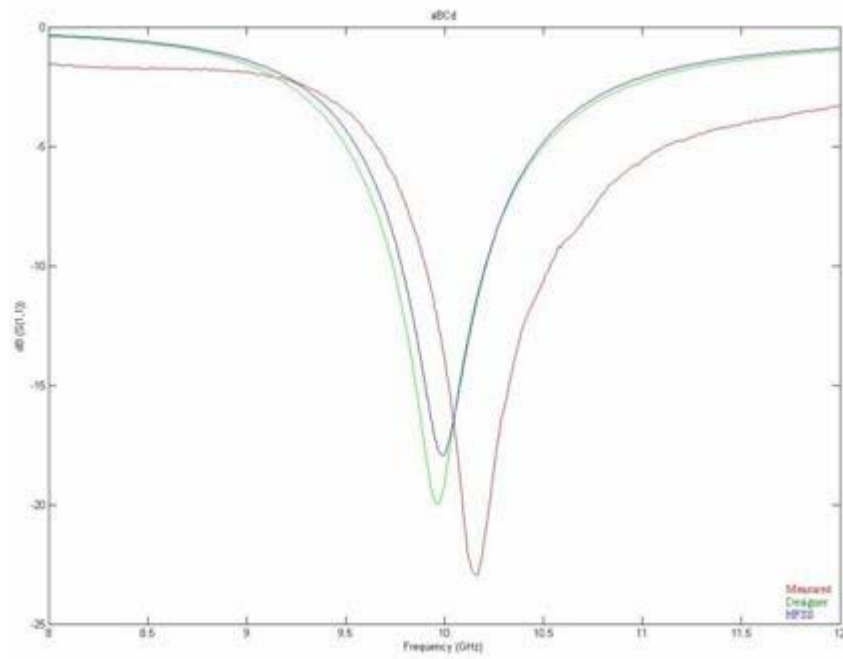


Figure 4.1.43 Log magnitude of the reflection coefficient of the fabricated aBCd design antenna measured (--) and simulated in Designer (--) and HFSS (--)

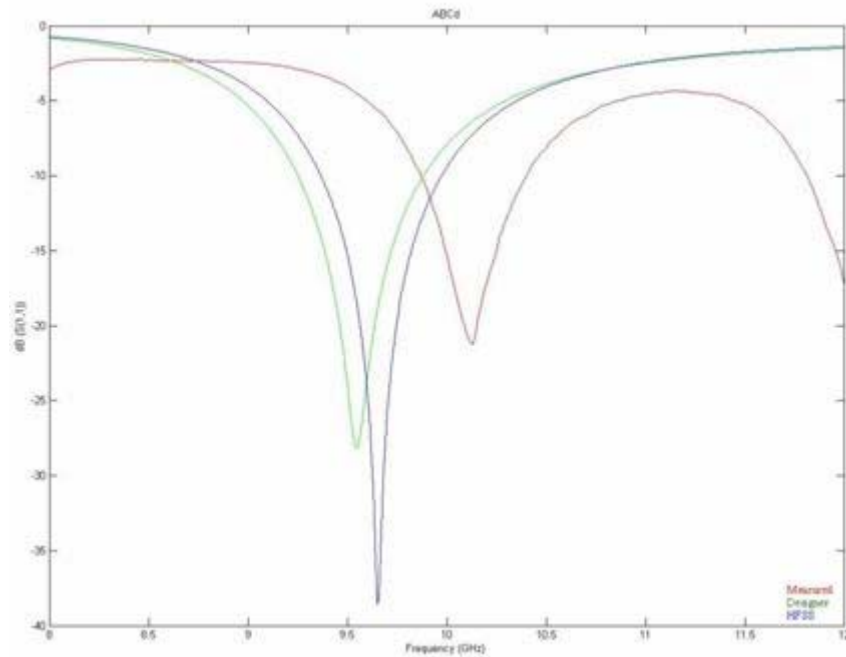


Figure 4.1.44 Log magnitude of the reflection coefficient of the fabricated ABCd design antenna measured (--) and simulated in Designer (--) and HFSS (--)

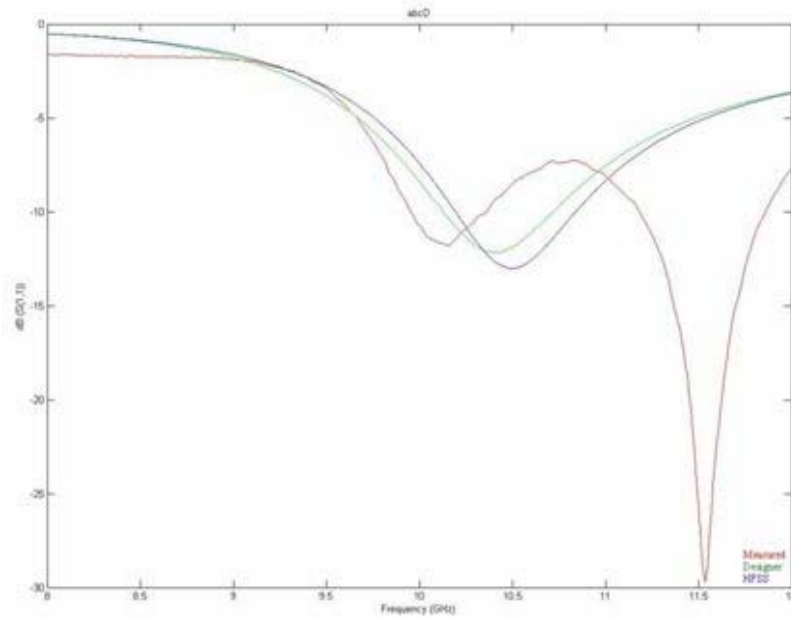


Figure 4.1.45 Log magnitude of the reflection coefficient of the fabricated abcD design antenna measured (--) and simulated in Designer (--) and HFSS (--)

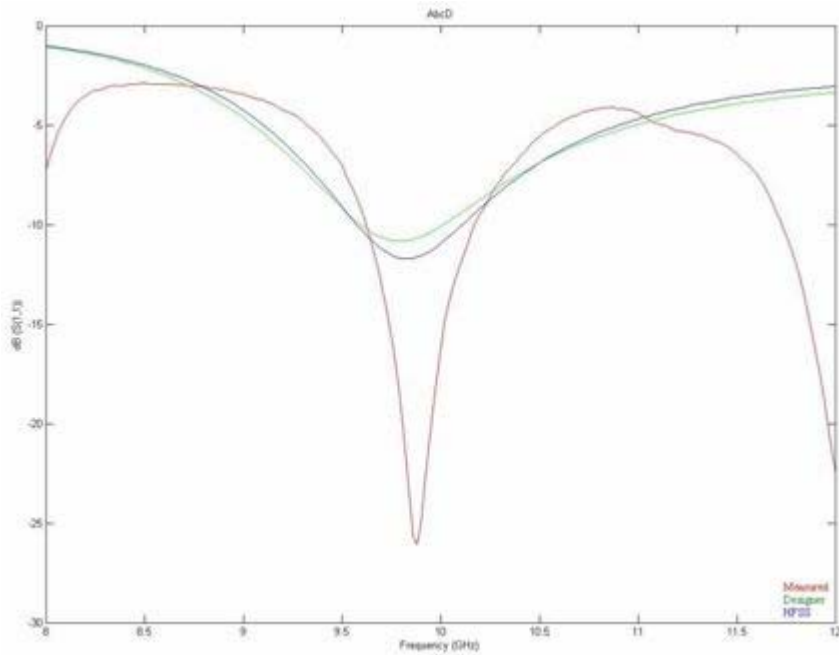


Figure 4.1.46 Log magnitude of the reflection coefficient of the fabricated AbcD design antenna measured (--) and simulated in Designer (--) and HFSS (--)

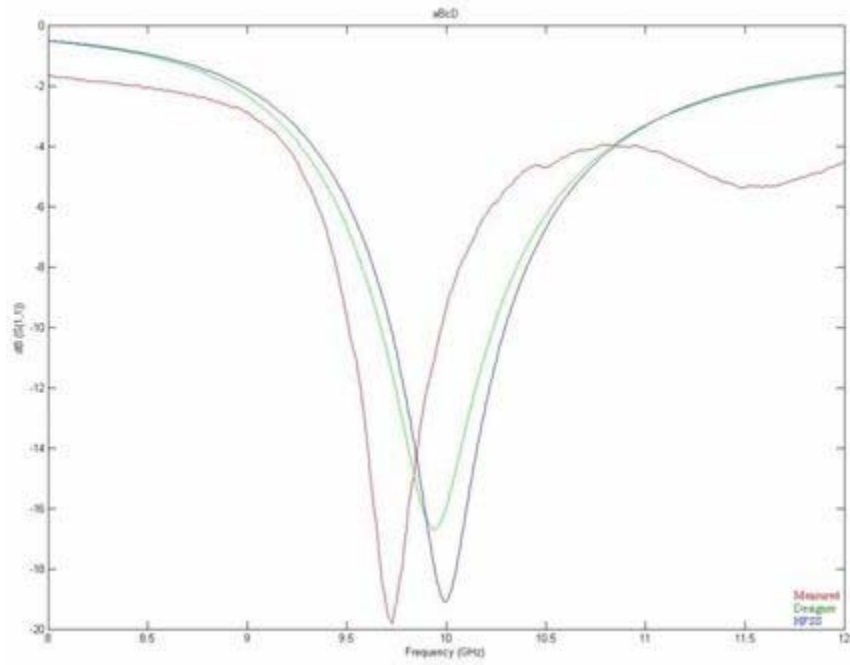


Figure 4.1.47 Log magnitude of the reflection coefficient of the fabricated aBcD design antenna measured (--) and simulated in Designer (--) and HFSS (--)

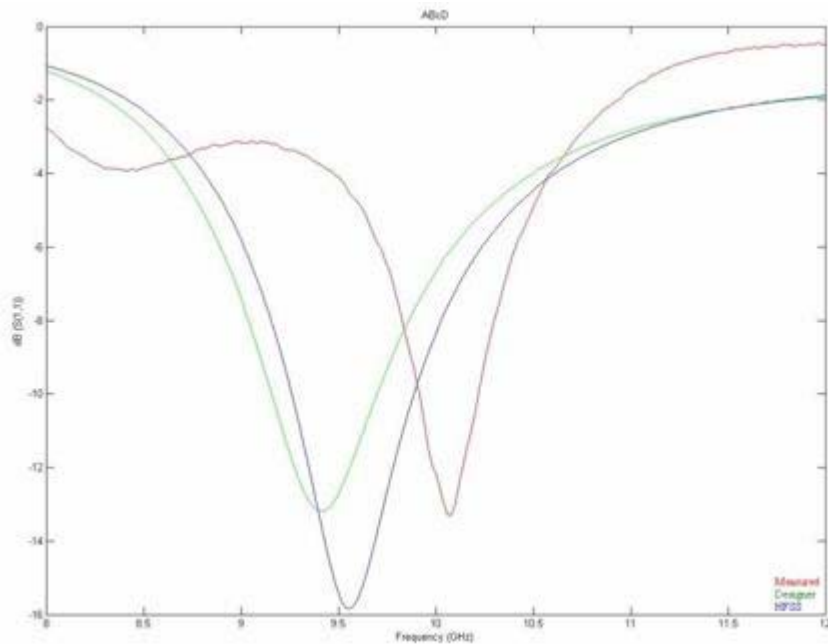


Figure 4.1.48 Log magnitude of the reflection coefficient of the fabricated ABcD design antenna measured (--) and simulated in Designer (--) and HFSS (--)

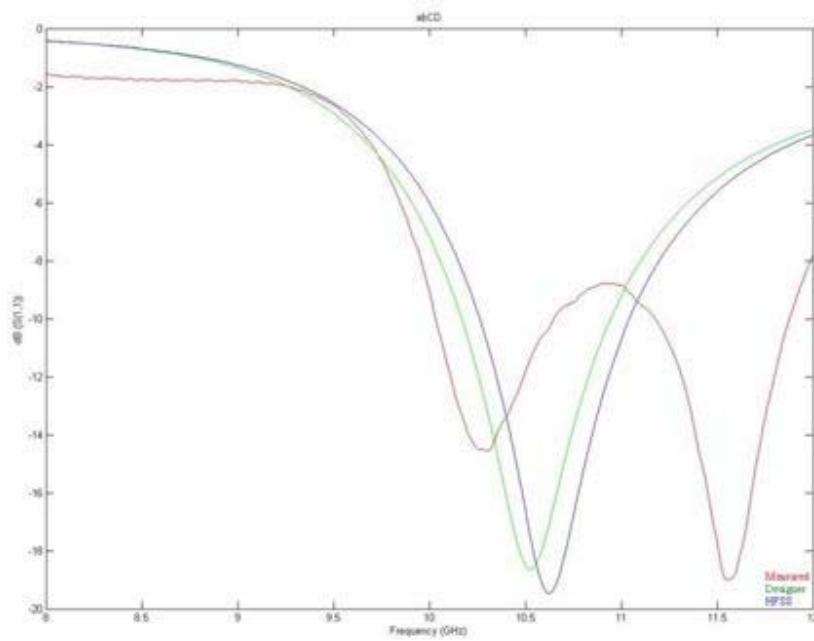


Figure 4.1.49 Log magnitude of the reflection coefficient of the fabricated abCD design antenna measured (--) and simulated in Designer (--) and HFSS (--)

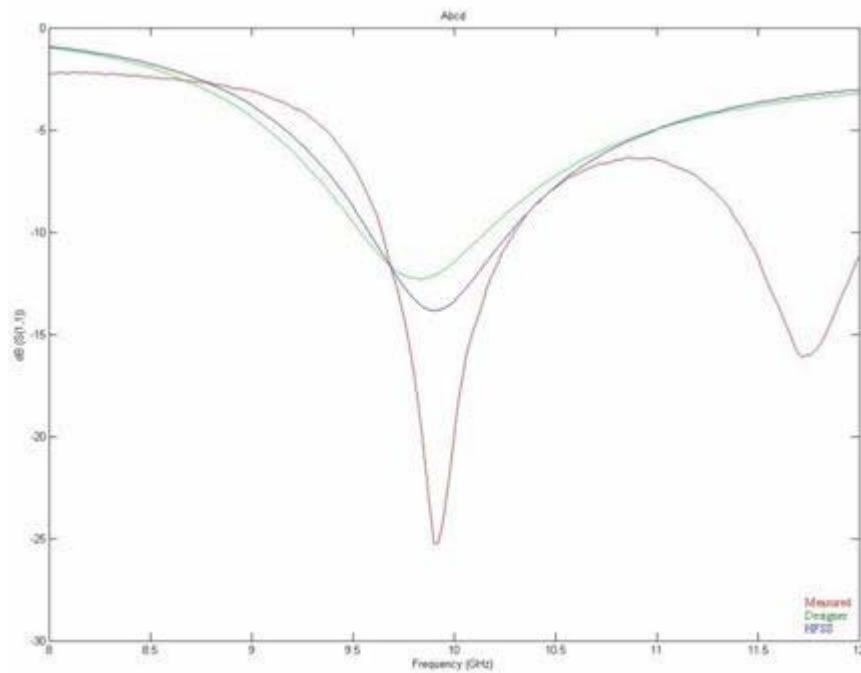


Figure 4.1.50 Log magnitude of the reflection coefficient of the fabricated AbCD design antenna measured (--) and simulated in Designer (--) and HFSS (--)

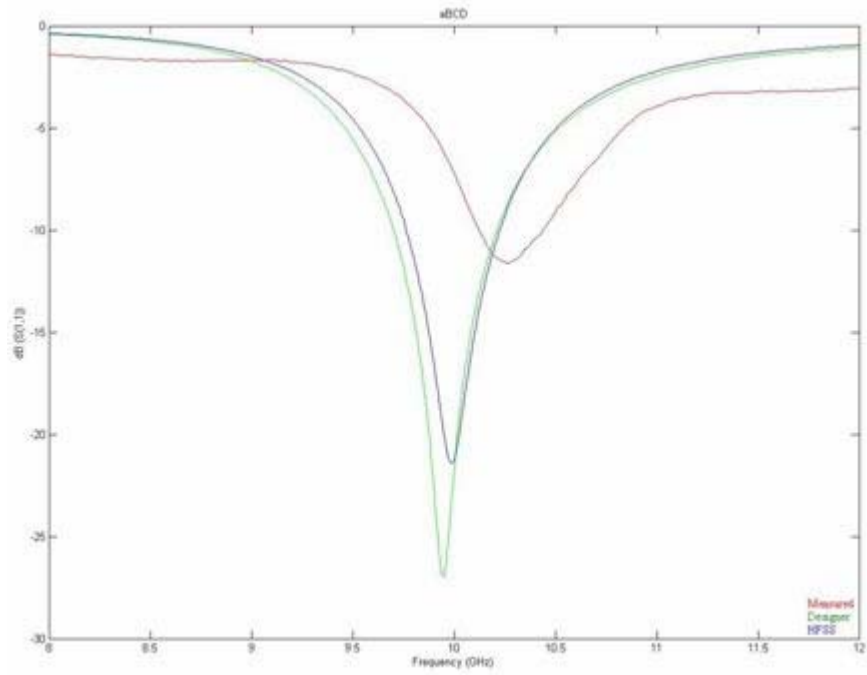


Figure 4.1.51 Log magnitude of the reflection coefficient of the fabricated aBCD design antenna measured (--) and simulated in Designer (--) and HFSS (--)

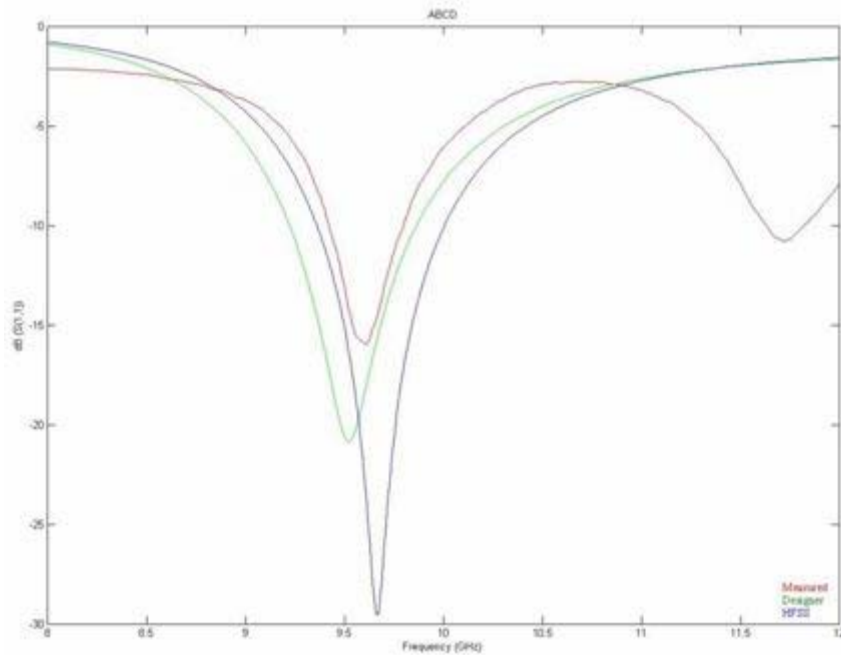


Figure 4.1.52 Log magnitude of the reflection coefficient of the fabricated ABCD design antenna measured (--) and simulated in Designer (--) and HFSS (--)

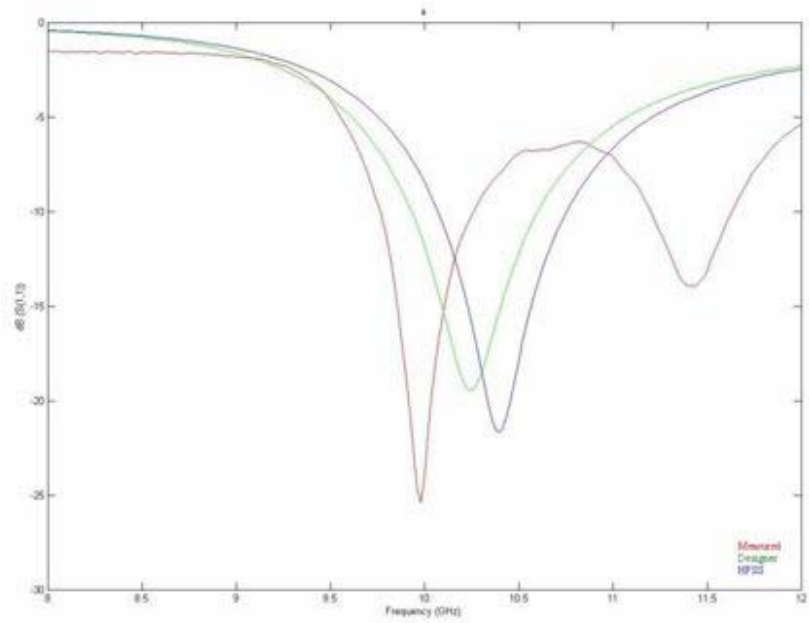


Figure 4.1.53 Log magnitude of the reflection coefficient of the fabricated a design antenna measured (--) and simulated in Designer (--) and HFSS (--)

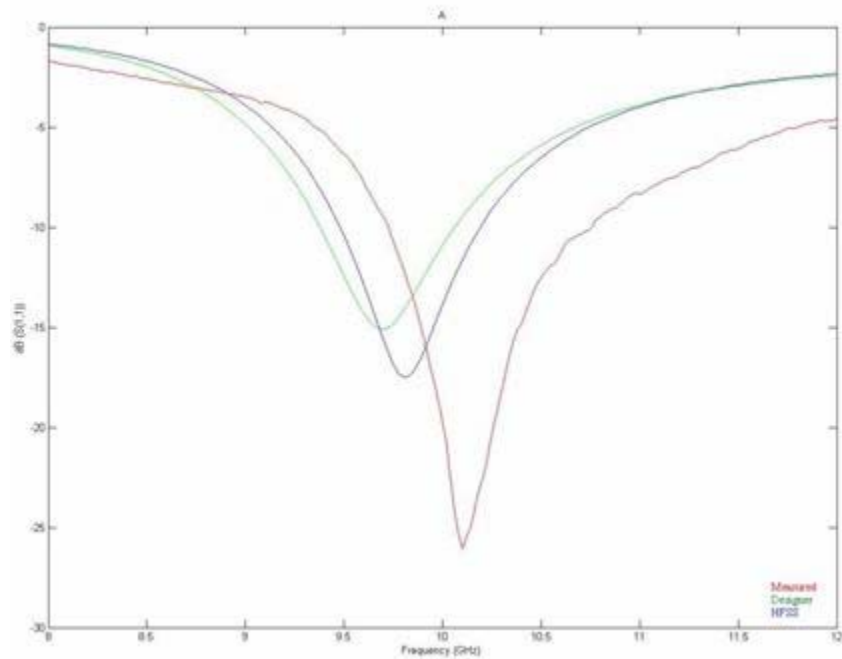


Figure 4.1.54 Log magnitude of the reflection coefficient of the fabricated A design antenna measured (--) and simulated in Designer (--) and HFSS (--)

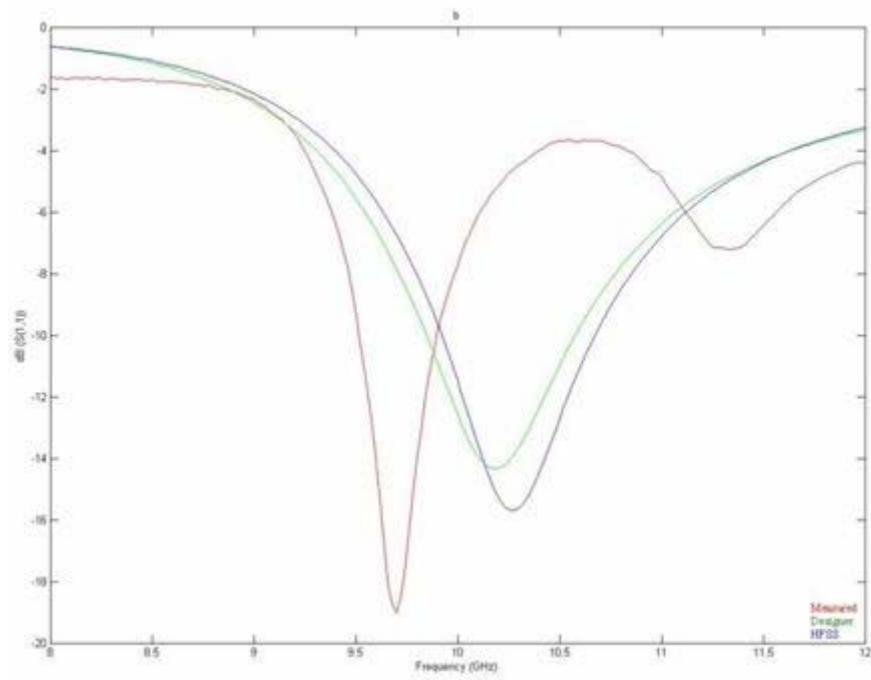


Figure 4.1.55 Log magnitude of the reflection coefficient of the fabricated b design antenna measured (--) and simulated in Designer (--) and HFSS (--)

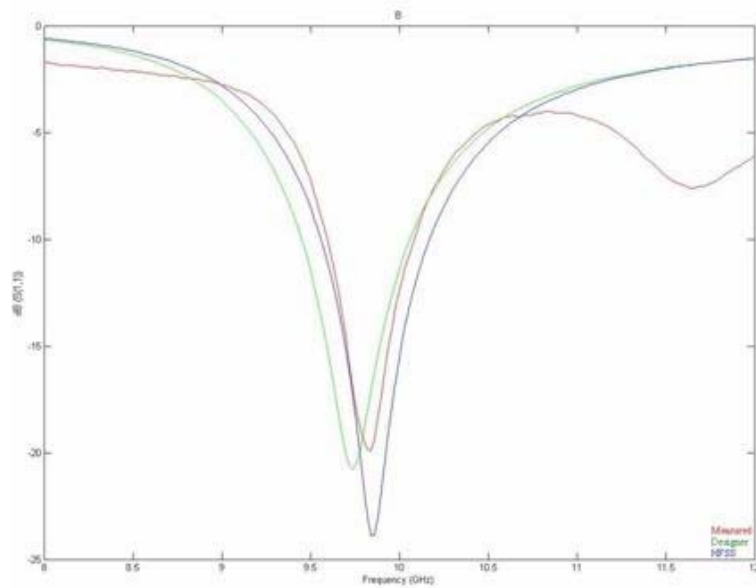


Figure 4.1.56 Log magnitude of the reflection coefficient of the fabricated B design antenna measured (--) and simulated in Designer (--) and HFSS (--)

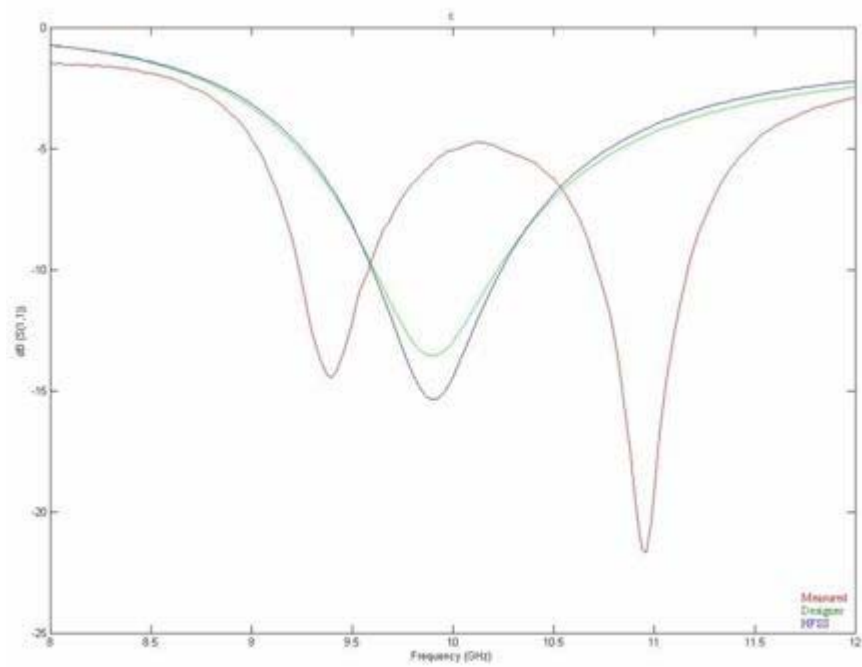


Figure 4.1.57 Log magnitude of the reflection coefficient of the fabricated c design antenna measured (--) and simulated in Designer (--) and HFSS (--)

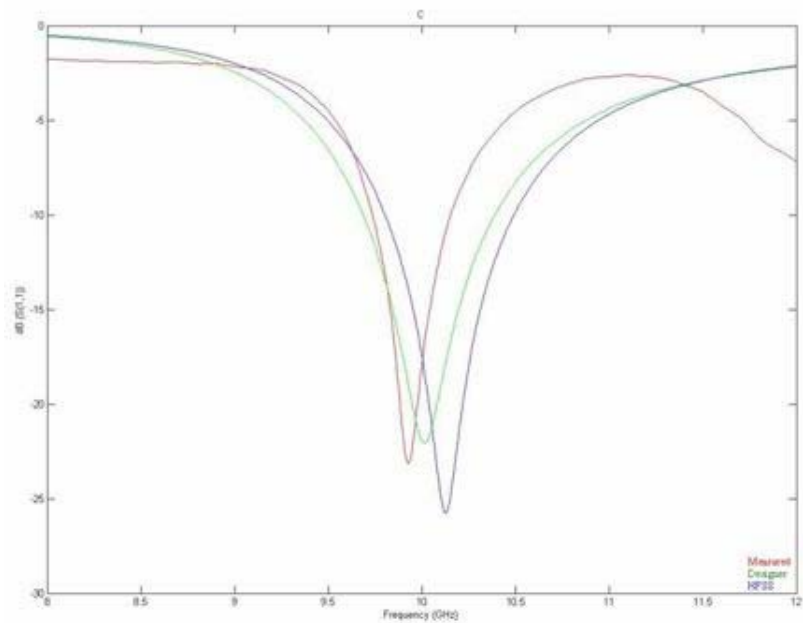


Figure 4.1.58 Log magnitude of the reflection coefficient of the fabricated C design antenna measured (--) and simulated in Designer (--) and HFSS (--)

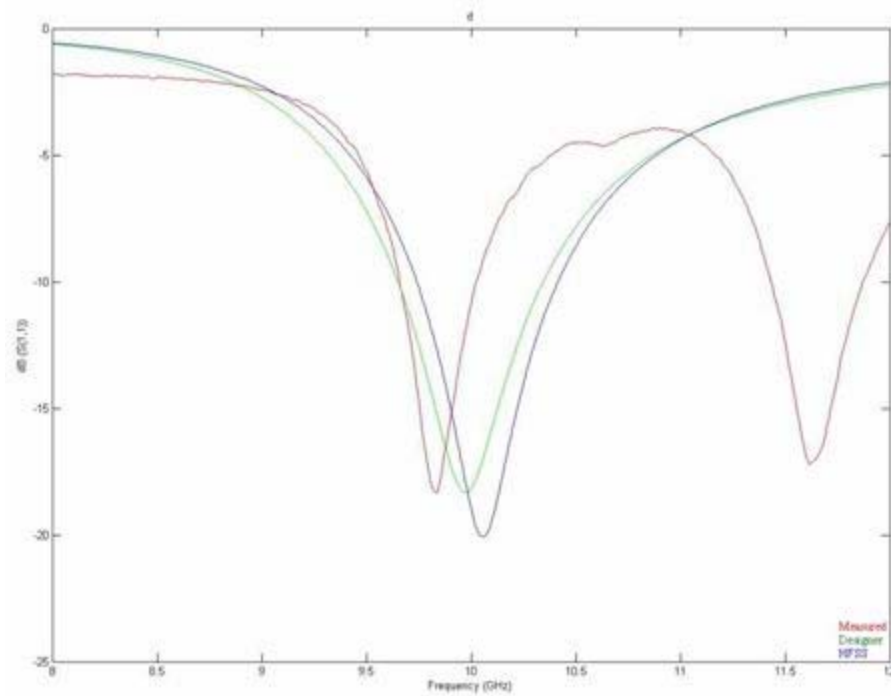


Figure 4.1.59 Log magnitude of the reflection coefficient of the fabricated d design antenna measured (--) and simulated in Designer (--) and HFSS (--)

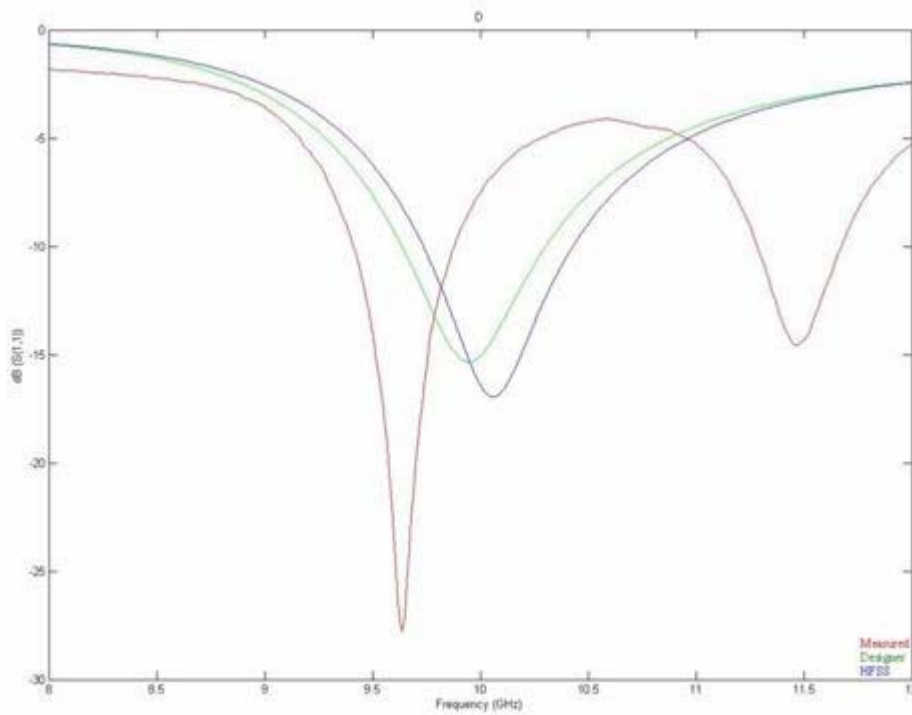


Figure 4.1.60 Log magnitude of the reflection coefficient of the fabricated D design antenna measured (--) and simulated in Designer (--) and HFSS (--)

These plots show that, in general, the simulated results and the fabricated results are in agreement. Around 11.5 GHz there is a second frequency range where the antenna is showing a reflection coefficient value lesser than -10 dB. This can be an effect caused by the connector of the fabricated antenna. Figures 4.1.41 (abCd design), 4.1.49 (abCD design), 4.1.53 (a design), 4.1.55 (b design), 4.1.57 (c design), and 4.1.60 (D design) have a frequency shift that could be caused by a phase change introduced by the connector

A DOE model was made with the measured data from the antennas. Table 4.1.8 shows the data from the antennas. Each antenna was measured in the network analyzer and in the anechoic chamber twice in order to minimize the error.

Table 4.1.8 Result data from fabricated antennas.

	f_0 (GHz)		R at f_0 (Ohm)		Bandwidth (MHz)		Max. Dir. at f_0 (dB)	
	1 st test	2 nd test	1 st test	2 nd test	1 st test	2 nd test	1 st test	2 nd test
central	9.88	9.88	49.42	49.21	480	500	7.01	7.05
abcd	10.25	10.33	46.39	51.51	630	630	7.42	7.39
Abcd	9.90	9.9	48.18	48.32	700	700	7.02	7.04
aBcd	9.88	9.88	44.53	44.57	380	350	7.02	7.01
ABcd	9.52	9.56	40.41	44.07	360	360	6.67	6.71
abCd	10.10	10.10	50.50	5.23	510	500	6.63	6.67
AbCd	10.13	10.12	51.25	50.24	500	560	6.88	6.85
aBCd	10.16	10.17	45.62	46.13	670	670	7.03	6.98
ABCd	10.13	9.41	51.25	40.96	560	300	7.46	7.62
abcD	10.15	10.11	53.72	49.13	460	470	6.30	6.21
AbcD	9.88	9.88	52.03	51.67	600	600	6.76	6.88
aBcD	9.73	9.73	51.76	51.68	490	480	6.66	6.40
ABcD	10.08	10.06	40.77	39.51	340	340	6.85	6.89
abCD	10.30	10.29	51.47	50.33	740	730	6.51	6.49
AbCD	10.01	9.99	52.58	51.42	750	670	6.98	7.01
aBCD	9.99	10.31	37.15	38.99	480	360	7.30	7.11
ABCD	9.61	9.63	45.26	47.66	400	410	6.88	6.88
a	9.98	9.98	51.84	51.90	520	530	6.92	6.93
A	10.10	10.01	50.09	50.03	1100	1080	7.34	7.32
b	9.70	9.7	56.05	56.13	420	410	6.68	6.60
B	9.84	9.82	49.67	47.31	520	490	7.24	7.23
c	9.40	10.94	60.13	58.23	380	480	6.63	6.66
C	9.93	9.99	56.20	48.84	450	470	7.49	7.53
d	9.84	9.82	48.91	46.2	390	400	7.12	7.11
D	9.64	9.64	50.57	50.42	500	500	6.23	6.23

The analysis generated models for each of the four responses. Those models are presented in equations 4.1.13 to 4.1.16. Table 4.1.9 compares the results of the DOE made with the data of the measured antennas with the ones from the antennas simulated by designer and HFSS

$$F = 9.85 - 0.095A - 0.092B + 0.033C + 0.14C^2 \quad 4.1.13$$

$$R = 52.62 - 0.33A - 3.16B - 0.29C + 0.47D - 2.66A^2 + 2.23C^2 - 4.59D^2 + 1.52AC - 1.05CD \quad 4.1.14$$

$$BW = 524.82 + 20.28A - 72.78B + 27.22C + 4.17D + 241.56A^2 - 120.94C^2 - 118.44D^2 \quad 4.1.15$$

$$D = 7.04 + 0.10B + 0.11C - 0.17D - 0.18D^2 + 0.13BC \quad 4.1.16$$

Table 4.1.9 Comparison between the fabricated antenna model and the simulated antenna models

	f _{res}			R at f _{res}			Bandwidth			Gain		
	Fab	Des	HFSS	Fab	Des	HFSS	Fab	Des	HFSS	Fab	Des	HFSS
constant	9.85	10.00	10.04	52.62	67.56	62.48	524.82	734.17	733.33	7.04	2.19	3.70
A(R _o)	-0.095	-0.25	-0.24	-0.33	5.54	3.61	20.28		31.11		0.003	-0.072
B(R _i)	-0.092	-0.24	-0.23	-3.16	-6.78	-7.42	-72.78	-75.56	-88.33	0.10		-0.110
C(d)	0.033			-0.29	-9.75	-8.25	27.22	38.33	12.78	0.11		
D(s)				0.47	3.57	3.16	4.17			-0.17		
A ² (R _o ²)				-2.66			241.56				0.044	
C ² (d ²)	0.14			2.23			-120.94	-50.28	-35.00			
D ² (s ²)				-4.59			-118.44			-0.18		
AB(R _o R _i)					1.49	0.9			38.12			0.021
AC(R _o d)				1.52					25.62			
BC(R _i d)								-53.12	-49.38	0.13		
CD(ds)				-1.05								

Table 4.1.9 shows that there are some differences between the models of the measured antennas and the simulated ones. The measured data showed that the factor with the biggest impact in increasing the resonant frequency is the square of increasing the separation between the circles. That was not a significant factor in the simulations. The inner radius and outer radius are the second most significant factors; these two factors are the only significant factor in the simulations. The difference is due to the effect of the connector.

The square of the inset was the most significant factor for the resistance. It reduces the impedance as it is increased. The square of the outer radius and the square of the difference of the circles are also very significant. The rest of the model is very similar to the ones from the simulation. For the bandwidth the most significant factor was the square of the outer radius which did not appear in the simulation model. The square of the inset also appears as a significant factor. These differences are attributed also to the connector.

Measuring gain using the spherical near-field antenna measurement system requires a characterization of the losses in the system and can be difficult to do. Instead, we measured the directivity of the antennas. The efficiency of the antenna is not considered in the directivity and therefore its values are higher than the simulated gain. Nevertheless, the factors must have a similar effect on the response. The inset and the square of the inset are the factors that have the biggest coefficient but none of the factors really has a big effect on the directivity. This is due to the fact that both gain and directivity are related to the effective area of the antenna and the antenna's area is changing very little.

To validate the model we fabricated the antennas used to validate the simulated antenna models and compared them with the predictions of the fabricated antenna models. Tables 4.1.10 to table 4.1.13 show the results.

Table 4.1.10 Validation of Fabricated Antenna Resonant Frequency Model

				Resonant Frequency (GHz)	
R_o	R_i	d	s	Predicted	Actual
-0.5	-0.5	-0.5	-0.5	9.96	10.16
-0.5	-0.5	-0.7	0.7	9.99	10.08
0.5	0.7	-0.5	-0.7	9.76	9.97
0.7	0.5	0.7	-0.5	9.83	10.59
0.7	-0.7	-0.7	-0.7	9.89	10.09
0.7	-0.7	-0.7	0.7	9.89	9.68

Table 4.1.11 Validation of Fabricated Antenna Resistance at Resonance Model

				Resistance at f_r (Ohms)	
R_o	R_i	d	s	Predicted	Actual
-0.5	-0.5	-0.5	-0.5	53.14	48.22
-0.5	-0.5	-0.7	0.7	54.12	29.81
0.5	0.7	-0.5	-0.7	46.96	47.98
0.7	0.5	0.7	-0.5	50.13	56.06
0.7	-0.7	-0.7	-0.7	50.77	51.35
0.7	-0.7	-0.7	0.7	52.45	37.84

Table 4.1.12 Validation of Fabricated Antenna Bandwidth Model

				Bandwidth (MHz)	
R_o	R_i	d	s	Predicted	Actual
-0.5	-0.5	-0.5	-0.5	540	280
-0.5	-0.5	-0.7	0.7	480	0
0.5	0.7	-0.5	-0.7	440	770
0.7	0.5	0.7	-0.5	550	460
0.7	-0.7	-0.7	-0.7	570	490
0.7	-0.7	-0.7	0.7	570	270

Table 4.1.13 Validation of Fabricated Antenna Directivity Model

R_o	R_i	d	s	Directivity (dB)	
				Predicted	Actual
-0.5	-0.5	-0.5	-0.5	7.01	6.69
-0.5	-0.5	-0.7	0.7	6.76	6.56
0.5	0.7	-0.5	-0.7	7.05	5.36
0.7	0.5	0.7	-0.5	7.25	5.41
0.7	-0.7	-0.7	-0.7	6.99	5.96
0.7	-0.7	-0.7	0.7	6.76	6.61

The tables show that these models were not as precise. To improve the models, multiple antennas would need to be fabricated for each design and average the results. This was not necessary in the Designer and HFSS models because the computer simulations would provide the same results no matter how many times you simulate a particular model.

4.2 Tunable antenna design results

The first design was an antenna with substrate thickness of 0.302 mm, an outer radius (R_o) equal to 0.92mm, inner radius (R_i) equal to 0.62 mm and an offset between circles (d) of 0.27 mm. The dimensions of the CPW line of 50 Ohm are a center conductor of 0.9 mm and slot of width equal to 0.02 mm. The inset used in the antennas for the Design of Experiments was eliminated because the impedance at resonance was too high. Figure 4.2.1 shows the top view of the antenna.

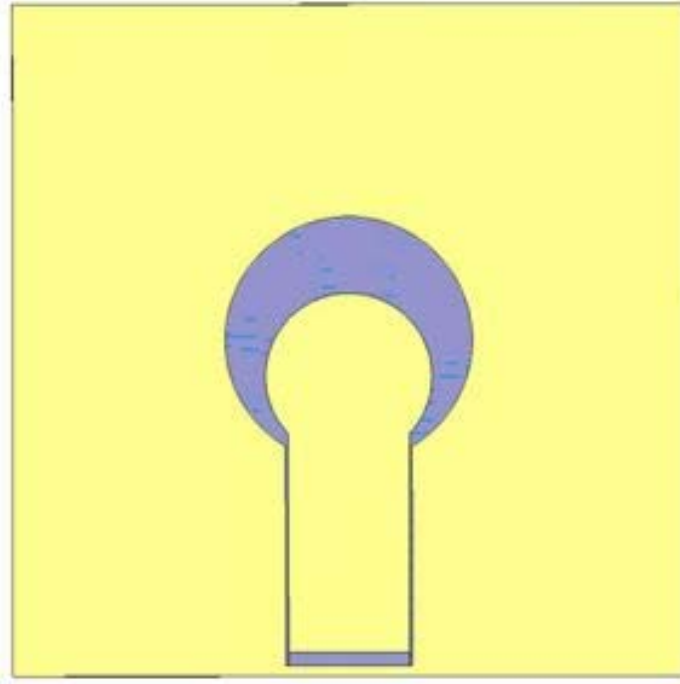


Figure 4.2.1 Tunable antenna with substrate thickness equal to 0.302 mm

The antenna was simulated in HFSS twice, once with a dielectric permittivity for the ferroelectric thin film of 600 and then changed to 1200. Figures 4.2.2 to 4.2.9 show the impedance, log magnitude of the reflection coefficient, the VSWR and the directivity of the antenna.

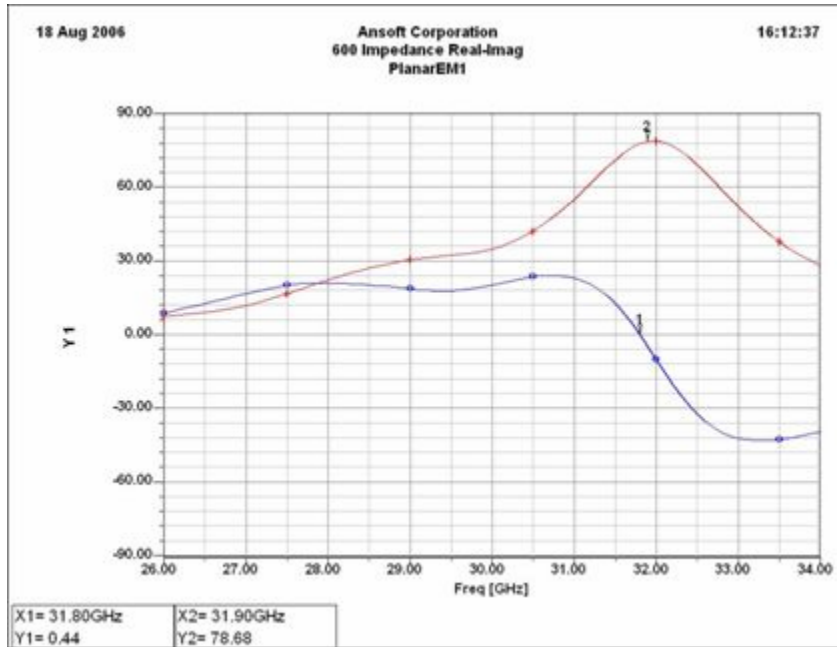


Figure 4.2.2 Resonance frequency and resistance at frequency of the 0.305mm substrate antenna with a ferroelectric material with relative permittivity equal to 600

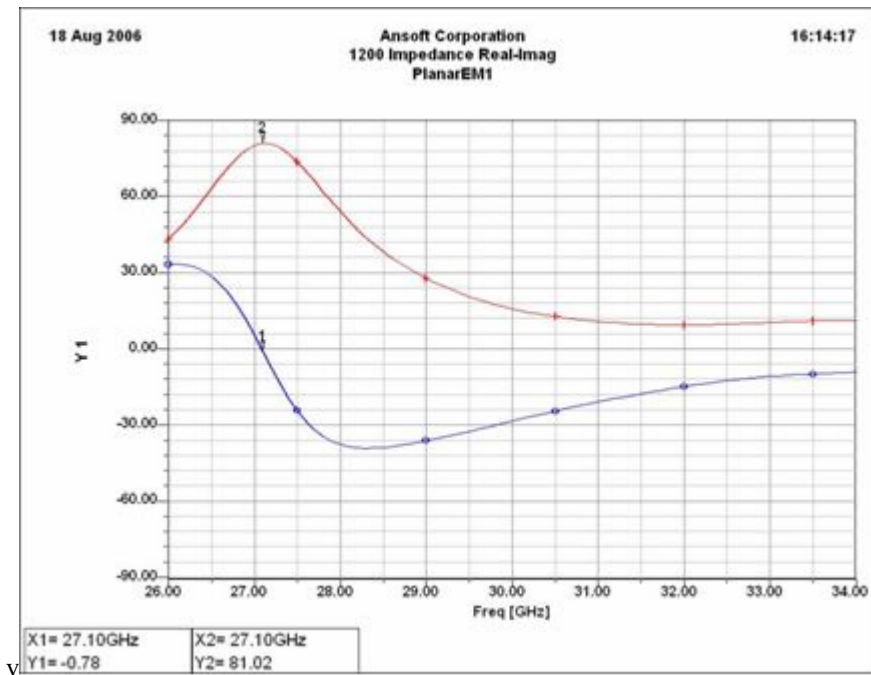


Figure 4.2.3 Resonance frequency and resistance at frequency of the 0.305mm substrate antenna with a ferroelectric material with relative permittivity equal to 1200

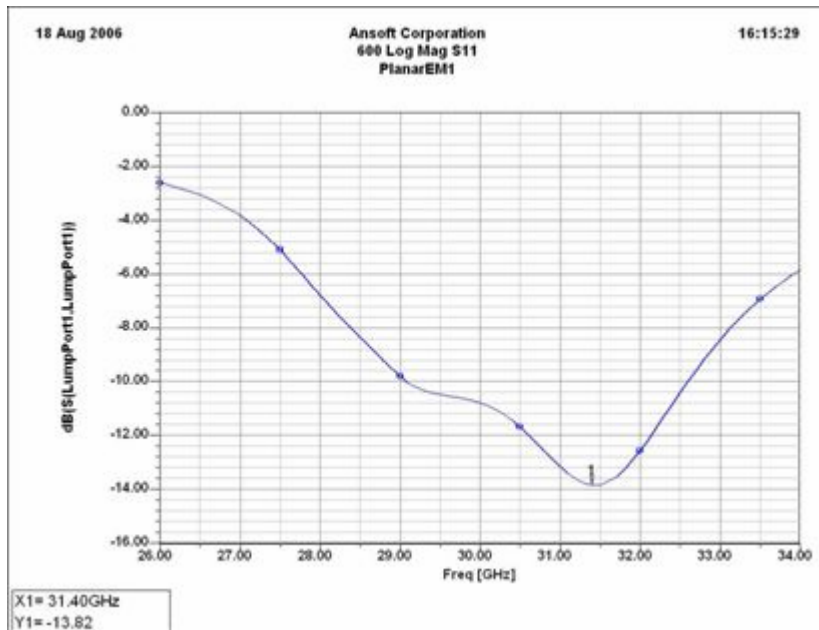


Figure 4.2.4 Log magnitude of the reflection coefficient of the 0.305mm substrate antenna with a ferroelectric material with relative permittivity equal to 600

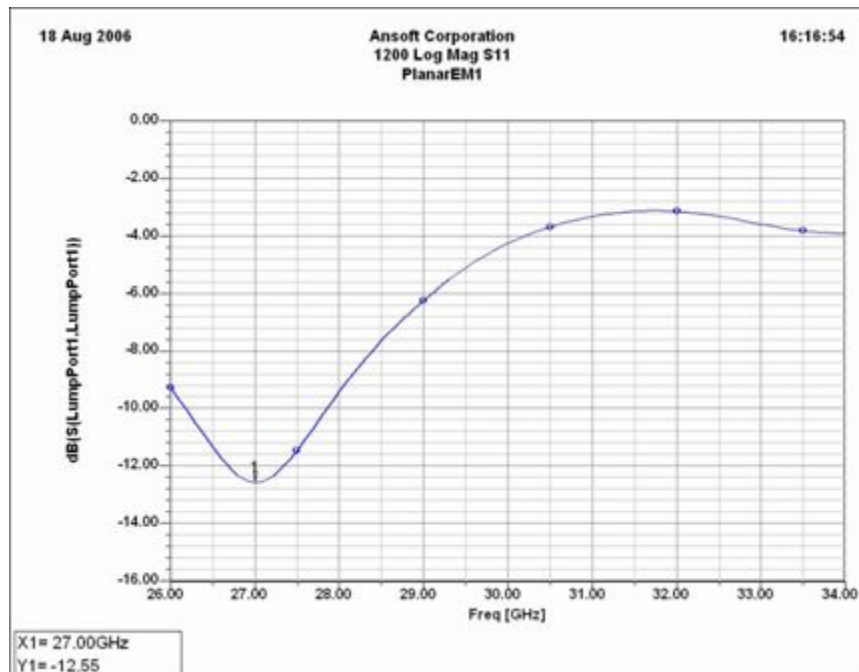


Figure 4.2.5 Log magnitude of the reflection coefficient of the 0.305mm substrate antenna with a ferroelectric material with relative permittivity equal to 1200

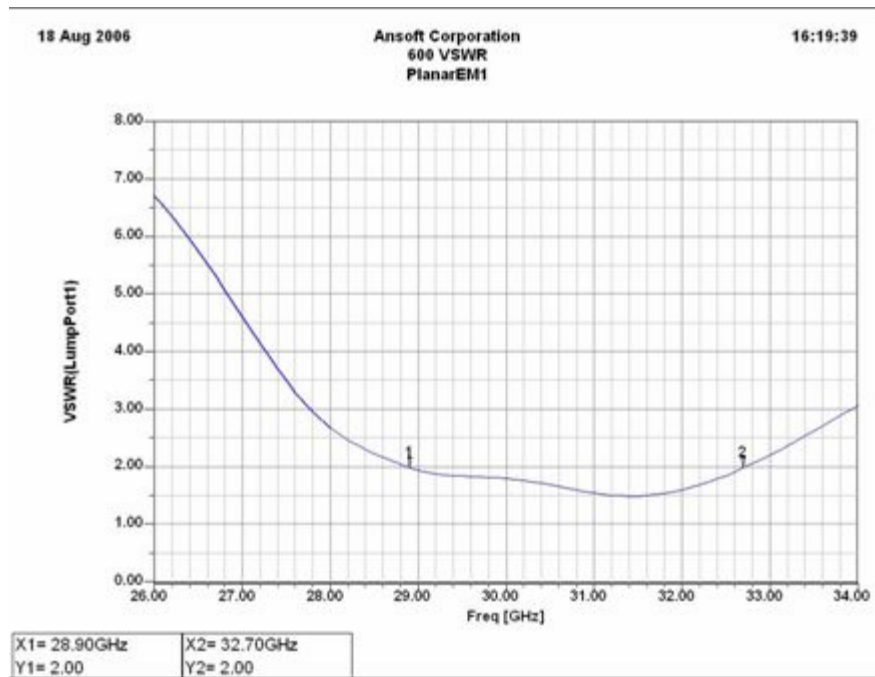


Figure 4.2.6 VSWR of the 0.305mm substrate antenna with a ferroelectric material with relative permittivity equal to 600

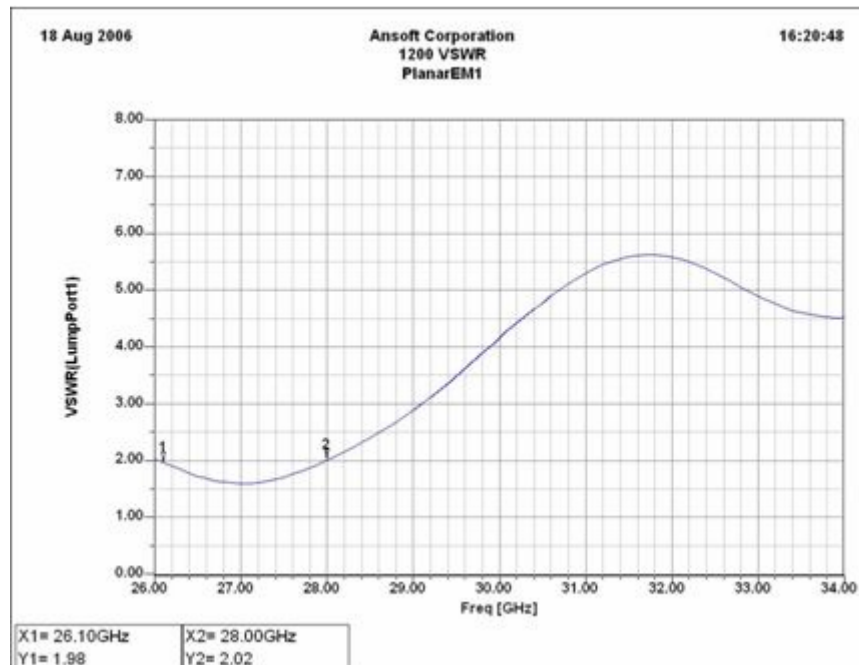


Figure 4.2.7 VSWR of the 0.305mm substrate antenna with a ferroelectric material with relative permittivity equal to 1200

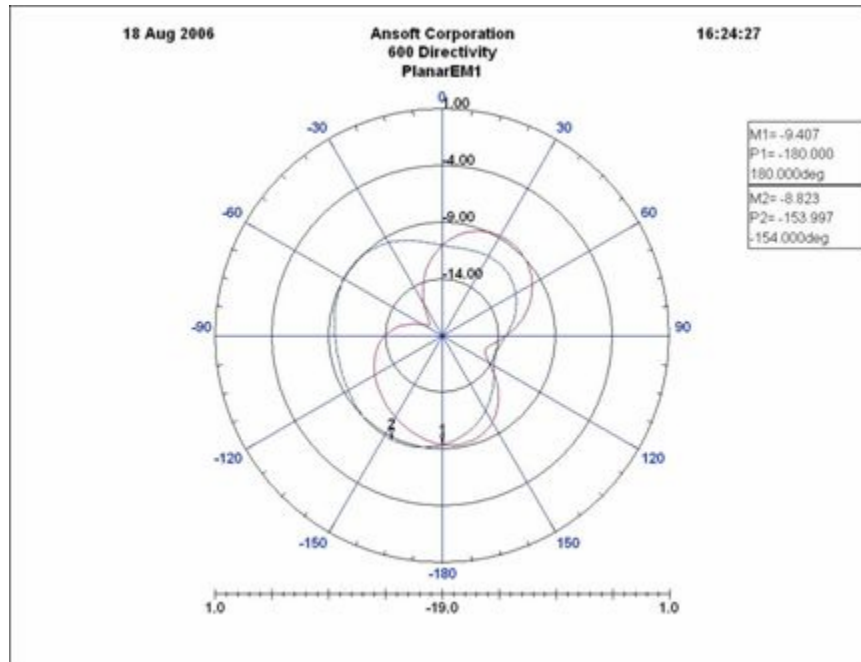


Figure 4.2.8 Directivity of the 0.305mm substrate antenna with a ferroelectric material with relative permittivity equal to 600

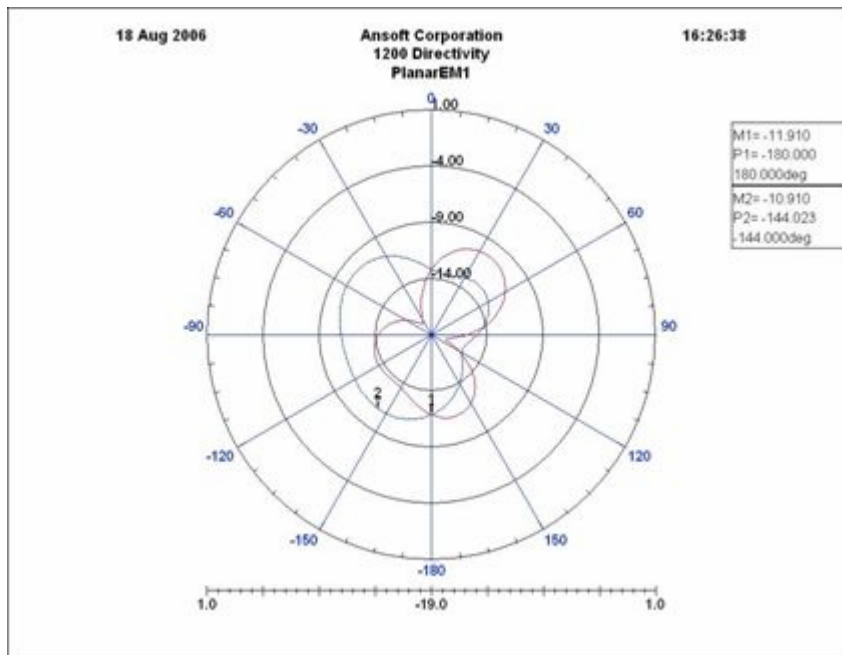


Figure 4.2.9 Directivity of the 0.305mm substrate antenna with a ferroelectric material with relative permittivity equal to 1200

Figures 4.2.2 and 4.2.3 show that as the dielectric constant of the thin film ferroelectric material is increase from 600 to 1200 the resonance frequency of the antenna changes from 31.8GHz to 27.1GHz for a tunability of 14.78%. Figures 4.2.6 and figure 4.2.7 show that the as the dielectric constant increase the bandwidth decrease from 3.8GHz to 1.9Ghz for a reduction of 50%. Also, figures 4.2.8 and 4.2.9 show that the directivity of the antenna is only about -8.8 dB.

To determine if the directivity of the antenna could be increased, another antenna was designed with a substrate thickness of 0.800mm. The dimensions of the antenna were an outer radius (R_o) equal to 0.95mm, inner radius (R_i) equal to 0.70 mm and an offset between circles of 0.0 mm. The dimensions of the CPW line of 50 Ohm are a center conductor of 0.34 mm and slot of width equal to 0.15 mm. Figure 4.2.10 shows the top view of the antenna and figures 4.2.11 to 4.2.18 show the impedance, log magnitude of the reflection coefficient, the VSWR and the directivity of the antenna.

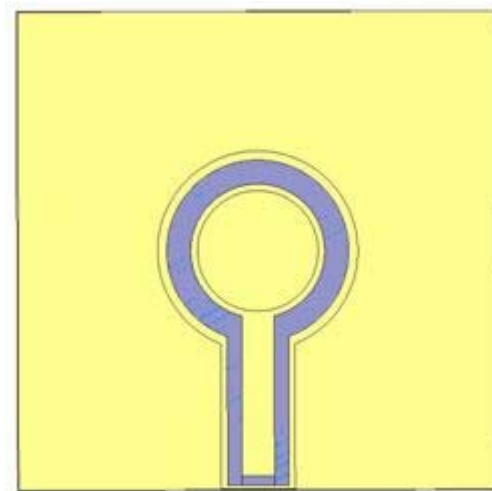


Figure 4.2.10. Tunable antenna with substrate thickness equal to 0.800 mm

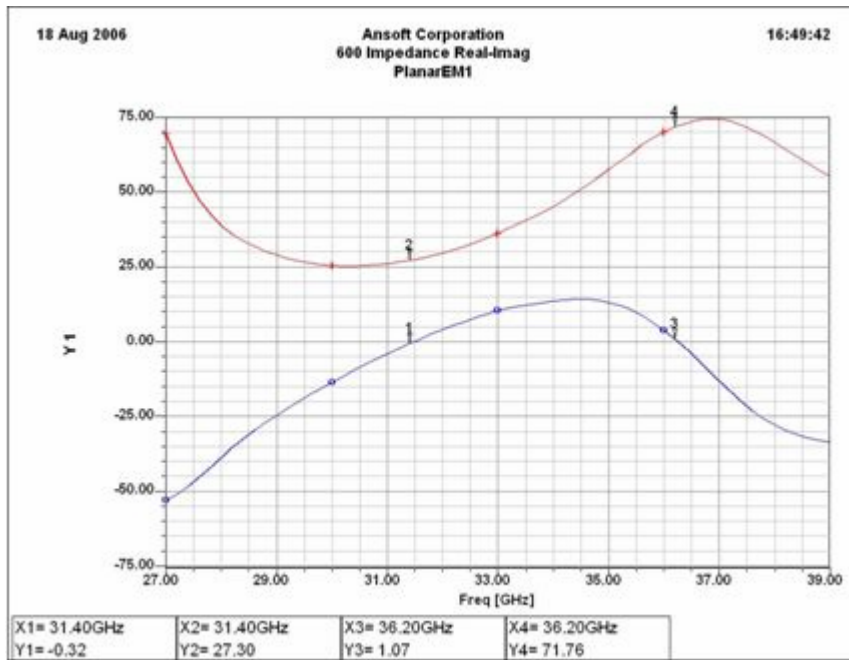


Figure 4.2.11 Resonance frequency and resistance at frequency of the 0.800mm substrate antenna with a ferroelectric material with relative permittivity equal to 600

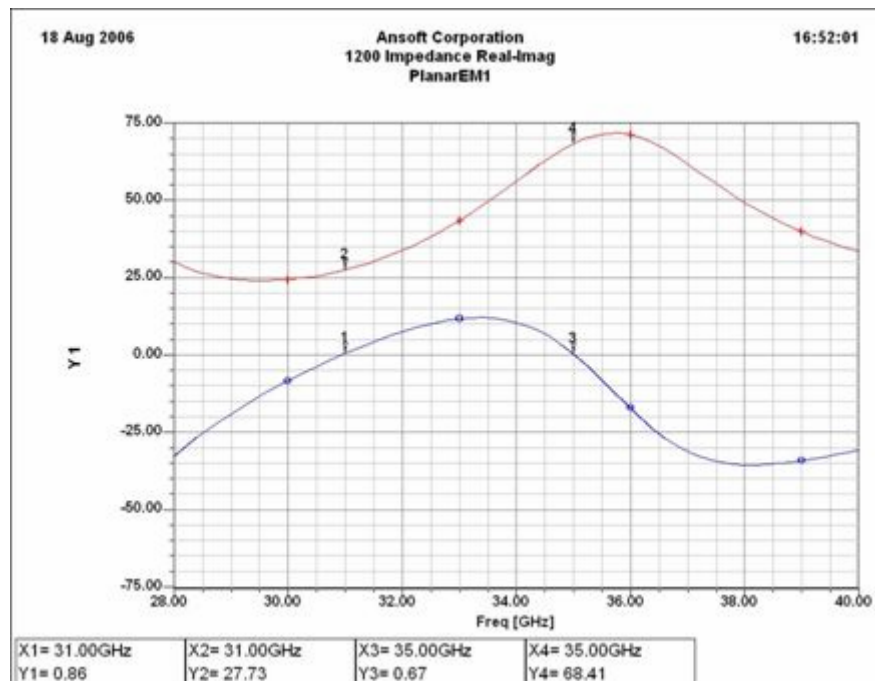


Figure 4.2.12 Resonance frequency and resistance at frequency of the 0.800mm substrate antenna with a ferroelectric material with relative permittivity equal to 1200

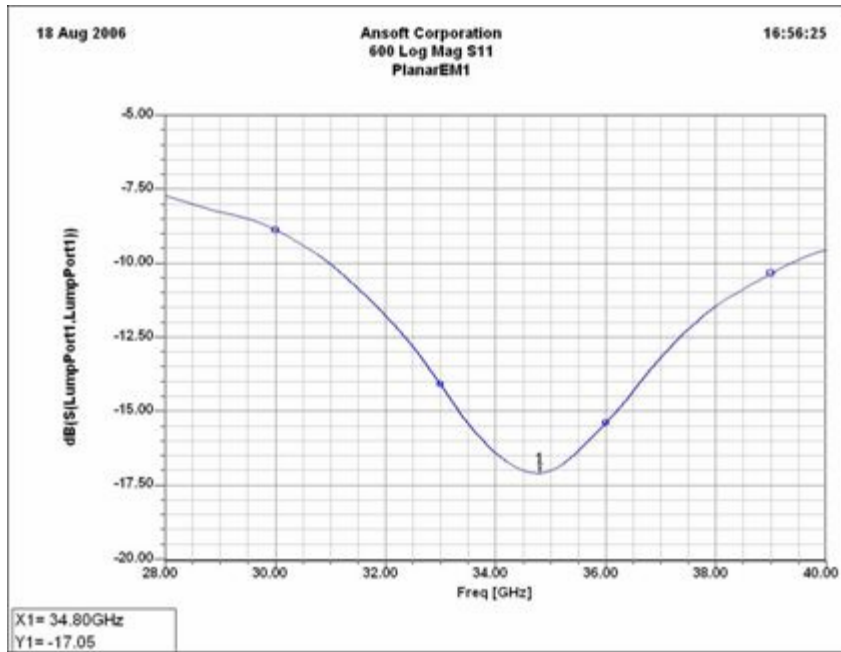


Figure 4.2.13 Log magnitude of the reflection coefficient of the 0.800mm substrate antenna with a ferroelectric material with relative permittivity equal to 600

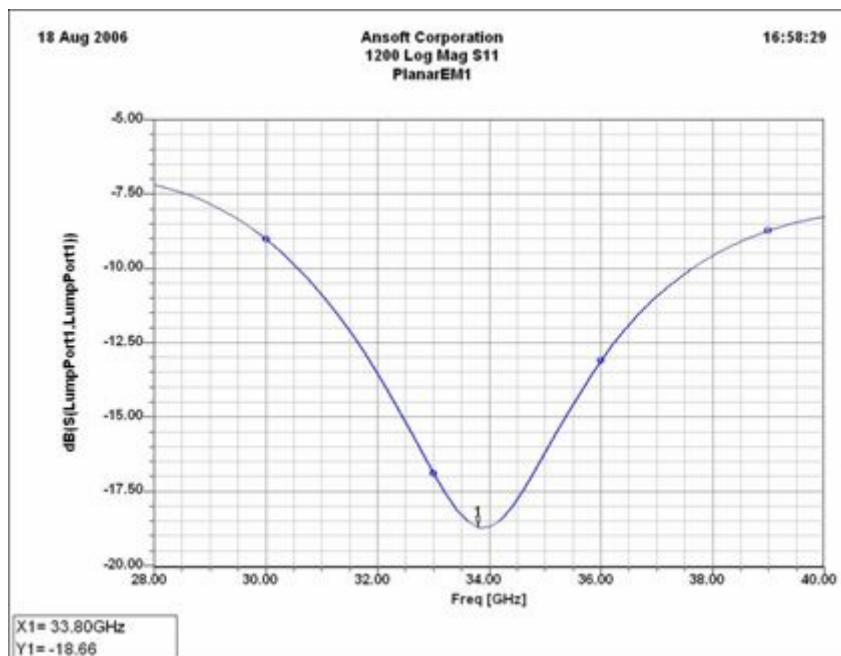


Figure 4.2.14 Log magnitude of the reflection coefficient of the 0.800mm substrate antenna with a ferroelectric material with relative permittivity equal to 1200

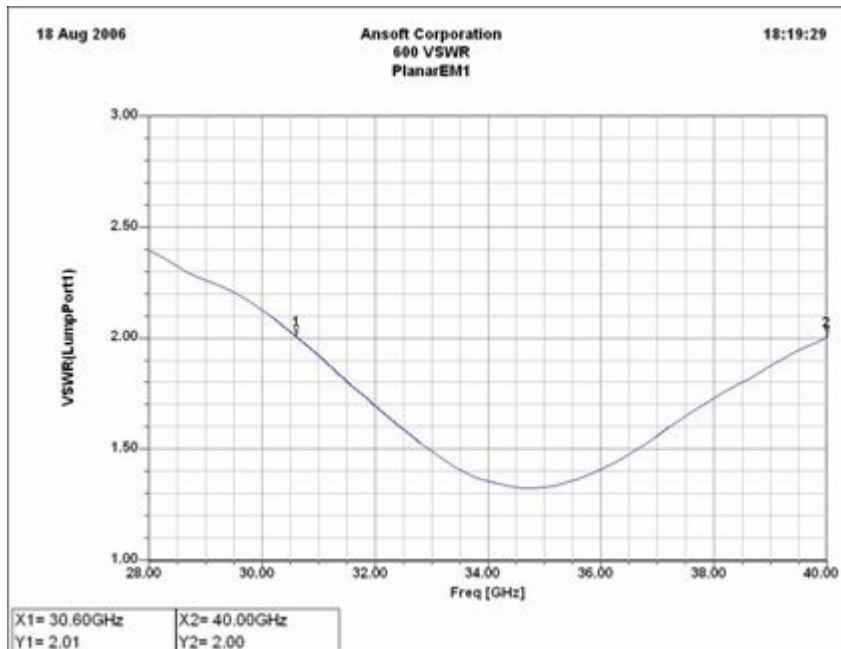


Figure 4.2.15 VSWR of the 0.800mm substrate antenna with a ferroelectric material with relative permittivity equal to 600

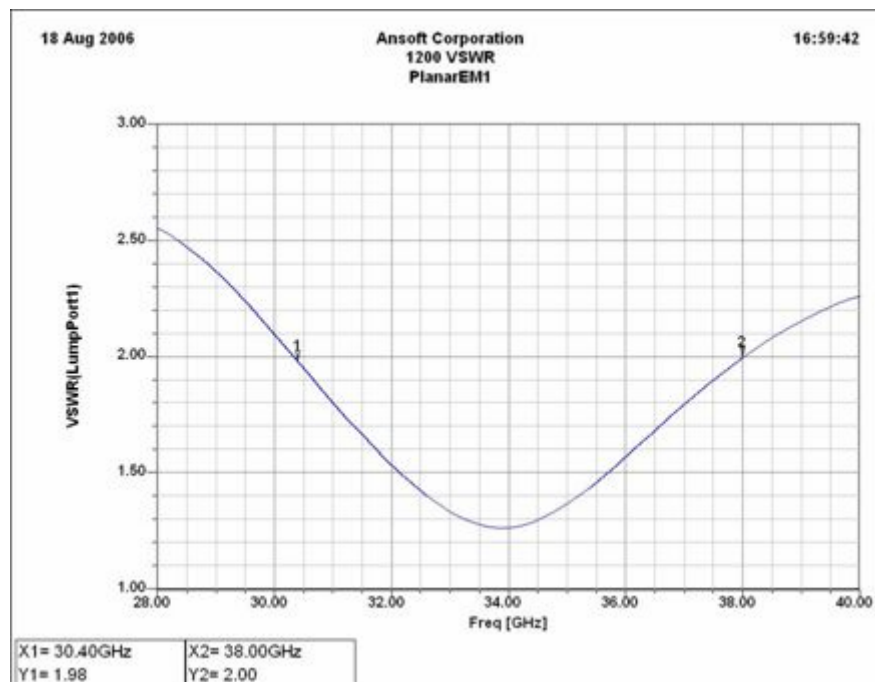


Figure 4.2.16 VSWR of the 0.800mm substrate antenna with a ferroelectric material with relative permittivity equal to 1200

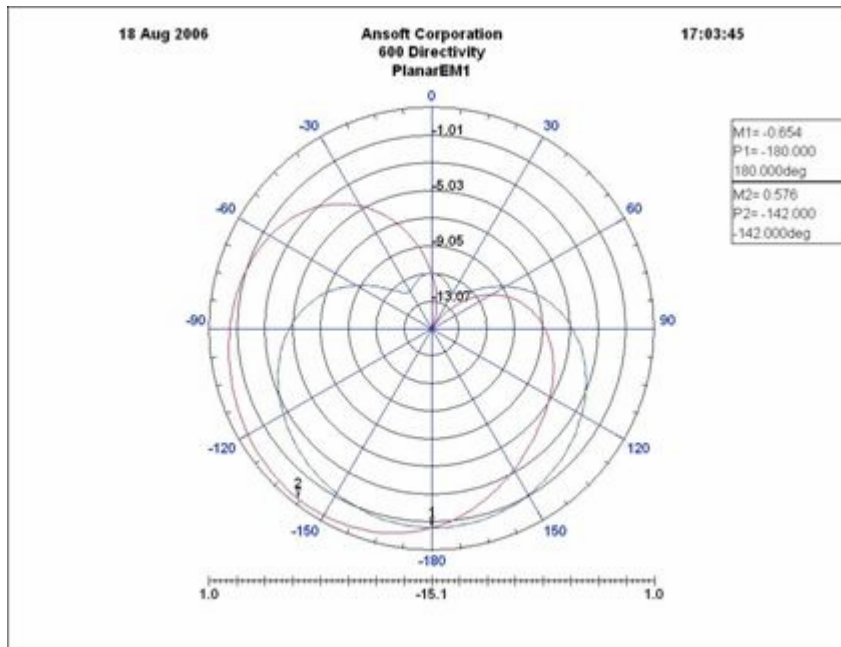


Figure 4.2.17 Directivity of the 0.800mm substrate antenna with a ferroelectric material with relative permittivity equal to 600

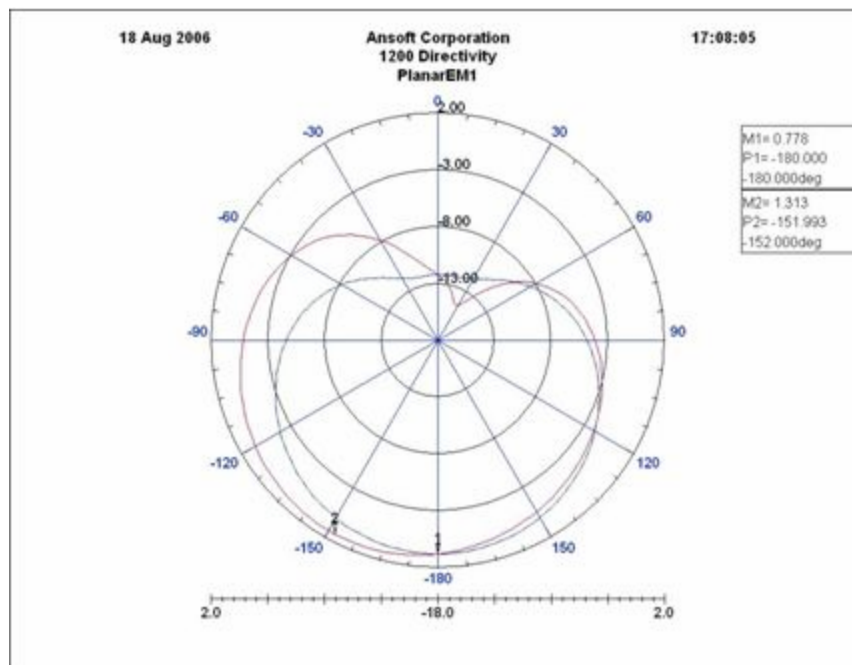


Figure 4.2.18 Directivity of the 0.800mm substrate antenna with a ferroelectric material with relative permittivity equal to 1200

Figures 4.2.11 and 4.2.12 show that this antenna has two resonance frequencies around 30 GHz. As the dielectric constant of the thin film ferroelectric material is increased from 600 to 1200, the first resonance frequency of the antenna changes from 31.4 GHz to 31.0GHz for a tunability of 1.27% and the second resonance changes from 36.2 GHz to 35.00GHz for a tunability of 3.31%. Figures 4.2.13 and 4.2.14 show that the frequency with minimum reflections change from 34.8GHz to 33.8GHz as the permittivity is increased for a tunability of 2.87%. Figures 4.2.15 and figure 4.2.16 show that as the dielectric constant increase the bandwidth decrease from 9.4GHz to 7.6 GHz for a reduction of 19.15%. Finally, figures 4.2.17 and 4.2.18 show that the directivity of the antenna increase from 0.567dB to 1.313dB as the permittivity is changed. The direction of greater directivity is not at -180 degrees but at an angle of -150 degrees. This 30 degree inclination is due to radiation of the CPW line.

4.3 Chapter Conclusions

In this chapter the results for the statistical characterization as well as for the design of the tunable antenna where presented, analyzed and explained. In the next chapter the general conclusions will be presented and in addition, recommendations for future works.

CONCLUSIONS AND FUTURE WORK

4.4 Conclusions

A statistical characterization of an annular slot ring antenna using DOE was presented. The models calculated give an understanding on the effects of the antenna design parameters on the responses of the antenna. These models were validated by comparing the values from simulated antennas with the values predicted by the models. Also, antennas were fabricated and measured to further validate the results and optimum models were obtained for maximum bandwidth and for perfect match.

The models showed that increasing the outer radius (R_o) or the inner (R_i) will increase the resonant frequency (f_{res}) as expected. They also show that the biggest effect on the resistance at resonance (R_f) is caused by the separation distance between the center of the circles (d). As the separation increases the resistance at resonance decreases. The resistance at resonance increases as R_o increases and R_i decreases.

Decreasing R_i or increasing the separation between the center of the outer and inner circle (d) will increase the bandwidth of the antenna. Also, the interaction $R_i d$ decrease the bandwidth as it is increased. R_i has a negative effect in the antenna gain. Only Designer shows that the interaction $R_i d$ has a negative effect and only HFSS shows that R_o also has a negative effect on the gain. It was determined that the discrepancy in the gain is due to the differences between the simulators.

A tunable antenna using ferroelectric material operating at around 30 GHz was presented. A design with a magnesium oxide substrate of thickness equal to 0.302mm showed that the resonance frequency of the antenna changes from 31.8GHz to 27.1GHz for a tunability of 14.78% when the dielectric permittivity of BSTO_3 was varied from 600 to 1200. The bandwidth decreased from 3.8GHz to 1.9GHz for a reduction of 50% and the directivity of the antenna was only about -8.8 dB.

A second design was presented with a substrate of thickness equal to 0.800mm, for this antenna has two resonance frequencies around 30 GHz. As the dielectric constant of the thin film ferroelectric material is increase from 600 to 1200 the first resonance frequency of the antenna change from 31.4GHz to 31.0GHz for a tunability of 1.27%, the second resonance changed from 36.2GHz to 35.00GHz for a tunability of 3.31% and the bandwidth decreased from 9.4GHz to 7.6Ghz for a reduction of 19.15%. The directivity of this antenna was between 0.567dB and 1.313dB. These antennas showed that increasing the thickness of the MgO crystal increases the gain but reduces the tunability of the antenna.

4.5 Future Work

A Design of Experiments should be performed to characterize the effects of the dimensions of the tunable antenna on its responses. Table 5.2.1 shows the propose

dimensions of a 2^3 factorial model. Those values correspond to -1 and 1 coded value and the values for the center design.

Table 4.5.1 Levels of the proposed DOE for the tunable antenna.

Factor	Low level	Center	High level
R_o	0.88mm	0.95mm	1.02mm
R_i	0.63mm	0.70mm	0.77mm
d	-0.07mm	0.00mm	0.07mm

More than one DOE should be done, one for various substrate thicknesses. If the thickness of the substrate is included as a factor in the DOE there will be complications due to the fact that the dimensions of the CPW line of the antenna are not independent from the substrate thickness.

REFERENCES

- [1] K. C. Gupta, R. Garg, I. Bahl, and P. Bhartia, *Microstrip Lines and Slotlines*, 2nd ed. Norwood, MA: Artech House, 1996.
- [2] Simons, R. N., *Coplanar Waveguide Circuits, Components, and Systems*, John Wiley & Sons, Inc., New York, 2001.
- [3] R.W. Jackson, "Considerations in the use of coplanar waveguide for millimeter-wave integrated circuits," *IEEE Trans. Microwave Theory and Tech.*, vol. MTT-34, pp. 1450–1456, Dec. 1986.
- [4] M. Sova, I. Bogdan, "Coplanar waveguide resonator design for array antenna applications" 6th International Conference on Telecommunications in Modern Satellite, Cable and Broadcasting Service, 2003. Vol. 1, pp. 57 – 59.
- [5] M.-H. Yen, P. Hsu, and J.-F. Kiang, "Analysis of a cpw-fed slot ring antenna," in *Proc. APMC 2001 Int. Conf.*, 2001, Vol. 3, pp. 1267–1270.
- [6] R. Garg, P. Bhartia, I. Bahl, and A. Ittipiboon, *Microstrip Antenna Design Handbook*. Norwood, MA: Artech House, 2001.
- [7] Chang, *Microwave Ring Circuits and Antennas*. New York: Wiley, 1996.
- [8] Suh, Y.H., and Park, I.: 'A broad eccentric annular slot antenna'. *IEEE AP-S Int. Symp.*, 2001, Vol. 1, pp. 94–97.
- [9] M. A. Habib, T.A. Denidni, G.Y. Delisle, "Design of a new wide-band CPW-fed circular slot antenna" *IEEE AP-S Int. Symp*, 2005 Vol. 1B, pp.565 – 568.

- [10] Montgomery, D.C. (2001), "Design and Analysis of Experiments", (5th edition), New York: Wiley.
- [11] N. D. Lopez-Rivera, and R. A. Rodriguez-Solis, "Input impedance and resonant frequency characterization for folded slot antennas through DOE techniques", IEEE AP-S Int. Symp., 2003, Vol. 2, pp. 545-548.
- [12] C. Jaramillo-Henao, R.A. Rodríguez-Solis, "Analysis of concentric slot ring antenna arrays using DOE and FDA", IEEE AP-S Int. Symp., 2004, Vol. 1, pp. 1074-1077.
- [13] D.A. Del Rio, R.A. Rodriguez-Solis, D.S. Filipovic, "Ways to improve the radiation pattern of a LPFSA", IEEE AP-S Int. Symp., 2005, Vol. 1B, pp. 410-413.
- [14] L. F. Chen, C. K. Ong, C. P. Neo, V. V. Varadan, Vijay Varadan, Microwave Electronics: Measurement and Materials Characterization, John Wiley & Sons, New York, 2004
- [15] M. J. Lancaster, J. Powell, and A. Porch, "Thin-film ferroelectric microwave devices," Superconduct. Sci. Technol., no. 11, pp. 1323–1334, 1998.
- [16] B. Acikel, Y. Liu, A. S. Nagra, T. R. Taylor, P. J. Hansen, J. S. Speck, and R. A. York, "Phase shifters using BaSrTiO thin films on sapphire and glass substrate," in IEEE MTT-S Int. Microwave Symp. Dig., 2001, pp. 1191–1194.
- [17] F.A. Miranda, G. Subramanyam, F.W. Vankeuls. R.R. Romanofsky, J.D. Warner and C.H. Mueller. "Design and Development of ferroelectric Tunable Microwave Components for Ku and K-Band Satellite Communication Systems", IEEE Trans. MicrowaveTheoryTech.Vol.48, July2000,pp. 1181-1189.

- [18] Jose, K.A., Varadan, V.K. and Varadan, V.V., “Experimental Investigations on Electronically Tunable Microstrip Antennas”, *Microwave and Optical Technology Letters*, Vol. 20, NO. 3, February 1999, pp 166-169.

- [19] Vinoy, K.J., Jose, K.A., Varadan, V.K. and Varadan, V.V., “Gain Enhanced Electronically Tunable Microstrip Patch Antenna”, Submitted to *Microwave and Optical Technology Letters*, 2000.

- [20] Teo, P.T., Vinoy, K.J., Jose, K.A., Varadan, V.K. and Varadan, V.V., “Design and Development of Tunable Multi- Layer Smart Antennas using Ferroelectric Materials”, Submitted to *IEEE Trans. Antennas Prop*, 2001.

- [21] A.M. Castro-Vilaro; R.A.R. Solis, “Tunable folded-slot antenna with thin film ferroelectric material” *IEEE AP-S Int. Symp.*, 2003, Vol 2, pp 549 – 552.